INFORMATION TO USERS

This manuscript has been reproduced from the microfilm master. UMI films the text directly from the original or copy submitted. Thus, some thesis and dissertation copies are in typewriter face, while others may be from any type of computer printer.

The quality of this reproduction is dependent upon the quality of the copy submitted. Broken or indistinct print, colored or poor quality illustrations and photographs, print bleedthrough, substandard margins, and improper alignment can adversely affect reproduction.

In the unlikely event that the author did not send UMI a complete manuscript and there are missing pages, these will be noted. Also, if unauthorized copyright material had to be removed, a note will indicate the deletion.

Oversize materials (e.g., maps, drawings, charts) are reproduced by sectioning the original, beginning at the upper left-hand corner and continuing from left to right in equal sections with small overlaps.

Photographs included in the original manuscript have been reproduced xerographically in this copy. Higher quality 6" x 9" black and white photographic prints are available for any photographs or illustrations appearing in this copy for an additional charge. Contact UMI directly to order.

ProQuest Information and Learning
300 North Zeeb Road, Ann Arbor, MI 48106-1346 USA
800-521-0600

Microscopic-level electrostatic behaviour in cytochrome *c*

By

Christian Blouin

Submitted in partial fulfillment of the requirements
for the degree of Doctorate of Philosophy

at

Dalhousie University
Halifax, Nova Scotia, Canada
January, 2001

DALHOUSIE UNIVERSITY
DEPARTMENT OF BIOCHEMISTRY AND MOLECULAR BIOLOGY

DALHOUSIE UNIVERSITY

FACULTY OF GRADUATE STUDIES

The undersigned hereby certify that they have read and recommend to the Faculty of Graduate Studies for acceptance a thesis entitled "Microscopic-level electrostatic behaviour in cytochrome *c*"

by Christian Blouin

in partial fulfillment of the requirements for the degree of Doctor of Philosophy.

Dated: February 23, 2001

External Examiner [redacted]

Research Supervisor

Examining Committee

DALHOUSIE UNIVERSITY

DATE: January 23, 2001

AUTHOR: Christian Blouin

TITLE: Microscopic-level electrostatic behaviour in cytochrome *c*

DEPARTMENT: Biochemistry and Molecular Biology

DEGREE: Ph.D. **CONVOCATION**: MAY **YEAR**: 2001

Permission is herewith granted to Dalhousie University to circulate and to have copied for non-commercial purposes, at its discretion, the above title upon request of individuals or institutions.

Signature of Author: [redacted]

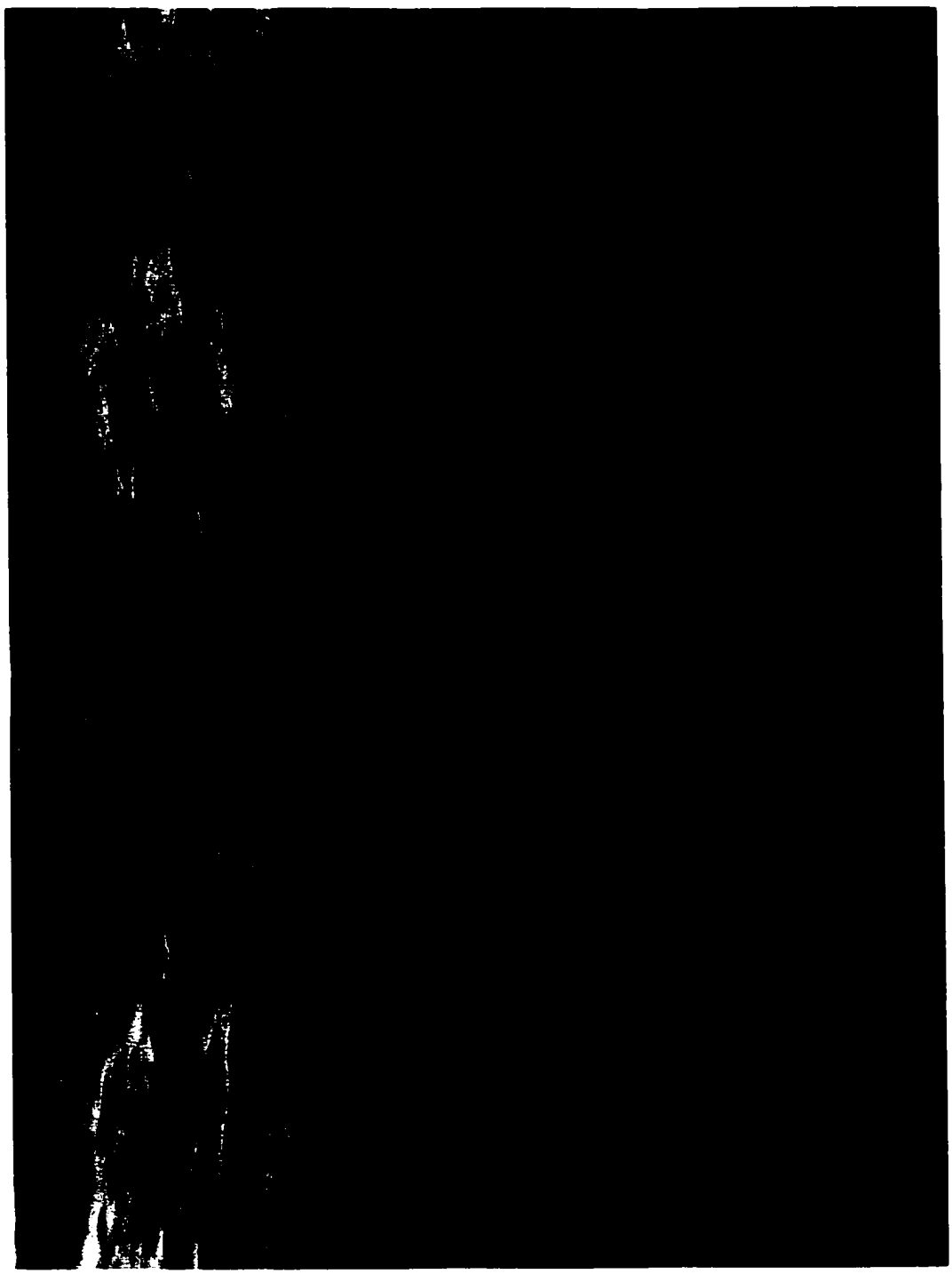

TABLE OF CONTENTS

TABLE OF CONTENTS (CONT'D)

TABLE OF CONTENTS (CONT'D)

TABLE OF CONTENTS (CONT'D)

LIST OF FIGURES

LIST OF TABLES

ABSTRACT

Although it is recognized that electrostatic potential roughly shapes the energetic landscape of macromolecules, the scale and the number of interacting entities in these systems hinders the quantitative appreciation of this contribution. The biophysics of two electrostatically-sensitive equilibria in cytochrome *c* has been studied using protein engineering. First, a pH-induced ligand exchange known as the alkaline transition was investigated using an (alternative) linear regression of titration curves. The alkaline transition proved to be a 2 step equilibrium that is led by the deprotonation of the high-pH ligands and another ionization, thought to trigger this cooperative change. Second, the thermodynamics of oxido-reduction of cytochrome *c* was investigated by point-charge probing and by engineering the internal polarity of the protein matrix. From the discrimination between enthalpic and entropic contribution to the equilibrium, it appears that the dielectric susceptibility is constant within the protein matrix. However, an entropic factor thought to be conformational polarisability dominates the dielectric effect. This explains why no predictable dielectric constant can be derived directly from Coulom's law. It also appears that dipolar and conformational susceptibilities combine in a form of homeostasis that preserves the function of the cytochrome. This functional cooperativity is proposed to confer the robustness and flexibility necessary for the protein to survive (near-)random mutations throughout evolution.

Abbreviations

*	Conventional set of one letter code for nucleotides, three and one letter nomenclature for amino acids and mutations
A(D,T)P	Adenosine di- tri- phosphate
CAMMS	Carboxyamidomethylmethionine sulfonium ion
CD	Circular Dichroism
CoQ	Coenzyme Q, ubiquinone
FAD*	Flavin Adenine Dinucleotide
HPLC	High Pressure Liquid Chromatography
NAD*	Nicotinamide Adenine Dinucleotide
NDM	Net Dipolar Moment
NMR	Nuclear Magnetic Resonance
Pi	Inorganic Phosphate
RMSD	Root Mean Square Deviation
Tml	Trimethyl-lysine
TMPD	Tetramethyl-p-phenylenediamine
XRD	X-Ray diffraction

ACKNOWLEDGEMENTS

First, I would like to thank Dr. Wallace for his guidance and trust in me to let me go through wherever the story led me, to wherever I am now.

I would like to thank Janet Hankins, Angela Brigley and Joclyn Keil for technical assistance, Dr. F. Sherman (U. Rochester), Dr. J.G. Guillemette (U. Waterloo), Dr. A.G. Mauk (U. British Columbia) for providing me with mutant cytochromes. Dr. J. Kornblatt for providing our laboratory with soluble cytochrome *c* oxidase preparation. Dr. S. Bearne, Dr. D. Byers and Dr. K.V. Ewart for sitting on my graduate committee.

I also would like to thank the Sumner Doctoral fellowship for its financial support as well as the members, student and staff of the department of Biochemistry and molecular biology for offering a pleasant working environment.

I would like to thank Karen Black who got more than her fair share of me in the last few years.

I want to thank the Blouins, the Mackays, Daniel, Neeraj, Graham, Sandy, the Blacks and the Vats for having nothing to do with this stack of paper.

Finally, thanks to Liz and Zach who make of this stack of paper means much more than biochemist talk.

Chapter 1: Introduction

1.1 Conformation of biomolecules

Multifunctional molecules and polymers display physical and biological properties that accord with their conformation. The number of possible conformations grows exponentially with the number of freely rotating bonds in the molecule, to attain some billions of theoretical conformations in a small protein. However, this number usually narrows down to a single, native, conformation determined by a complex ensemble of atomic interactions. This ensemble is in part explored through protein engineering and molecular modeling in this work.

This thesis focuses on the role played by electrostatic forces in the determination of native conformations and biophysical properties.

1.2 Concepts of physics

1.2.1 Coulomb's law

The electrostatic force is one of the five fundamental forces affecting matter. Two bodies of identical or opposite polarity will respectively repel or attract each other. The energy required to bring two of these bodies from an infinite to a finite distance apart defines their electrostatic potential. In the macroscopic

world, the relationship between two charges (q_x), distance (r) and potential (U_E) is defined by Coulomb's law (**Equation 1**).

$$U_{Elec} = \frac{q_1 q_2}{(4\pi\varepsilon_o)\,\varepsilon\, r} \qquad (1)$$

Two other terms are present in this relationship: ε_o; the permittivity of the vacuum (8.85419 10^{-12} kg^{-1} m^{-3} s^4 Å) and ε; the dielectric constant. The dielectric constant represents an environmental factor by which the electrostatic potential of a charge is decreased.

A vacuum has an ideal ε value of 1. The dielectric constant ranges in liquids from 4 (cyclohexane) to 110 (HF), with a value of 78.54 for water at 25°C (Eisenberg and Crother, 1979). The effective dielectric constant of dried protein powder varies from 1 to 5 (Takashima *et al.* 1965; Bone *et al.*, 1982). This value is also thought to be representative of the apolar interior of a protein in solution. However, the broad range of chemical properties found in the interior of a protein matrix and the ensuing dielectric screening is likely to

yield ε values around 10-40 (Moore, 1983). Finally, an effective value of 50-80 is typically observed for solvent exposed charges (Rees, 1980).

1.2.2 Physical meaning of dielectrics

The dielectric susceptibility, historically referred to as dielectric constant or effective dielectric constant (Rees, 1980), is a factor by which the electrostatic potential is dissipated by the polarisation of the medium subjected to an electrostatic field. This medium-specific property has a "constant" nature only if one can treat the medium as a continuum of matter. This assumption formally fails in microscopic systems where the polarisability of individually defined molecules must be accounted for.

The microscopic dielectric susceptibility has been broken down by theoreticians into dipolar relaxation and electronic relaxation (Simonson *et al.*, 1991). It was also postulated that the biological functions of catalysis, binding, and electron transport in proteins, all exploited this paradoxical distinction between

polarity and dielectric susceptibility (Simonson *et al.*, 1990).

Due to its high polarisability, solvent water is a potent dielectric material. The study of the structure and function of proteins therefore must account for this major factor.

1.3 Concepts of physical chemistry

1.3.1 Historical perspective

The early model to represent a protein in solution was that of an oil droplet surrounded by a polar environment: a core of low dielectric properties made of hydrophobic side chains surrounded by a high dielectric environment made of polar side chains and a solvent shell (Tanford, 1961). This model was later shaken by the resolution of crystal structures of proteins. In these structures, many polar groups were observed to interact with each other *inside* proteins. With this new information, the model of the low dielectric, non-polar, nature of the protein interior seemed to be too reductionist to be applicable.

From a theoretical point of view, the treatment of a protein as a homogenous dielectric entity was thus becoming impossible. However, recent molecular dynamics experiments showed that it is reasonable to treat the interior of a protein as a low dielectric environment, despite the polar nature of its components (Simonson, 1995; Simonson, 1998). The rationale is that the motion of these buried groups is restrained in a lattice of interactions and hence cannot polarize in response to an electrostatic field.

1.3.2 Oxido-reduction couples

Oxido-reduction (redox) potential and hydrogen ion potential (pH) are two analogous characteristics of a solution. They determine, respectively, the oxidation and ionic states of compounds in solution capable of such equilibria. **Equations 2** and **3** show the two relationships. In **Equation 2**, $\mathbf{E_m}$ is the redox potential of a solution (in Volts) and $\mathbf{E_m^{\circ\prime}}$ is the standard redox potential of an oxido-reduction couple. In **Equation 3**, $\mathbf{pK_a}$ is the ionisation constant of an ionisable group and **HA** and $\mathbf{A^-}$ represent the acid and the base forms of this group.

$$E_m = E_m^{o'} - \quad 0.06 \quad \log \quad \left[\frac{reduced}{oxidized}\right] \tag{2}$$

$$pH = pK_a - \quad \log \quad \left[\frac{A^-}{HA}\right] \tag{3}$$

The standard reduction potential of an oxido-reduction couple reflects how well a molecule stabilizes its reduced state over the oxidized. In a protein, prosthetic groups and metal ions are common redox centres. In cytochrome *c*, the bonds between the iron and its ligands determine roughly the standard redox potential while the protein environment finely tunes it (Moore, 1983), with electrostatic interaction playing an important role (Churg *et al.*, 1986; Langen *et al.*, 1992; Gunner *et al.*, 1991; Davies *et al.*, 1993; Berghuis *et al.*, 1994a). This contribution to the redox potential reflects the ability of a protein to differentially solvate the reduced state versus the oxidized.

1.3.3 Cooperative nature of biopolymers

In the native conformation of globular domains, the ensemble of chemical functionalities form a coherent system that behaves as a unit. The energetics of conformational stability thus depend on a geometrical factor in which all interacting components have to maintain their favourable states. This was observed first in protein unfolding experiments where the plot of the heat capacity of a protein with respect to temperature yields a sharp peak at the midpoint temperature. This binary behaviour in globular domains is known as cooperativity.

The local variations in stability have thus to match the global transition midpoint, which implies that the strongest and the weakest interactions have to form or break in the same event. It is likely that a global transition midpoint does not correspond to any of the isolated local properties: however, all interactions see their energetics focused to this single event. Most of the non-ideal microscopic behaviours observed in macromolecules, such as altered pK_as, thermal denaturation or interaction energetics, can thus be attributable to cooperativity.

1.4 Concepts of molecular modeling

Molecular modeling is a discipline that would benefit from an enhanced quantitative treatment of the electrostatics of macromolecules. Due to the lack of computing technology to model accurately at the orbital level large molecules and their solvent milieu, molecular mechanics is used to perform conformational searching. This method proves itself invaluable in geometrical optimization of a near-native protein. However, it fails to consistently and accurately fold an extended polypeptide into its 3D structure in a timely fashion.

1.4.1 Assumptions of forcefield calculation modeling

An empirical set of optimizations replaces sub-atomic properties.

The computing cost of applying quantum chemistry modeling to large molecules is beyond our current level of technology. The bonded and non-bonded atomic interactions are modeled using a best-fitting algorithm based on spectroscopic observations, electronic structure calculations or simply reproducing empirically known XRD

structures (Jensen, 1999). In forcefield calculations, each atom is assigned a precise coordinate and a parameter commonly known in modeling as "potential". The potential defines a large number of characteristics such as the valence, van der Waals radius, bond length and angles, partial electrostatic charge with regards to its connected atoms, and a series of factors (in kJ * mol^{-1}) with which the potential energy of each of these parameters can be weighted. The bonds are modeled as either harmonic oscillators or using a more realistic "morse" function (tending to 0 $KJ*Mol^{-1}$ for long bonds). A collection of these potentials is compiled in a forcefield file. The reliability of a modeling calculation will largely depend on the relevance of the modeled structure to the purpose of a given forcefield. The forcefield used in this study is cvff_heme; a derivative of the Constant Valence ForceField (cvff), a general purpose forcefield for proteins, with added parameters to model heme proteins.

A cutoff range for non-bonded interactions

The large number of calculations per iteration limits the practical length of simulations. Since this number increases exponentially with the number of interacting elements in the model, the significance of distant atoms is arguably low. To avoid cluttering the modeling process with non-significant contributions, a cutoff system is introduced. The use of cutoff distances can be tailored differentially for van der Waals and electrostatic potential in order to further minimize the number of calculations per iteration. It is common practice to use cutoffs between 8 and 14 Å. This means that any group of atoms found beyond this distance will have no direct influence on the triple derivative of the chemical potential of an atom. It has been demonstrated that the contribution of the interactions neglected by the cutoff does not significantly affect the course of a simulation (Simonson, 1998).

These two main assumptions of forcefield calculation explain why this type of molecular modeling is a fast and reliable means to explore the conformational space by restraining the conformational freedom to a **native** or **near native** fold. The large scale rearrangement involving the high energy barrier of partial unfolding of

a model cannot be reproduced using empirical forcefield simulation in the picosecond time scale.

1.4.2 Triple derivative calculations

This iterative process is commonly known as energy minimisation. During minimisation, the ensemble of all energy terms is first calculated for each atom so a derivative of potential energy is determined. Depending on the algorithm used, each atom is then moved along this triple derivative vector by a certain value. This process is repeated for as many iterations required to balance the attractive and repulsive forces. At this point, the model protein is at a local minimum. Which is not guarenteed to be the global minimum of the model.

The two most common algorithms used in minimization are: Steepest Descent and Conjugate Gradient. Steepest Descent performs fewer calculations per iteration, is more stable in distorted structures, but will approach the local minimum hyperbolically. Conjugate Gradient requires more calculations per iteration but does better at reaching a local minimum when the potential gradient is very small.

1.4.3 Molecular dynamics

Molecular dynamics allows the exploration of the conformational space by initially providing a vector of kinetic energy to each atom. The direction of the vector is randomly generated in the initialization of the simulation, and its energy value is a function of the simulated temperature. This additional energy allows the model to adopt transitory structures between potential minima and settle on the most stable of them. This minimum is expected to be the global minimum, assumed to be the native conformation.

1.5 Cytochrome c as model protein

The protein cytochrome *c* is a classic model protein to investigate structure-function relationships. Its solubility, stability, and its extensive characterization permit numerous experimental approaches.

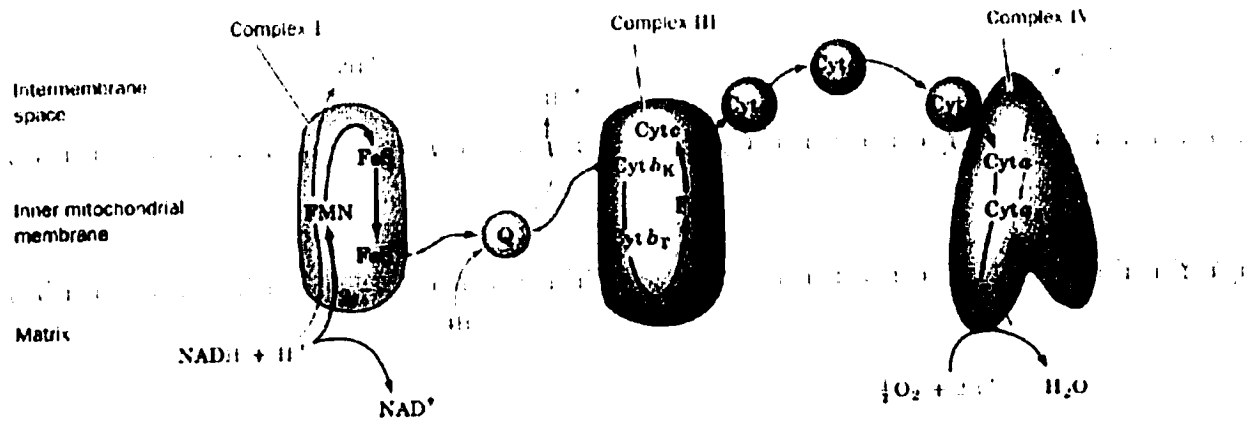

Figure 1.51 Electron transport in the oxidative phosphorylation chain. The pathway of electron transfer is shown in black, and proton pumping in grey. Electrons are transferred from complex I to II by the membrane soluble CoQ and between complexes III and IV by the peripheral membrane protein cytochrome *c*. Adapted from Voet and Voet (1990).

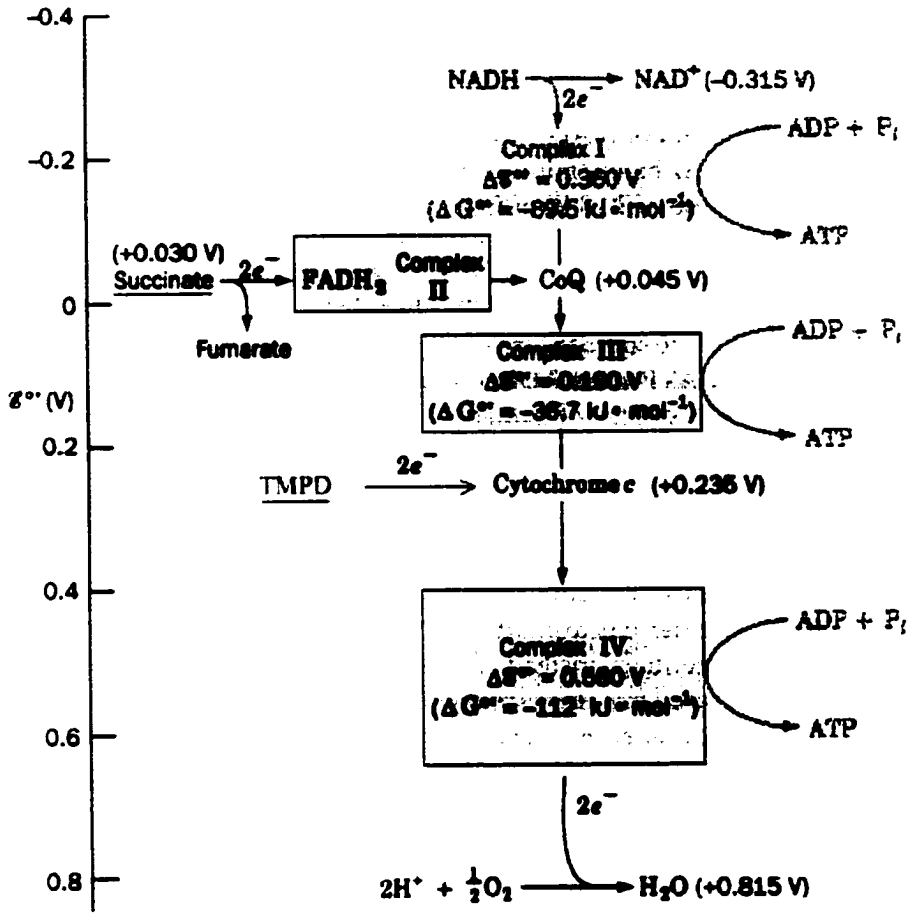

Figure 1.51a Metabolic pathway used in the succinate oxidase and cytochrome c oxidase assays. The standard redox potential is indicated for each natural component of the pathway. Blurred components are irrelevant to the assays described in the text. This figure was adapted from Voet and Voet (1990).

Also, the large number of determined structures (see section 2.4.1 for a partial list) of variant cytochromes and its small size are two assets to undertaking a parallel study using molecular modeling.

1.5.1 Biological function and assays of cytochrome *c*.

Cytochrome *c* acts as an electron carrier for a variety of metabolic pathways. The best known of these pathways is the respiratory chain that drives oxidative phosphorylation in which one cytochrome *c* carries one electron from cytochrome c_1 to cytochrome *a* of complexes III and IV respectively (**Figure 1.51**). In the succinate oxidase assay, the activity of a sample cytochrome *c* in its biological context can be expressed relative to the activity of the wild type protein. This assay uses osmotically shocked, outer membrane depleted mitochondria, and succinate as an electron source (**Figure 1.51a**). Also, the activity of cytochrome *c*, specifically with the cytochrome *c* oxidase, can be assayed using tetramethylphenylenediamine (TMPD) as artificial reducing agent for the cytochrome *c*.

1.5.2 Interaction of cytochrome *c* with its physiological partners

The fast electron transfer from cytochrome *c* to a variety of physiological partners makes this protein a model of choice to study protein-protein interactions. Extensive spectroscopic characterization has been undertaken to study the interactions of cytochrome *c* with cytochrome b_5 (Mauk *et al.*, 1995), cytochrome *c* peroxidase (Mauk *et al.*, 1994) and cytochrome *c* oxidase (Döpner *et al.*, 1999 and references therein). The cytochrome b_5 - cytochrome *c* interaction fostered pioneering work in molecular modeling, first on electrostatics of rigid body binding (Salemme *et al.*, 1976) and later on a flexible binding mechanism (Guillemette *et al.*, 1994).

A trend has been identified, for all of these intermolecular interactions, that the highly basic protein is interacting via its lysine-rich surface with negatively charged surfaces such as lipid bilayers (Hildebrandt *et al.*, 1993) and acidic proteins. The electrostatic potential is responsible for steering the cytochrome into favourable binding conformations and salt-bridge mediated specific binding (Moore and Pettigrew, 1990). There is also evidence that the heme crevice of the cytochrome *c* is

altered (Döpner *et al.*, 1999) and may even substitute Met^{80} as the iron-ligand with another ligand. This is thought to reduce the standard redox potential of the protein, and thereby increase the thermodynamic driving force of the electron transfer reaction (Döpner *et al.*, 1999). These data revived the interest in the ligand exchange isomerization that cytochrome *c* undergoes at alkaline pH.

1.5.3 pH-dependent spectroscopic states

The ligation of the heme iron in ferricytochrome c by the side chains of the protein is a pH-dependent process and yields 5 spectroscopically distinct states (I - V) (Theorell and Åkesson, 1941). The functional conformation is known as state III. In state III, the presence of a band at 695 nm is the result of a charge transfer between the ferric ion and the δ-sulphur atom of Met^{80}, the sixth ligand of heme iron (Schejter *et al.*, 1964; Harbury *et al.*, 1965; Eaton *et al.*, 1967; Schejter *et al.*, 1991). During the transition from state III to IV, the 695 nm band disappears with an apparent pK value ranging between 8.5 and 9.5 depending on the species of

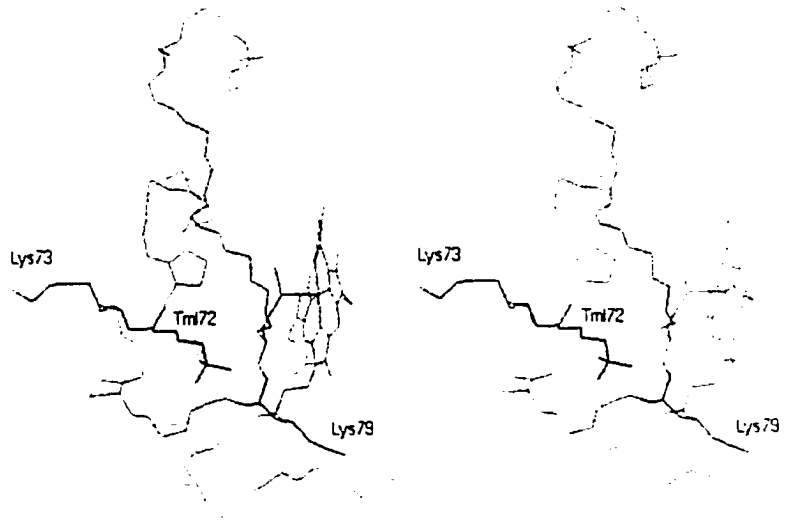

Figure 1.53 Position of the putative lysine ligands in the state III of yeast iso-1 ferricytochrome c. All lysines are in the Ω-loop including residues 69 to 83. Lys^{79} is interacting with the carbonyl group of Ser^{47}, Lys^{73} is fully exposed to the solvent. Tml^{72} is displayed as reference since the untrimethylated Lys^{72} in the horse variant occupies a similar position. Only the backbone from residues 45 to 93 is displayed.

origin (9.35 in the horse variant)(Moore *et al.*, 1990) and titration conditions (Pearce *et al.*, 1989). The replacement of Met^{80} at pH ~ 8.5-10 by another iron ligand is commonly referred to as the alkaline transition of cytochrome c.

The iron in state IV remains low spin due to its coordination by strong field ligands. In yeast cytochrome *c* (isoform 1), NMR spectroscopy was used to show that state IV consists of two possible conformations. Each has either of two deprotonated ε-NH_2 groups as ligands at the sixte position (Hong and Dixon, 1989). These ligands were identified in the yeast cytochrome c (iso-1) as Lys^{73} and Lys^{79} (Ferrer *et al.*, 1993; Rosell *et al.*, 1998; Döpner *et al.*, 1998). In the yeast variant, the apparent pK of the alkaline transition (pK' = 8.7) is an intermediate value between the pKs of two ionisations (pKs = 8.44 and 8.82) (Rosell *et al.*, 1998). In the bacterially expressed yeast cytochrome c iso-1, the apparent pK of the alkaline transition is decreased by 0.6 pK units, to about 8.1. This is hypothesized to be due to the absence of post-translational trimethylation at position 72 that makes this lysine side-chain a plausible ligand, once deprotonated. Animal cells do not undertake this

trimethylation modification (Moore and Pettigrew, 1990); for that specific reason, the alternative ligands for these variants were proposed to be Lys^{72} and Lys^{79} (Pollock *et al.*, 1998). Further observations showed that no major conformational rearrangement occurs in the protein other than the iron ligand replacement (Rosell *et al.*, 1998).

1.5.4 A complex hydrogen bond network inside the protein

The work of Churg *et al.* (1986) showed that the dielectric nature of the heme crevice is ambiguous: A - It serves as a low dielectric environment to favour the ferrous form over the ferric cytochrome *c* and, B - It acts as a high polarity medium to stabilize the positive charge on the heme. This paradoxical situation is the result of a finely tuned network of hydrogen bonds around the heme prosthetic group. **Figure 1.54** shows the various components of this network.

Heme propionates

The heme has two propionate groups named Hpr^6 and Hpr^7. Hpr^6 is partially buried while Hpr^7 is entirely buried inside the heme crevice. Hpr^7 has been the focus of

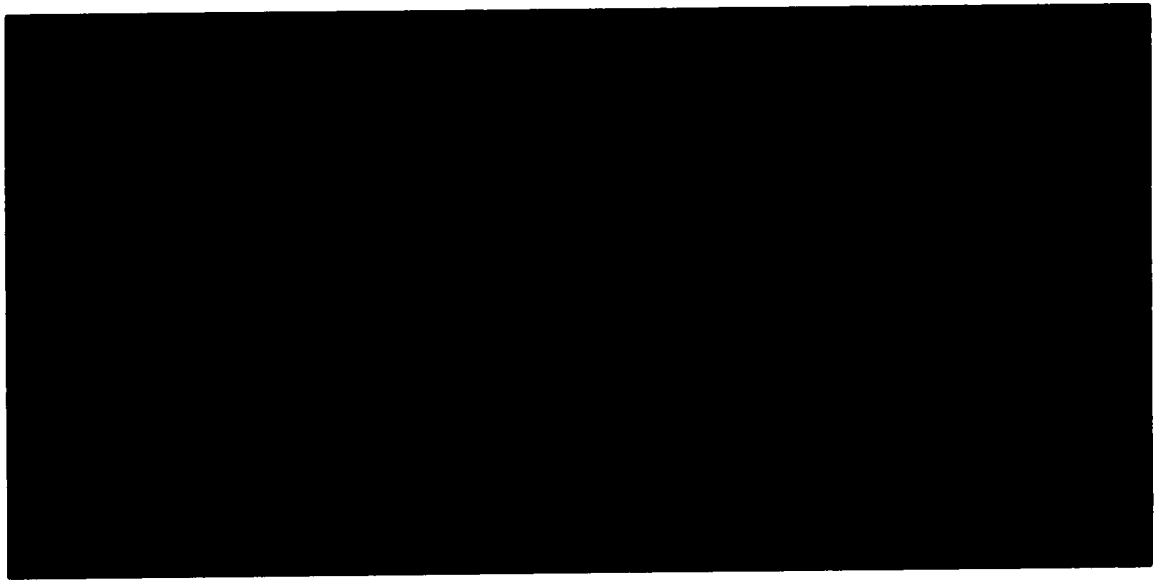

Figure 1.54 Hydrogen bond network in Yeast iso-1 ferricytochrome *c*. Prepared from the Cartesian coordinates of 1YCC (Louie *et al.*, 1990). Water molecules resolved by XRD that belong to the network are shown in blue. Interactions based on hydrogen bonding are indicated by green dotted lines.

interest for the study of the standard redox potential (Moore *et al.*, 1980) of mutants at position 38 (Cutler *et al.* 1989), and for its interaction with the absolutely conserved residues Trp^{59} (Davies *et al.* 1993).

Only one of these carboxylic groups is thought to be ionized at pH = 7, most probably Hpr^{7} (Hartshorn *et al.* 1989). This propionate group is shielded from the solvent by the alkane portion of Lys^{79} and tightly held in place by the amide hydrogen and the γ-OH of Thr^{49}. Also, one of the oxygens is in contact with Thr^{78} and water 166.

Threonine 78

This residue is conserved in 95 known sequences (Moore and Pettigrew, 1990) except for that of *Chlamydomonas reinhardtii* where the residue is replaced by an asparagine (Amati *et al.*, 1988). Mutant T78G (Rafferty *et al.* 1996) was observed to have an apparent pK for its alkaline transition of ~7 (Guillemette, unpublished) and a semisynthetic derivative having a N-butyric group as side chain at this same position, a pK' < 7 (Wallace *et al.*, 1989). The alteration of the chemical nature of this side chain has the largest effect on the pK' of the alkaline transition. In fact, as shown in **Figure 1.55** (see page 27), a close inspection of the chemical context of this

residue indicates that Thr^{78} is the sole potential hydrogen bond acceptor for the propionic group of Hpr^{6}. This residue is thus likely to play a critical role in increasing the microscopic pK of Hpr^{6}.

Asparagine 52

This amino acid interacts with Hpr^{7} and the buried water 166 (Louie *et al.*, 1990). It plays a critical role in the thermodynamics of oxido-reduction (Schejter *et al.*, 1994; Langen *et al.*, 1994; Berghuis *et al.* 1994), thermal denaturation (Linske-O'Connell *et al.*, 1995; Koshy *et al.*, 1994), electron transfer kinetics (Whitford *et al.*, 1991) and the alkaline transition (Schejter *et al.*, 1994) of the cytochrome *c*. Along with the Wtr^{166}, this is the only side chain undergoing a significant rearrangement upon oxido-reduction (Takano *et al.*, 1981;1981a) (**Figure 1.54**).

Much attention was drawn to this position when the mutation N52I was reported to increase both the thermal stability and the pK' of the alkaline transition. In mutant N52I, the Wtr^{166} cavity is filled by the bulkier Ile side chain, and in mutant N52A, the amide group of the asparagine is replaced by a second water molecule.

Tyrosine 67

As visible in **Figure 1.55**, Tyr^{67} interacts via its hydroxyl group with Wtr^{166} and the δ-sulfur of Met^{80}. The contribution of this chemical group has also been extensively studied by semisynthetic (Wallace *et al.*, 1989) and mutagenic approaches (Berghuis *et al.*, 1994; Lett *et al.*, 1996). The mutation Y67F, responsible for a drop in standard redox potential of 56 mV, was suggested to modulate the redox equilibrium by electron withdrawal on the sulfur ligand (Berghuis *et al.*, 1994), and was later shown to contribute both enthalpically and entropically to the equilibrium (Feinberg *et al.*, 1999). In the reduced state of mutant Y67F, XRD crystallography resolved a second buried water molecule located where the hydroxyl of Tyr^{67} used to be (Berghuis *et al.*, 1994). This second water molecule could not be resolved in the oxidized form. This latter mutation has a strong stabilizing effect on the fold of the protein ($T_m \approx 107$ °C) and increases the pK'_{AT} to 10.65 (Wallace *et al.*, 1989).

Isoleucine 75

This residue is conserved in all mitochondrial cytochromes *c* except for a few protists where it is replaced by a methionine or a valine (Moore and Pettigrew, 1990). This residue is part of the polar cavity in which Wtr^{166} is located and is shielded from the bulk solvent. The mutation I75M was studied by XRD and electrochemical characterization (Rafferty *et al.*, 1996). This minor structural alteration provoked a drop in standard redox potential of 33 mV. On the basis of the solved crystal structure, the investigators proposed that the increased polarity of the cavity was diverting the hydrogen bond donor potential of Wtr^{166} from the hydroxyl group of Tyr^{67}. This data set provided little information on the role of this physically neutral residue. However, it reveals more on the role of Wtr^{166} as a modulating element of the protein's standard redox potential (Berghuis and Brayer, 1992; Berghuis *et al.*, 1994a; Lett *et al.*, 1996).

1.5.5 Redox dependent conformations

A redox state change breaks the crystals of cytochrome *c* (Swanson *et al.*, 1977), suggesting a significant conformational difference between the two oxidation states. The alteration of the pKs of surface lysines 53 and 55 (Bosshard *et al.*, 1980) and histidines 33 and 39 (Cutler *et al.*, 1989) also suggested a change in the chemical nature of their immediate environment. The comparison of the two redox state crystal structures in tuna (Takano *et al.*, 1981 and 1981a) and *S. cerevisiae* isoforms-1 (Berghuis and Brayer, 1992), however, indicates that the protein does not undergo any redox state-associated conformational change. According to these studies the buried water molecule 166 of the heme crevice moves toward the iron atom in the oxidized state, extending the side chain of Asn^{52} and altering Wtr^{166} interaction with Tyr^{67} (**Figure 1.55**). Subsequent work using NMR solution structures of the horse variant has shown that, in the oxidized state, the heme solvent access is increased by a slight rearrangement of residues 81-82 (Qi *et al.*, 1994). Also, that the number of bound water molecules increases in the oxidized conformation

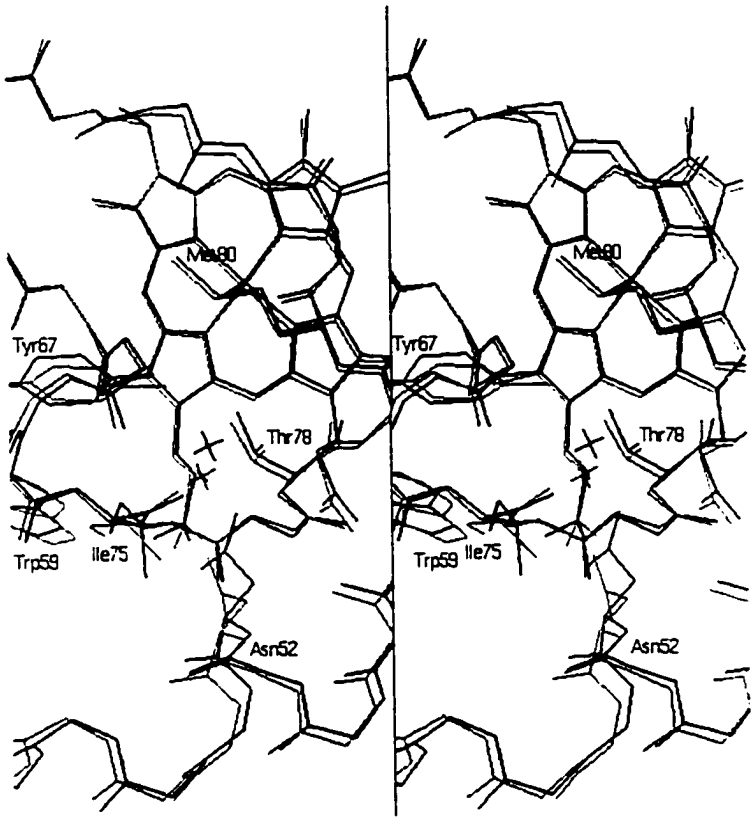

Figure 1.55 Superposition of crystal structures of Tuna cytochrome c in the oxidized (Black) and reduced (grey) form. The oxidized structure was determined by Takano *et al.* (1981a) and the reduced by Takano *et al.* (1981). The key residues interacting with the buried water 166 are labeled. The measured RMSD for the two models is 0.43 $Å^2$.

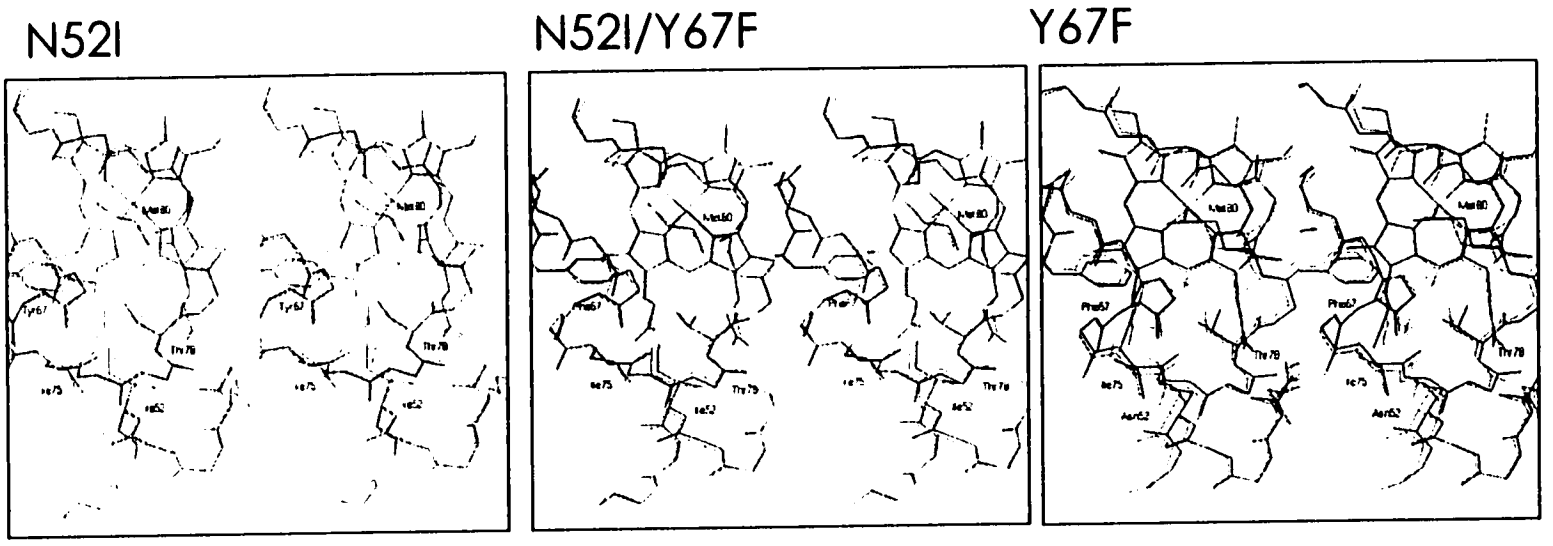

Figure 1.55 Redox dependent conformations of cytochrome *c* mutants. Oxidized and reduced structures are shown respectively in black and grey. Hydrogen bonds are shown in light grey. Prepared from the crystal structure 1CRG, 1CRH, 1CRI and 1CRJ (Berghuis *et al.*, 1994a); 1CTW and 1CTZ (Berghuis *et al.*, 1994).

(Qi *et al.*, 1994). This observation was however contested by another group whose solution structure resembled the crystal structure more closely (Banci *et al.*, 1997). These diverging data at least agree that no major rearrangement is occurring upon oxido-reduction, and that the structural reaction of the protein to the charge on the iron is of a dynamic nature.

Solution structures of the horse cytochrome *c* indicates that one of two water molecules in the heme crevice (water 166) can reorient and act as a microscopic dielectric element to the iron charge (Qi *et al.* 1994a; Battistuzzi *et al.*, 1997). Also, it was suggested that this water molecule influences the standard redox potential via charge withdrawal on the ligating sulfur of Met^{80} by interacting with the hydroxyl group of Tyr^{67} (Berghuis *et al.*, 1994).

1.6 Objectives of this Study

1.6.1 Partial electrostatic scan of the cytochrome *c*

The chemical modification of proteins is a powerful means to extend the variety of side chain functionalities beyond the range of naturally encoded

amino acids. However, the limitation of this approach is the difficulty in attaining site specificity. A selective modification of amino acids can be achieved by exploiting the differential reactivity of some protein side chains (Bosshard *et al.*, 1980), or by limiting the number of target residues on the protein surface (Ando *et al.*, 1966,1966a). This section will report selective alkylation of single methionine residues in cytochrome *c*, using iodoacetamide to generate a non-titratable, non-delocalisable positive charge on a series of methionine mutant proteins.

The cytochrome *c* of *S. cerevisiae* (isoform-1) has two methionines found at position 64 and 80 (Narita *et al.*, 1969). Met^{80}, is the sixth ligand of the iron of this heme-protein, and was reported to be shielded from reactivity with iodoacetamide in bovine ferrocytochrome c (Ando *et al.*, 1966, 1966a). Our preliminary results have shown that this also holds for *S. cerevisiae* iso-1, a variant for which a partial methionine mutant scan comprising a single exposed methionine side chain was designed (Woods *et al.*, 1996). In this partial methionine scan, the wild-type Met^{64} was replaced by a leucine and a methionine was introduced at one of six other locations:

Pro^{25}, Val^{28}, Lys^{55}, Leu^{68}, Ile^{75} and Ser^{65}. From this series of mutants, a corresponding set of site-directed carboxyamidomethylmethionine-sulfonium ion (CAMMS) derivatives was generated. A similar approach to the generation of site-specific chemical modifications has been taken by other workers, using the introduction of unique cysteine residues to provide the target for derivatisation (Wang *et al.*, 1995).

Iodoacetamide reacts with nucleophilic chemical groups found in proteins. Under mild acidic conditions (Ando *et al.*, 1966), only the δ-sulphur of methionines attacks the acetamide methylene group of the halogenoamide using an SN2 mechanism which yields an iodide ion and a CAMMS side chain (**Figure 1.61**). The polarity of the adduct is greatly increased from that of the methionine side chain by the addition of a positive charge and an amide group. In this study, most of these chemical modifications occur at the surface of the protein, hence altered electrostatic properties are likely to be the most important consequence of this modification.

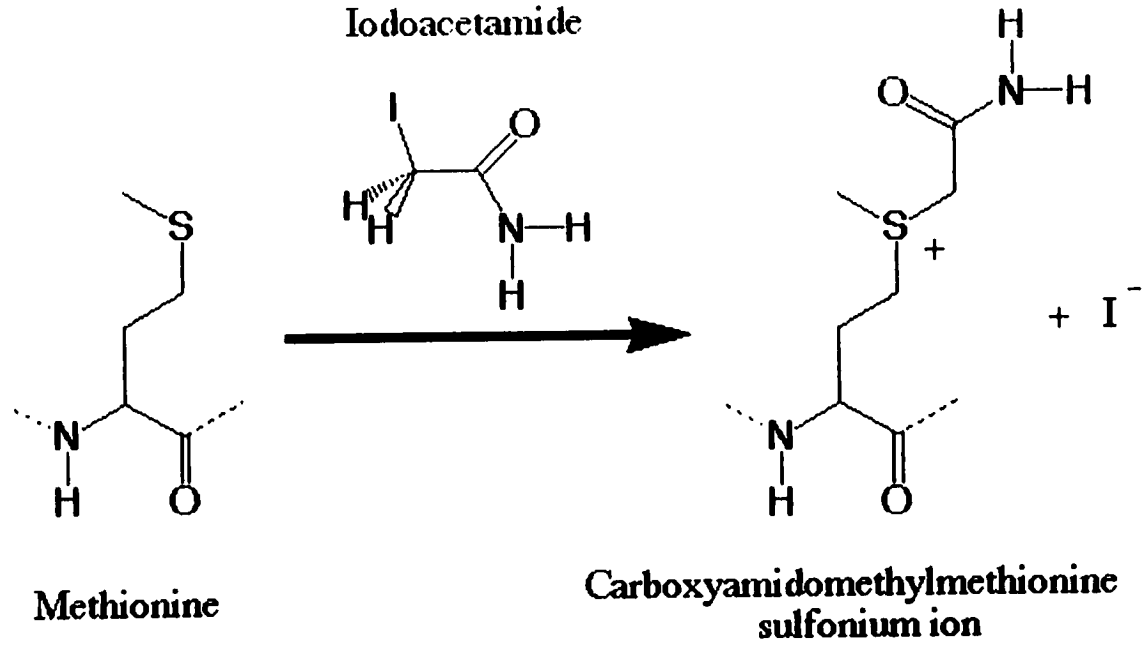

Figure 1.61 Modification of the methionine side chain by iodoacetamide. The δ-Sulfur of the methionine side chain reacts with a molecule of iodoacetamide to yield a carboxymethylmethionine-sulfonium salt (CAMMS) side chain and an iodide ion.

The selective alkylation of these mutant proteins was used as a model system to explore the biochemical and biophysical effects of the addition of a punctate positive charge at the surface of the cytochrome. In addition, the structural effects of the chemical change and consequent altered electrostatics were assessed using molecular dynamics.

1.6.2 Dissection of a pH-induced conformational change

Spectroscopic monitoring of pH-induced conformational changes often generates an irregular titration curve. This is due to the multiplicity of microscopic components involved. The nature of these components and the detail of their interactions define the structure and the properties of a molecule. As a molecule passes from one conformation to another, some of these components become limiting. It is thus possible to resolve these microscopic components from the macroscopic change. This study introduces the use of a linear regression of titration curves to identify the microscopic components of a ligand exchange isomerization in the protein cytochrome c.

This study shows that the determination of limiting microscopic components reveals details about the structure and mechanism of a transition that were not available previously: the mere absence of trimethylation at Lys^{72} in the yeast cytochrome c alters the process of its alkaline transition by generating a new conformer at a lower pH. This conformer must, to account for the hysteresis observed in the titration, overcome a high-energy barrier to equilibrate with the other, more stable, alkaline conformers. I also show that the loss of Met^{80} iron ligation is not solely determined by the ionisation of the lysine ligands, but is likely to involve a third microscopic trigger. I finally argue that the resolution of microscopic components can be applied to any spectroscopic technique to contribute to the investigation of the biophysics of structural biology.

1.6.3 Protein matrix and dielectric effect

This section investigates the premise that the standard redox potential of a redox centre is affected by the local structural effects (Springs *et al.*, 2000), the electrostatic landscape of the polypeptide (Moore, 1983), including the protein's own charges (Churg *et al.*, 1986;

Moore *et al.*, 1980), dipolar matrix (Simonson *et al.*, 1991; Simonson *et al.*, 1995) and surrounding solvent molecules (Edholm *et al.*, 2000).

Since the standard redox potential defines the thermodynamics of equilibrium between two redox states, E_m' can, therefore, be regarded as a measure of the dielectric response to the change in electrostatic charge by the environment (i.e., a higher level of polarisability will favour the +3 charge on the iron over the +2 state as a lower polarisable environment will disfavour it). Assuming that the nature of the iron-ligand interaction remains unchanged, the values of $\Delta\Delta E_m$'' of mutant proteins (versus a suitable control) can be regarded as a measure of the dielectric response of a mutated structural feature to the charge of the redox centre.

The Van't-Hoff method, based on the temperature dependence of equilibria, was chosen to measure the thermodynamics of oxido-reduction (K_{redox}) as shown in the thermodynamic cycle in **Figure 1.63**.

With virtually no redox dependent conformational change and ligand effects (Takano *et al.*, 1981,1981a;

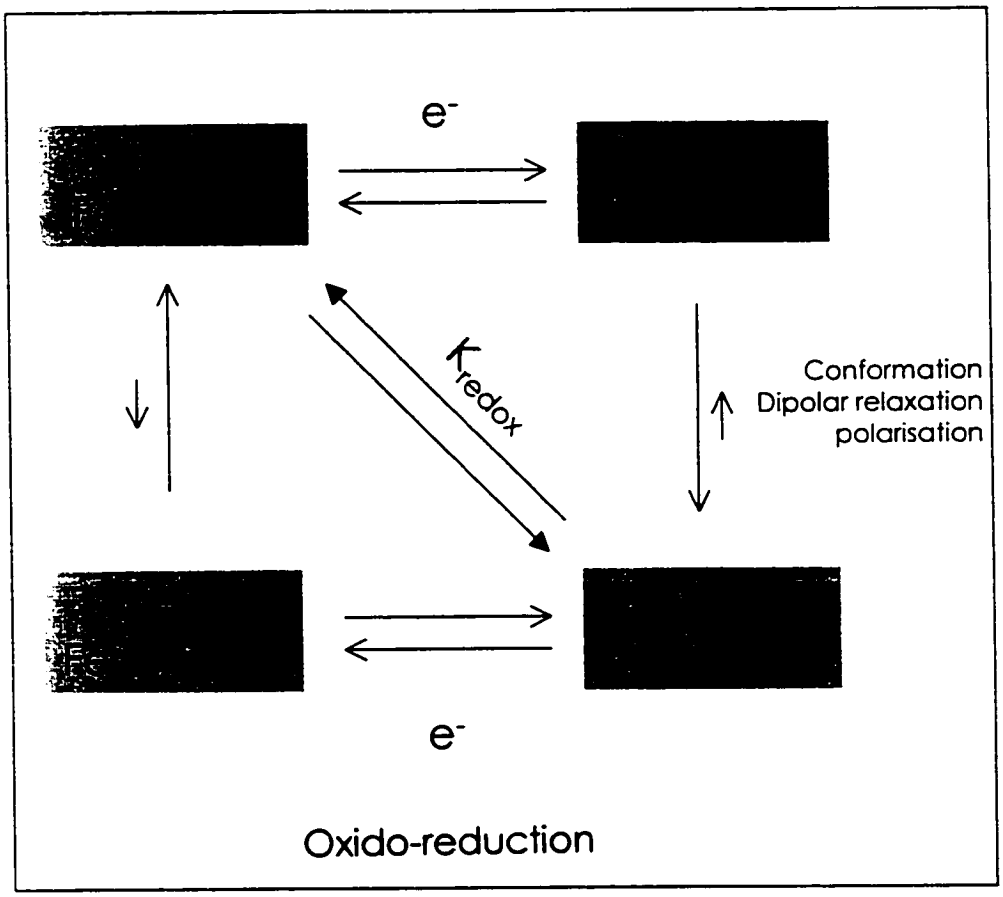

Figure 1.63 Thermodynamic cycle of redox of cytochrome c. The oxidation state of the iron and the polypeptide associated conformation are separately stated respectively in the first and second line in the boxes. The monitored equilibrium is labeled as K_{redox}.

Berghuis *et al.*, 1994; Banci *et al.*, 1997; Qi *et al.*, 1996), cytochrome *c* is an suitable model to investigate the dipolar and electronic contributions to dielectrics by using the standard redox potential of its iron as a measurement of solvation of the extra charge in the oxidized protein.

This section will exploit a series of mutants at position 52 (Linske-O'Connell *et al.*, 1995), three CAMMS derivatives (Blouin and Wallace, unpublished) using the methionine mutants (Woods *et al.*, 1996) as references; and the series of point mutations Y67F, N52I, N52V and their double mutants (Schroeder *et al.*, 1997). The effect on the redox centre will be, in most cases, correlated for these subtle modifications to the E_m'' of the protein and rationalized in terms of polarisability of the matrix in the context of the theory of microscopic dielectrics.

Chapter 2: Materials and Methods

2.1 Expression and purification of proteins

2.1.1 Site directed Mutagenesis of arginine mutants in plasmid pING4

Site directed mutagenesis was performed using a procedure based on the QuickChange method by Stratagene (La Jolla, Ca). The entire gene for the mutant R13K/R38K/M64L/C102T yeast iso-1-cytochrome *c* and parts of the upstream and downstream untranslated regions were cut from pING4 (Inglis *et al.*, 1991) using HindIII and subcloned into Bluescript KS^+ vector.

The resulting plasmid, named pWEE8, was used as the template for performing mutagenesis reactions to avoid problems originally encountered with the large 10.5 kbp pING4 phagemid when using this mutagenesis technique. For each mutagenic reaction, a set of complementary forward and reverse nucleotide primers carrying the desired mutation was synthesised by the MOBIX facility at McMaster University. For each mutagenesis reaction, 50 ng of plasmid pWEE8 DNA, 50 pmol of each of the appropriate forward and reverse primers, 5 µl of the 10X PWO buffer (supplied by the manufacturer) and 2.5 mM of each dNTP

were mixed together on ice and brought to a final volume of 50 µl, then 2 units of PWO polymerase (Boehringer Mannheim, Laval, Canada) were added per reaction. The PCR parameters used consisted of 22 cycles of sequential incubations of 30 s at 95°C, 1 min at 55°C and 3 min at 68°C. Upon completion of the amplification reaction, the samples were cooled to 37°C and 10 units of DpnI endonuclease (Boehringer Mannheim, Laval, Canada) added and the samples incubated for 2 h to selectively digest the methylated parental DNA template. The nuclease-treated DNA was used to transform electrocompetent *E. coli* DH5α cells. The mutant DNA was then fully sequenced to verify the incorporation of the desired modification and rule out the production of spontaneous mutations during amplification. The mutant cytochrome c genes were cut using HindIII from the respective plasmids and subcloned back into pING4 restricted with the same enzyme. The plasmids carrying the mutant cytochrome *c* genes were used to transform yeast GM3C-2 cells for expression of the protein as previously described (Inglis, 1991).

2.1.2 Mitochondrial *S. cerevisiae* iso-1 mutant protein expressed in *S. cerevisiae* strain GM3C-2

Cytochrome c protein was expressed in a strain of *S. cerevisiae* in which both isoforms of mitochondrial cytochrome c are knocked out. This strain retains its ability to grow with partially functional protein but is free from wild-type protein contamination. Cultures were grown at 30°C in 1% (w/v) yeast extract, 2% (w/v) bactopeptone, 0.17% (w/v) yeast nitrogen base without amino acids, 0.5% (w/v) ammonium sulphate and 3% (v/v) glycerol serving as carbon source. Cell density was monitored at 660 nm until stationary phase was just reached and the media was then supplemented with 1% lactic acid (pH 5.5) to stimulate the production of cytochrome c. This culture was then allowed to progress for three days and the cells were spun down at 4000 g for 15 min. Cell lysis was performed for 20 h in 0.5 M KCl and 25% (v/v) ethyl acetate in the presence of a cocktail of proteolysis inhibitors (35 µg/mL PMSF, 0.3 mg/mL EDTA and 0.1% β-mercaptoethanol). Lysate was spun down at 4000 g for 15 min and the supernatant was fractionated by bringing the solution to 50% ammonium sulphate. The supernatant

following centrifugation was dialysed once against 12.5 mM potassium phosphate (pH 7.0), 35 µg/mL PMSF, 0.3 mg/mL EDTA, 0.133 µL/mL β-mercaptoethanol, and twice against distilled water.

The protein solution was then diluted to reduce conductivity prior to loading into a cation exchange Trisacryl-SP Plus-M resin (Sigma) and eluted with a continuous potassium phosphate (pH 7.0) gradient from 100 mM to 250 mM. Appropriate fractions were pooled, desalted on G-25 gel filtration resin (1% acetic acid as eluant), lyophilised and stored at -20°C.

2.1.3 Mitochondrial *S. cerevisiae* iso-1 protein expressed in *E. coli*

The recombinant protein expressed in pBPCYC1-3 was expressed and purified as described in Pollock *et al.*, 1998. However, many attempts to recover the bulk of the product from the pellet of cell debris failed to produce yields as plentiful as those reported by the authors. The amount of purified cytochrome *c* was however suitable for biophysical characterization.

2.2 Chemical Modification of proteins

2.2.1 Selective Iodoacetamidation of Methionines

Ferrocytochrome c (10 mg/mL) and 0.65 M iodoacetamide (Sigma, Oakville, Can) were incubated at 38°C for 4 - 24 hours in an air tight syringe containing degassed 50 mM potassium phosphate pH 5.4 with a small amount of ascorbate (SIGMA, Oakville, Can) to keep the protein in the reduced state. The course of reaction was monitored using high pressure liquid cation exchange chromatography on a SP 5PW column (Waters Associates, Milford, MA) and the reaction product was separated at the preparative scale using SP trisacryl PLUS-M (Sigma, Oakville, Can) cation exchange resin eluted with a phosphate buffer gradient (50 -250 mM).

2.2.2 Reductive alkylation of Lysines

Alkylation was undertaken as previously described (Wallace and Corthésy, 1987), using acetone to produce a fully alkylated isopropyl-lysine derivative.

2.3 Biological and biophysical assays

2.3.1 Succinate oxidase assay

Mitochondria were isolated from rat liver homogenate by cell fractionation. The homogenisation was performed in 8.5% sucrose followed by low speed centrifugation (600 g, 10 min) to get rid of nuclei and cellular debris. Further centrifugation of the supernatant (8000 g, 10 minutes) yielded a mitochrondria-enriched pellet washed with and recentrifuged twice from 8.5% sucrose.

Removal of the organelle outer membrane and endogenous cytochrome c were performed consecutively by osmotic shock of the pellet in 15 mM KCl (10 min, 4°C) and centrifugation (6000 g, 10 min) of the preparation and then four iterations of resuspension/centrifugation of the sediment in 150 mM KCl. The resulting pellet was finally resuspended in 8.5% sucrose and kept on ice until used.

The biological activity of the mitochondria was followed by oxygen consumption monitored with a Clark-type oxygen electrode. A volume of 4.1 mL of assay buffer (300 mM sucrose, 75 mM glucose, 1 mM $MgCl_2$, 12 mM K_2HPO_4, 11 mM succinate, 2 mM ATP and 0.113 mg/mL hexokinase (ICN)) was mixed with 1 mL of mitochondrial suspension and left to

equilibrate until a steady consumption baseline could be established. Cytochrome c was incrementally added. Velocities were recorded and plotted with respect to the mass of cytochrome c present in the assay. First order initial rates were then established for each sample and expressed as % of activity with respect to the appropriate control cytochrome c.

2.3.2 Cytochrome c oxidase assay

The cytochrome c oxidase membrane complex was purified from cow hearts using the technique of Darley-Usmar *et al.* (1987). The activity was measured by molecular oxygen consumption using a Clark-type oxygen electrode. First, 5 mL of reaction buffer (50 mM MOPS and 0.3% Tween 80, pH 7.5) and ascorbate was added to a final concentration of 7 mM (70 µL of 0.5 M sodium ascorbate). TMPD was prepared by recrystallisation from 80% acidified ethanol and added to a final concentration of 0.7 mM (70 µL of 50 mM TMPD). The solution was left to equilibrate until a steady consumption baseline was established and a small volume (0.5 µL) cytochrome c oxidase was added, followed by incremental additions of sample cytochrome c.

First order initial rates were then established for each sample and expressed as % of activity with respect to the appropriate control cytochrome c.

2.3.3 Determination of Redox potential

The measurement of redox potential was made using the method of mixtures (Wallace *et al.*, 1986) in 50 mM potassium phosphate (pH 7.0). A series of ferro/ferricyanide redox buffers were used to assess the oxidation state of the heme iron by spectrophotometry and E_m' calculated using the following relationships:

$$E = E^{\circ'} - 0.06 \log\left[\frac{Reduced}{Oxidised}\right] \quad (2)$$

$$E^{\circ'}_{FeCN} - 0.06 \log\left[\frac{Ferrocyanide}{Ferricyanide}\right] = E^{\circ'}_{Cytochrome} - 0.06 \log\left[\frac{Ferrocytochrome}{Ferricytochrome}\right] \quad (3)$$

The ratio ferro/ferricytochrome c was assessed by comparing the peak height at 550 nm versus those of the fully oxidized and reduced protein at the same concentration. The redox potential of the buffer was set by incremental addition of ferricyanide to a ferrocyanide solution with molar ratio varying from 500 to 7.14. By plotting the logarithm of the ferro/ferricyanide ratio

with respect to the logarithm of the ratio of ferro/ferricytochrome c, we obtain the linear relationship:

$$\log\left[\frac{Ferrocyanide}{Ferricyanide}\right] = \log\left[\frac{Ferrocytocrome}{Ferricytochrome}\right] + \left(\frac{E^{\circ'}_{FeCN} - E^{\circ'}_{Cytochrome}}{0.06}\right) \qquad (4)$$

From this relationship, the standard redox potential of the sample cytochrome c could be calculated using equation (5). However, a correction factor for the deviation from the theoretical slope of one was applied and proved to accurately recover data failing to achieve a slope of 1. The actual equation used to determine redox potential was then equation 6 (**Appendix A**).

$$E^{\circ'}_{Cytochrome} = E^{\circ'}_{FeCN} - 0.06\ b \qquad (5)$$

$$E^{\circ'}_{Cytochrome} = E^{\circ'}_{FeCN} - 0.06\left(\frac{3+m}{2}\right) b \qquad (6)$$

The value of the standard redox potential for the couple ferro/ferricyanide ($E^{\circ'}_{FeCN}$) was taken to be +0.43 V (Wallace *et al.*, 1986).

2.3.4 Determination of REDOX potential with the Fe-EDTA buffer system

The use of an alternate redox buffer system was found necessary for a better coverage of the lower redox potential range in the study of mutant proteins with low E_m'. A method using EDTA-complexed iron in both oxidation states was adapted from Moore *et al.* (1984). Samples were added to 50 mM potassium phosphate (pH = 7.0) and 10 mM EDTA, in the presence of ~0.5 mM of ferric ammonium sulphate (this solution was prepared by dissolving 96.4 mg of ferric ammonium sulphate in 5 mL of 0.5 M EDTA, left to rest for a few hours, then diluted to approximately 0.5 mM in degassed 50 mM phosphate/ 10 mM EDTA). Incremental addition of ferrous ammonium sulphate was made to cover buffer redox values of 180 to 300 mV (5 X 1 µL, 5 µL, 10 µL of 0.05 mM and then 5 µL and 10 µL of 0.5 mM ferrous ammonium sulphate).

Buffer redox potential was calibrated with the parallel titration of two C102T yeast iso-1 cytochrome c (E_m' = 275 mV) and the ratio of mutant ferrous over ferricytochrome c was plotted against the solution redox

potential value. The data was best fitted with a suitable relationship and the mid-point potential evaluated.

2.3.5 Thermodynamics of oxido-reduction

Temperature dependence of the equilibrium between the reduced and the oxidized form of the cytochrome c was measured in 50 mM potassium phosphate (pH 7.0) with its redox potential set at 268 mV using a ferro/ferricyanide ratio of 500. The sample was first prepared, then degassed for 15 min under vacuum, flushed with argon and kept in an airtight quartz cuvette for the whole experiment.

The temperature sweep occurred between 16 and 30°C with a 2°C increment using a HP89090A Peletier element thermostated cuvette holder (Hewlett-Packard, Missisauga, Canada) and the 550 nm absorption band was monitored with a HP8452A diode array spectrophotometer. Fully oxidized and reduced protein were generated respectively by addition of ferricyanide up to a ferro/ferricyanide ratio of 3 and then a small amount of ascorbate.

Despite multiple precautions to overcome apparent autooxidation of the sample protein, the data collection has to proceed in such a way to correct for this minor, but critical, source of error. The temperature sweep proceeded from 30°C to 16°C and then back to 30°C. Corresponding measurements in both direction could be compared to evaluate the constitutive autooxidation. In practice, the two titrations superimposed well up to 26°. Control runs evaluating the temperature dependence of E_m of the buffer indicated that no correcting factor was necessary to be applied.

2.3.6 Titration of the 695nm charge transfer band

Sample cytochromes c were fully oxidised using excess potassium ferricyanide, then desalted on a Sephadex G-25 PD-10 column (Pharmacia, Baie D'Urfé, Canada) and brought to a final concentration of about 2.5 - 8 mg/mL in 50 mM potassium phosphate. The charge transfer band at 695 nm was evaluated by subtracting the absorbance at 710 nm (baseline) from that at 695 nm measured using a HP 8452A diode array spectrophotometer (Hewlett-Packard, Mississauga, Canada). The titration was performed for pH

values typically ranging from 6.5 to 10.5 and at approximately 0.15 pH unit intervals using small volumes of 0.01, 0.1, 1 and 5 M KOH or HCl. Special care was taken to avoid large pH swings in the pH range of 8.2-8.9 since direction of titration was important in some samples and therefore no backward step could be performed.

2.3.7 Mathematical processing of titration data

Equation 7 is derived from the mathematical definition of an ionisation constant with its signal decreasing as the pH increased. In this equation, $A_{695\ nm}$ corresponds to the absorbance at 695 nm, A_{max} is the maximal peak height at neutral pH and K_a is the ionisation constant of the ionizing group:

$$A_{695\,nm} = \frac{A_{max}}{1 + (K_a / [H^+])} \qquad (7)$$

$$\frac{A_{695\,nm}}{[H^+]} = \frac{A_{max}}{K_a} - \frac{1}{K_a} A_{695\,nm} \qquad (8)$$

The titration curve was evaluated with a non-linear regression algorithm to determine the offset in absorbance of the sigmoid best fit. This offset was then subtracted from the data. By plotting $A_{695nm}/ [H^+]$ vs A_{695nm},

the slope of a linear segment determined using the least-squares method could be used to calculate discrete K_a values. Most samples assayed yielded two or three of these linear segments and their slopes were determined separately. The precision in measurements of pK was typically within +/- 0.05 unit of pH.

2.3.8 Partial titrations of the 695 nm charge transfer band

Freeze dried commercial horse heart cytochrome c (Boeringer Mannheim, Laval, Canada) was dissolved in 50 mM sodium phosphate buffer (pH 7.0). The protein was totally oxidized using potassium ferricyanide and buffer exchanged to 50 mM sodium phosphate pH 9.2 or 10.5 using a G-25 resin in a PD-10 desalting column. The titration was then either immediately performed in ~0.1 pH unit increments back to pH 7.4, or to pH 10.5, or incubated at room temperature for 10 minute prior to titration. Finally, the titration curve was sampled over a few data points in the pH range of 10.5-11 to determine the titration curve baseline. The corresponding fragments of the titration

pseudosigmoid were then mathematically processed as described.

2.3.9 Thermodynamics of the alkaline transition

This was performed using the graphical method of van't Hoff. Samples were dissolved in 50 mM sodium phosphate, pH 6.5, to measure the maximum of the 695 nm band using a UV spectrometer. The samples were then taken to a pH corresponding to their apparent transition midpoint and left to equilibrate in a thermostated cuvette holder HP 89090A (Hewlett-Packard, Mississauga, Canada). The 695 nm peak height was monitored over 20 - 34 °C using increments of 2 °C. A final measurement was made at pH ≈ 10.5 to assess the baseline of the titration curve.

2.3.10 Secondary structure analysis by circular dichroism

Sample cytochromes *c* were prepared in 10 mM phosphate pH 7.0 in a 1 mm quartz cuvette and the spectra were recorded from 260 nm to 180 nm at 10 $nm*s^{-1}$, at 25°C. Molar ellipticity was then calculated with exact

cytochrome concentrations measured at 410 nm (ε=106 $M^{-1}cm^{-1}$) in a regular UV-vis spectrometer. The typical domain of good signal-to-noise ratio was 183 - 260 nm.

2.4 Computer modeling

Computer modeling was carried out on a INDIGO2 SGI platform running under IRIX 6.5.5 using MSI's modeling package INSIGHTII v.98.0 with licenses to BIOPOLYMER, DISCOVER 2.7.7, DISCOVER 3.0 and SKETCHER. A custom forcefield was used to accommodate the peculiar character of the type-c cytochromes. This force field, named cvff_heme (gift from Dr. G. Brayer, UBC), is a derivative of the standard Constant Valence Force Field (cvff) with the necessary parameters to process the heme prosthetic group. Cvff_heme was further modified to allow the modeling of the sulfonium sulfur atom found in the chemical derivative CAMMS.

2.4.1 Starting structures

Protein DataBase (PDB) structures were downloaded from the Entrez database (http://www.ncbi.nlm.nih.gov) for a variety of X-Ray and

NMR solution structures with the accession numbers as shown on **table 2.41.**

PBD file format is a simple system including information on molecular coordinates, atom type and crystallographic temperature factor for each atom. These were then processed into a functional molecular model with the addition of hydrogen atoms to cap open valences and adjust the ionisation states of basic and acidic groups as typically charged at pH 7.0. Potential was then assigned to each atom using the automated feature of the modeling environment. The output was manually checked and adjusted for the heme prosthetic group and the trimethylysine at position 72 in the yeast models. A typical minimisation step (Steepest descent, 5000-10000 iterations, Morse and Cross terms turned on) was then performed using DISCOVER 2.7.7 with all the atoms belonging to the protein fixed in space to generate an appropriate solvent-mediated hydrogen-bond lattice.

Balanced structures were then soaked using a layering algorithm with 5 Å of discrete solvent molecules and this solvation shell was in turn solvated with an extra 5 Å of water molecules that will form the shell of "frozen" water molecules, decreasing the rate of

evaporation during the course of molecular dynamics. This method was preferred over the use of Periodic Boundary Conditions (PBC) given available computing resources.

Initial structures were assayed for stability as control.

2.4.2 Modeling mutant proteins

Mutant and chemical derivatives were modeled using the closest related initial structure, modified using BIOPOLYMER. Side chain replacement was performed automatically and then bond torsions were manually adjusted to minimise steric clashes and initialise the calculation with the highest local stability. The modified side chain was then allowed to minimise (Steepest descent, 1000 iterations, harmonic bond, no cross terms), then the neighbouring side-chains and finally the protein was fixed and the solvent shell was relaxed prior to the actual modeling calculation. Addition or omission of one or many steps of initial minimisation was decided on a case-by-case basis with respect to the magnitude of the modeled modification versus the geometry of the original structure.

Table 2.41 Crystallographic coordinates used to model the cytochrome c in this study.

PDB Key	Structure description	Reference
1AKK	Ferricytochrome c *E. caballus* NMR min., RMSD = N/A	Banci *et al.*, 1997
1AKK	Ferricytochrome c *E. caballus* NMR min., RMSD = N/A	Banci *et al.*, 1997
1CRG	N52I / C102T Ferricytochrome c *S. cerevisiae* isoforms-1 X-Ray, RMSD = 2.00 Å	Berghuis *et al.*, 1994a
1CRH	N52I Ferrocytochrome c *S. cerevisiae* isoforms-1 X-Ray, RMSD = 1.90 Å	Berghuis *et al.*, 1994a
1CRI	N52I/Y67F/C102T Ferricytochrome c *S. cerevisiae* isoforms-1 X-Ray, RMSD = 2.00 Å	Berghuis *et al.*, 1994a
1CRJ	N52I/Y67F/C102T Ferrocytochrome c *S. cerevisiae* isoforms-1 X-Ray, RMSD = 2.05 Å	Berghuis *et al.*, 1994a
1CTY	Y67F/C102T Ferricytochrome c *S. cerevisiae* isoforms-1 X-Ray, RMSD = 2.20 Å	Berghuis *et al.*, 1994
1CTZ	Y67F/C102T Ferrocytochrome c *S. cerevisiae* isoforms-1 X-Ray, RMSD = 1.90 Å	Berghuis *et al.*, 1994
1GIW	Ferrocytochrome c *E. caballus* NMR (minimised), RMSD = N/A	Banci *et al.*, 1999
1IRV	I75M / C102T Ferricytochrome c *S. cerevisiae* isoforms-1 X-Ray, RMSD = 1.9 Å	Rafferty *et al.*, 1996
1IRW	N52A / C102T Ferrocytochrome c *S. cerevisiae* isoforms-1 X-Ray, RMSD = 2.00 Å	Berghuis *et al.*, 1996a
1OCD	Ferricytochrome c *E. caballus* NMR (minimised), RMSD = N/A	Qi *et al.*, 1996

1YCC	C102T Ferrocytochrome c *S. cerevisiae* isoforms-1 X-Ray, RMSD = 1.23 Å	Louie *et al.*, 1990
1YIC	C102S Ferricytochrome c *E. caballus* NMR (minimised), RMSD = N/A	Qi *et al.*, 1997
1FRC	Ferrocytochrome c *E. caballus* NMR (minimised), RMSD = N/A	Qi *et al.*, 1996
1YCC	C102T Ferricytochrome c *S. cerevisiae* isoforms-1 X-Ray, RMSD = 1.9 Å	Berghuis *et al.*, 1994
1HRC	Cytochrome c Horse heart X-Ray, RMSD = 1.9 Å	Bushnell *et al.*, 1990

A typical calculation involved first a minimisation step of 10000 iterations of steepest descent or Conjugate Gradient. This was followed by over 100000 iterations (100 ps) of Leapfrog molecular dynamics at 300 K, 1 fs per iteration with a trajectory sampling rate of 200 steps.

Unavoidable evaporation of some of the solvent molecules forbids the potential energy of the system from perfectly levelling. However, the course of the molecular simulation was assessed for stable conformation using a matrix of Root Mean Square Deviations (RMSD) for clusters of parent conformations (< 0.33 Å RMSD). These matrices were typically calculated using 3-5 key amino acids to optimise reliability versus computing time. The members of the identified families of conformation were then averaged and the resulting structures used for analysis. This method was preferred over a complete process of averaging-minimising because raw averaged structures give a better feel of the dynamics of motion in the actual model than a minimised model. The exception was in the case where freely rotating groups were critical for the analysis.

2.4.3 Modeling Alkaline Isomers

The replacement of the sixth iron ligand required special considerations. The ligation bond between the δS of Met^{80} had to be broken and the potential of δS restored to the forcefield methionine default values. The bond between the target nitrogen of the amino group destined to ligate the iron was then defined and the potential was approximated to that of the His^{18} ligating nitrogen. This highly distorted structure was minimised for 10 000 iterations of Steepest descent and visually assessed for further structure stabilisation prior to a typical molecular dynamic calculation for 100 to 150 ps and processed the same way as described in section 2.4.2.

2.4.4 Calculating Net Dipolar moment

Net dipolar moment was calculated by analysing the trajectory file of a molecular simulation of a given model cytochrome c. A RMSD matrix was generated to identify domains of local stability. Cartesian coordinates of atoms were averaged over the life span of a chosen cluster of conformation and the relevant water molecules

were extracted into separate files for spreadsheet processing.

The value for the dipole moment of a relaxed water molecule was 1.85 Debyes and the length of the vectorial sum of O-H bonds was calculated from a model water molecule and found to be 1.278 Å. The vectorial sum of each water molecule was then calculated relative to the vectorial sum of a relaxed molecule and then multiplied by the full dipole moment of a water molecule (equation 9).

$$d = \frac{1.85 Debyes}{1.278 A} \sqrt{\sum_{\psi=x,y,z} \left(\left(\overline{\psi}_{H1} - \psi_O \right) + \left(\overline{\psi}_{H2} - \psi_O \right) \right)^2} \qquad (9)$$

Where Ψ_{Hx} refers to the averaged coordinate of one of the two hydrogen atom and $\Psi_{O'}$, the averaged position of the oxygen atom that is considered as reference point.

Chapter 3: Results

3.1 Stability and validity of the model of wild type ferrocytochrome c

A control dataset was collected on the model of ferrocytochrome *c* to assess the stability and validity of the model protein versus the original crystallographic coordinates.

3.1.1 Stable conformation of the model protein

Two matrices of RMSD were determined to identify groups of stable conformations (**Figure 3.11**). The first matrix involved all heavy atoms (77 atoms) of the following residues: Tyr^{67}, Thr^{78}, Asn^{52}, Ile^{75} and the heme ring. This matrix indicated that the heme crevice stays within 1 Å RMSD for the duration of the simulation (100.5 ps) and that a stable structure (RMSD < 0.66 $Å^2$) was adopted at t=60 ps and maintained for the remaining 40.5 ps. It appears, then, that the 50 ps early in the simulation were necessary to recover the exact native heme crevice conformation following the initiation of the simulation.

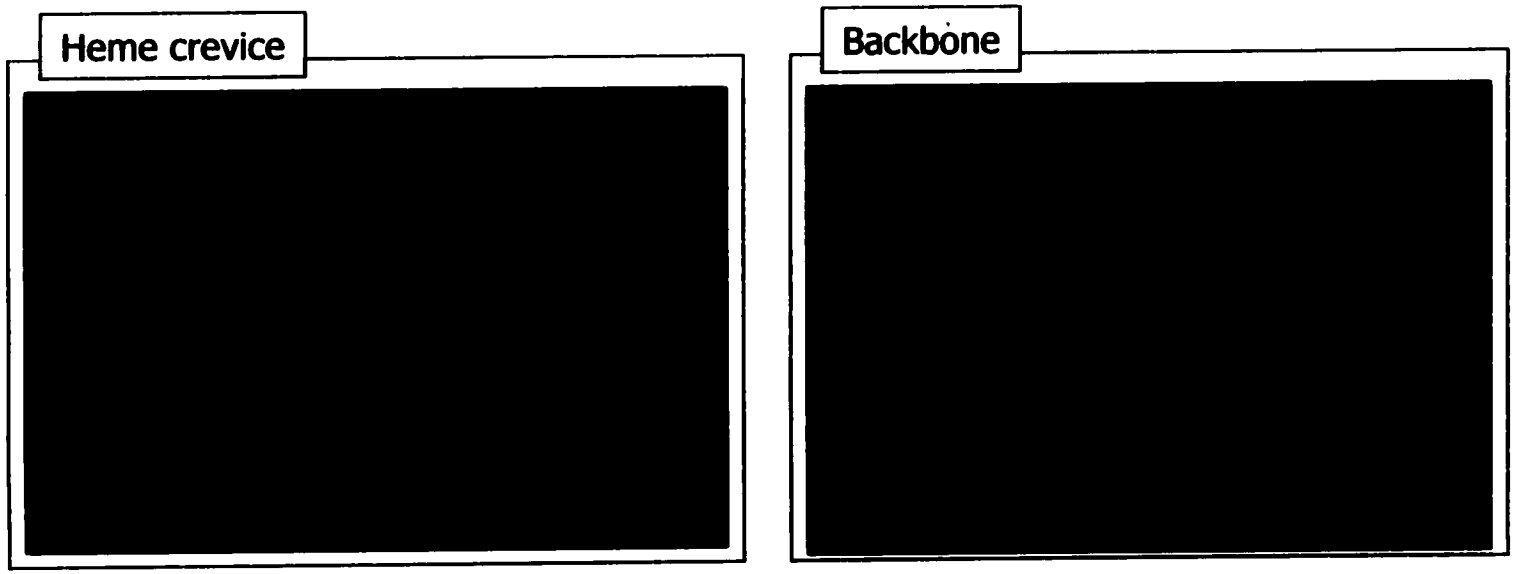

Figure 3.11 Matrices of trajectory RMSD comparisons. The left panel was calculated using the C, N and O atoms of the residues Asn^{52}, Tyr^{67}, Ile^{75}, Thr^{78} and the heme ring. The right panel was calculated with all Cα atoms of the model protein. One frame corresponds to 0.2 ps. The sampling frequency in either case was 1 ps.

A similar matrix was established for the positions of all Cα atoms of the protein backbone that adopted a stable structure within 20 ps (**Figure 3.11**), with RMSD ranging between 0.33 to 1 Å throughout the entire simulation.

3.1.2 Validity of the model protein

A moving window RMSD scan was then run on the averaged coordinates of the protein for the last 40 ps of the simulation. This averaged structure (1.55 Å RMSD vs. crystal coordinates) was then compared to the original coordinate file using the moving window RMSD data analysis script (**Appendix C**). **Figure 3.12** shows that no region of the protein is distorted above the background noise, except for a slight drift in the vicinity of residue 40. Also, the RMSD scan of the backbone with a window of 12 residues shows that the Ω-loop, including the residues 20 to 30, drifts slightly more than the rest of the protein.

Figure 3.12 also shows that there is no correlation between the crystallographic temperature factors (B-factor), the backbone and the local RMSD.

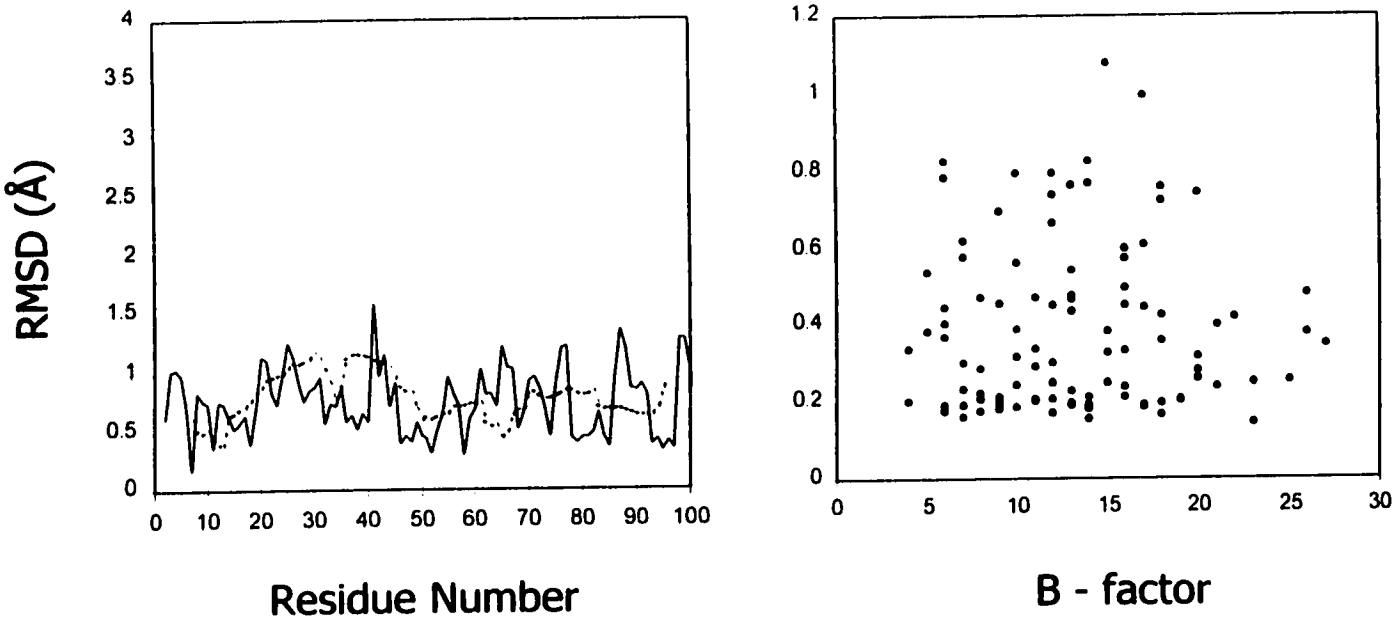

Figure 3.12 Stability of the modeled cytochrome *c* fold during molecular mechanics. Study carried over 40 ps of stable conformation during a 100.5 ps simulation on ferrocytochrome c (1YCC). Left panel: RMSD moving window of 12 backbone amino acids (dotted) is compared to a window of 2 amino acids (solid line). Right hand panel shows that local RMSD of the model (scan window of 2 residues) does not correlate with the B-factor of the back bone of the crystal structure.

3.2 Selective alkylation of methionines in cytochrome c

3.2.1 Alkylation of Methionines

The alkylation of a surface methionine is efficient and highly specific at most of the positions chosen for methionine insertion. Under reducing conditions, unreacted protein was left, in most cases, only in trace amounts after 2 - 8 h of reaction (**Figure 3.21**), and polyalkylation was not observed unless exposure was prolonged. The variant L68M failed to be specifically alkylated. Leu^{68} is a completely buried residue situated in the left loop of the cytochrome c. When Leu^{68} was mutated to methionine, the apparent pK of the alkaline isomerization is shifted to a lower value (**Table 3.21**) indicating a significant distortion of the chemical nature of the heme environment. Upon prolonged treatment with this substrate the reaction generates polyalkylated derivatives, most probably including the double derivative Met68 / Met80.

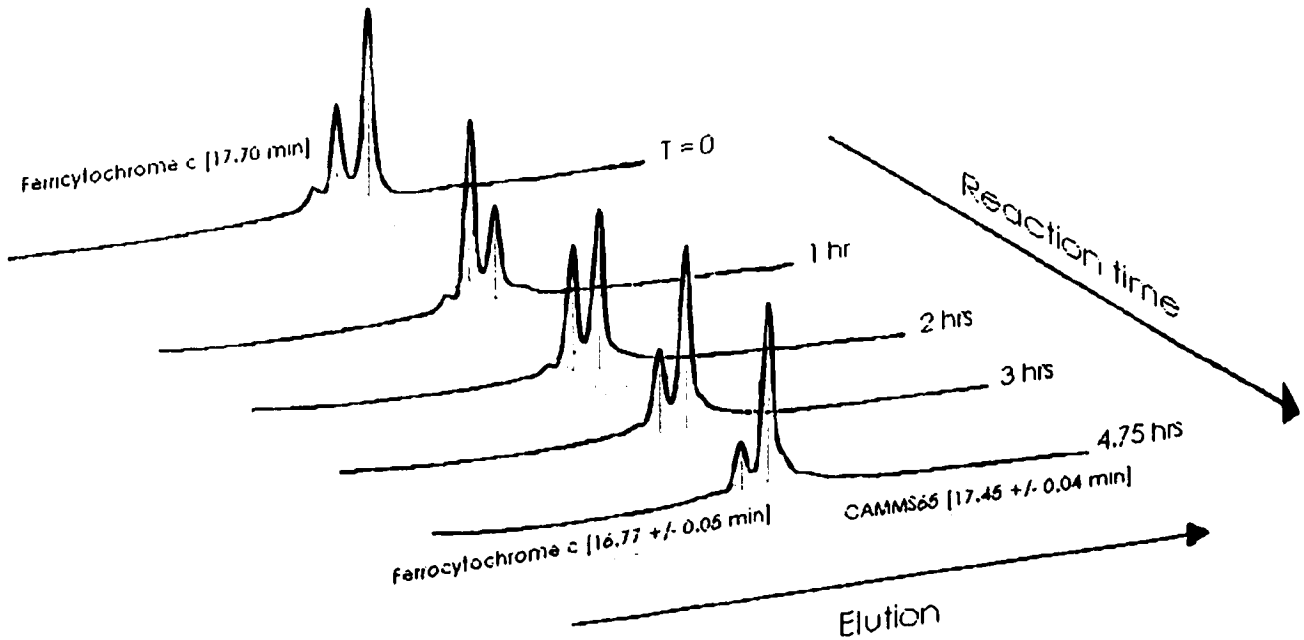

Figure 3.21 Time resolved alkylation of mutant S65M. As determined by analytical cation exchange high performance liquid chromatography. The peaks were assigned according to their relative retention times (as labeled on the graph). Time zero was run prior to reduction with ascorbate to show S65M ferricytochrome c retention time versus the alkylated species.

Table 3.21 Biological and biophysical properties of the methionine mutants and their CAMMS derivatives

	Succinate oxidase (% Native)		Cytochrome c oxidase (% Native)		$E^{\circ\prime}_m$ (mV)		pK'[b] (695 nm)	
		CAMMS		CAMMS		CAMMS		CAMMS
C102T[a]	100	105	100	103	276	277	8.4	8.6
S65M	100	**33**	72	76	270	276	8.5	8.3
P25M	100	95	103	105	288	287	8.5	8.5
V28M	63	65	85	**10**	**268**	**284**	8.1	8.1
K55M	55	58	46	**95**	**284**	**267**	**7.8**	**7.3**
L68M[c]	73	N/A	52	N/A	268	N/A	**7.6**	N/A
I75M	48	56	92	**65**	**247**	**278**	8.1	8.1

[a] Mutant protein C102T is considered as the wild type in this study.

[b] Apparent pK of the alkaline transition evaluated by non-linear regression.

[c] Mutant L68M failed to selectively alkylate at position 68.

3.2.2 Activity of CAMMS derivatives with physiological partners

The activity of mutant cytochromes *c*, and their chemical derivatives, with physiological partners was assayed. **Table 3.21** presents the results of these assays for each type of cytochrome *c*. The alkylation of Met^{64} in the wild type protein does not significantly change the activity with cytochrome c oxidase nor in the succinate oxidase assay. Yet alkylating the next position (CAMMS65) decreases the relative activity of the cytochrome *c* in the succinate oxidase assay by 66%, though only by 25% in the cytochrome *c* oxidase assay.

The effects of methionine alkylation on the activity of these mutants with the purified cytochrome *c* oxidase can also be quite pronounced. Derivative CAMMS28 has an activity decreased by one order of magnitude while the restoration of the positive charge at position 55 regenerates the wild type activity level in the derivative CAMMS55 (**Table 3.21**).

3.2.3 **Alkaline transition of CAMMS derivatives**

The apparent pK of the alkaline transition is affected by the mutation K55M (pK'_{AT}=7.8) and the pH lability of the spectroscopic state III is further increased by the alkylation at this position (**Table 3.21**). Mutant L68M also shows a significant decrease in the midpoint of its state III to IV conformation transition with a pK' = 7.6. Other mutants and derivatives show no substantial $\Delta pK'_{AT}$.

3.2.4 **Modeling of the CAMMS28 derivative**

The modeling of the CAMMS28 derivative yielded two possible conformers, varying by a bond rotation in the CAMMS side chain. The CAMMS side chain either extends across the heme edge and interacts with the backbone carbonyl group of Lys^{79} (**Figure 3.24**), or has its amide moiety within hydrogen bonding distance of the neighbouring Gln^{16}. In both conformations, the positive charge of the sulfonium ion contacts the heme edge and none of these surface structural alterations are seen to affect the wild type fold of the cytochrome *c*.

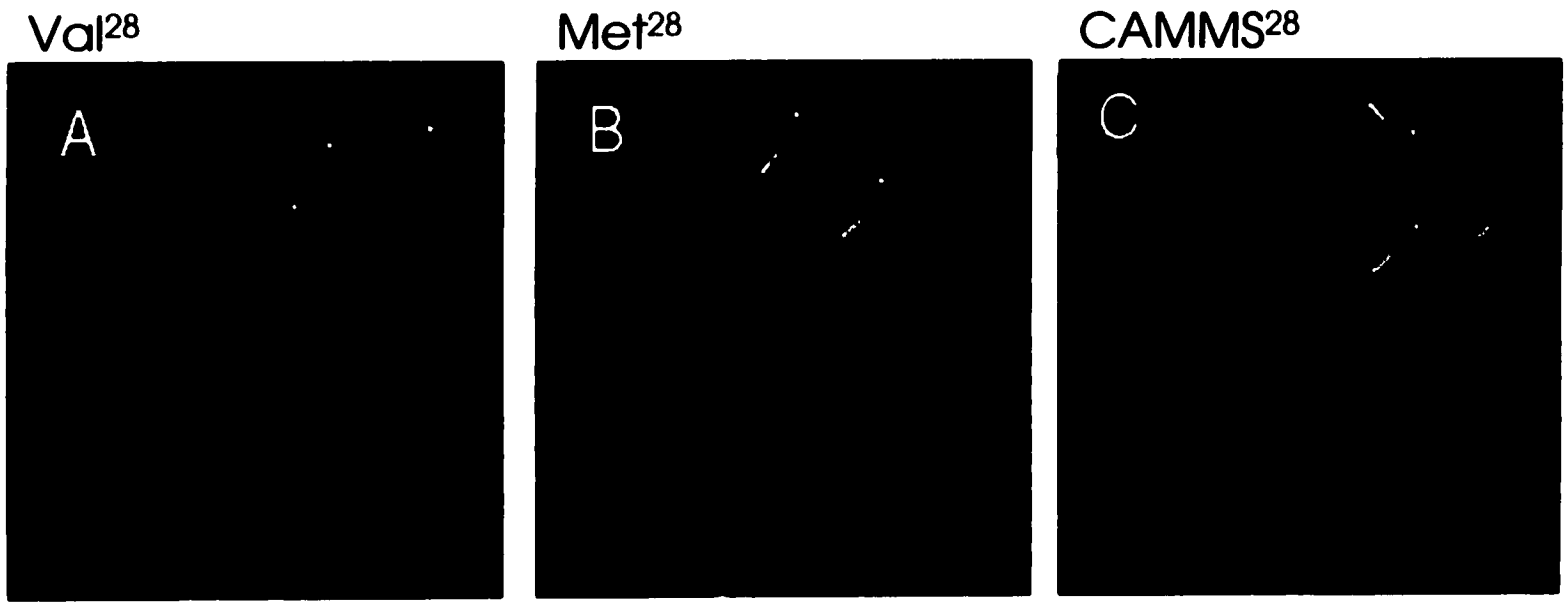

Figure 3.24 Effect of mutation V28M and chemical modification CAMMS28 at the surface of the ferrocytochrome c. Model V28M and CAMMS28 were generated using the average coordinates of a stable cluster of conformation, and then minimized. The backbone carbonyl group of Lys^{79} is shown in the CAMMS28 panel to indicate the site where the amide group of CAMMS28 is binding.

3.2.5 **Modeling of CAMMS55 derivative**

The modeling of the mutation K55M and its CAMMS derivative did not show any modification of the fold of the protein. As shown in **Figure 3.25**, the mutation of the lysine residue to methionine negated the ability of this side-chain to bind to the backbone carbonyl of Tyr^{74}. This potential is, however, regained with the acetamidation of the δ-sulfur: the amide hydrogens are able to bind to this carbonyl oxygen in the model of the CAMMS derivative (**Figure 3.25**). The longer side chain changes the geometry of the interaction and the average hydrogen bond length is increased by about 1 Å. In the absence of other changes, the structural basis for all alterations of the physical characteristics of these cytochrome c variants will lie in the energetics of the hydrogen bonding potential and/or the electrostatic charge on the side chain and this role is governing the stability of the local protein fold.

3.2.6 **Modeling of CAMMS75 derivative**

The model of CAMMS75 was derived from the crystal structure of the mutant cytochrome *c* I75M (PDB accession key:

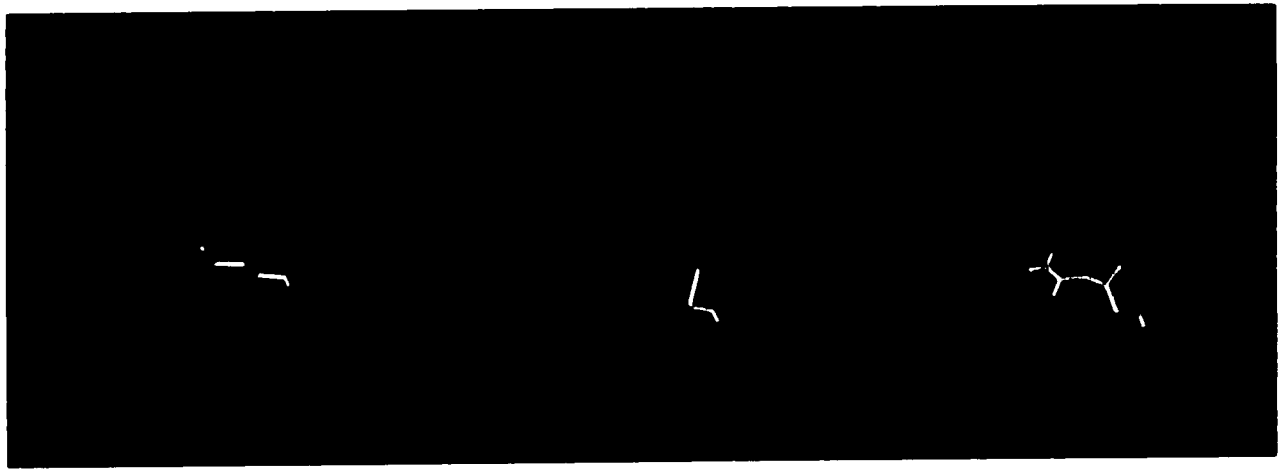

Figure 3.25 Modeled interaction between the side chain of position 55 and the backbone carbonyl of Tyr^{74}. Only the backbone for the segments 53-59 and 68-77 is displayed (Blue). The side chain of Tyr^{74} is also displayed for reference. Side chain of position 55 is displayed in white and the interacting carbonyl oxygen atom is in red. The hydrogen bond in the wild type and the CAMMS derivative models have a respective length of 1.8 Å and 2.8 Å.

1IRV (Rafferty *et al.*, 1996)). The assumption was made, supported by a near native pK' of the alkaline transition of this variant, that the amide group would occupy the heme crevice cavity filled in part by a structural water molecule. In the model, the polar SP2 nitrogen component of the CAMMS amide is stabilized within the protein interior in a similar fashion to that of the amide of Asn^{52} in the wild type structure, pushing this latter residue slightly away from the heme. As shown in **figure 3.26**, the modeled amide group of the CAMMS side chains is interacting with the carboxyl group of heme propionate 7 and with Thr^{78} via its amide hydrogen atom and its carbonyl group respectively. Finally, the dipole of the amide group of Asn^{52} aligns itself with the electrostatic field of the sulfonium charge, with its carbonyl group pointed at the positive charge that stays buried in the modeled cytochrome *c*. The model also suggests that a polar cavity in this area would be sufficiently large to accommodate a structural water molecule, although this water molecule occupies a binding site unrelated to these of Wat^{166} in the wild type protein (**Figure 3.25**).

Figure 3.26 The heme crevice in model of chemical derivative CAMMS75 of *S. cerevisiae* cytochrome c isoform 1. Structure averaged over 50 ps. The water molecule displayed (white) is a solvent molecule that introduced itself during the simulation and plays a structural role. Residue displayed for reference are (clockwise): Tyr^{67}, Val^{57}, Lys^{55}, Asn^{52} and Thr^{78}.

3.3 Modeling of the alkaline conformers

The study of the mechanism of the alkaline transition is complicated by the lack of structural information on the alkaline isomers. This section presents models of these isomers.

3.3.1 Modeling of conformer IV_{79}

The existence of state IV_{79} was long hypothesised before its existence was finally confirmed. The relatively small movement that the backbone must undergo to replace Met^{80} by Lys^{79} makes IV_{79} a plausible isomer. A conformational search using molecular mechanics shows that Lys^{79} can replace Met^{80} at the sixth coordination position with a displacement of $C\alpha^{79}$ of only 2.20 Å and a minimal amount of rearrangement (**Figure 3.31**).

The alteration of the local conformation upon ligand exchange is minor within the heme crevice. As indicated in the **Figure 3.31a**, the local RMSDs of the backbone and the backbone/side chains are altered in the second half of the 70s loop, past the double proline turn that rigidifies this area. Most of the backbone rearrangement appears in the extended

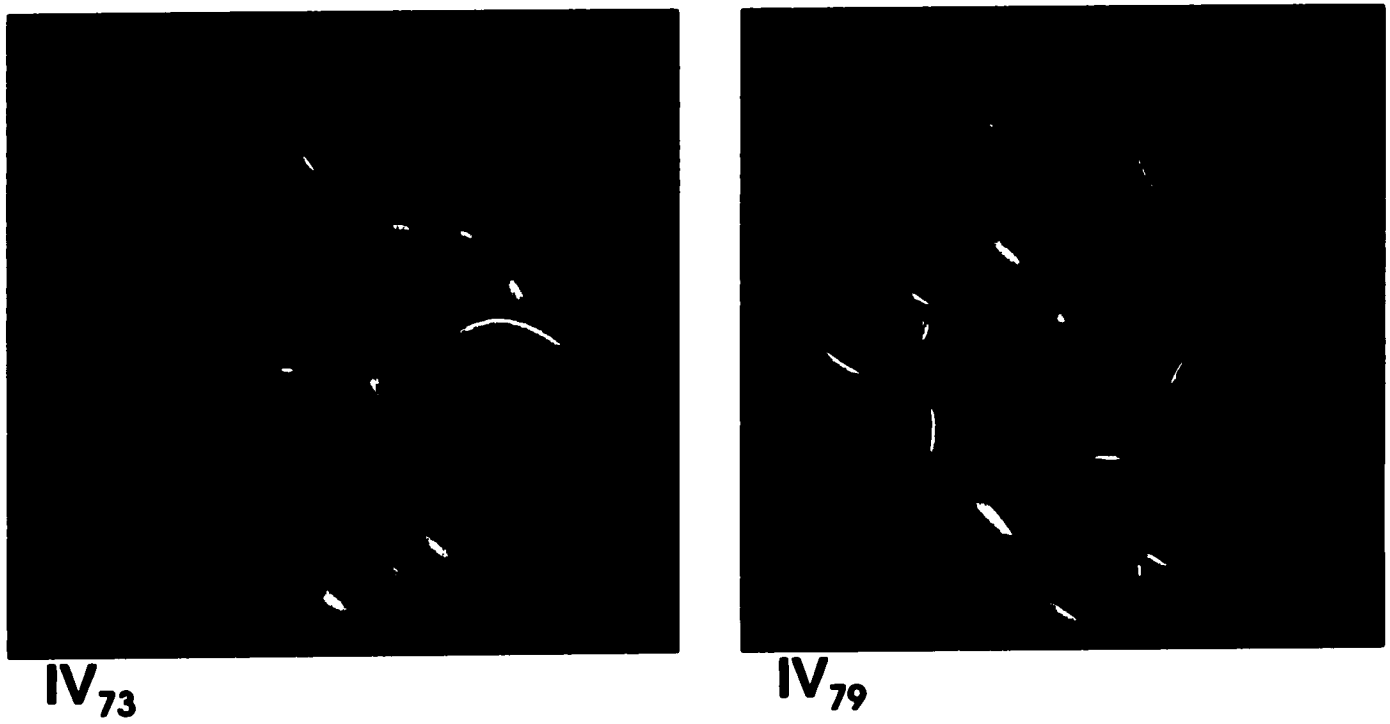

Figure 3.31 Backbone rearrangement upon ligand replacement of the alkaline transition. The backbone fold of residues 49 to 90 in state III mitochondrial cytochrome *c* is superimposed on models of state IV alkaline isomers (Gold). State III proteins (purple) correspond to the crystal structure of ferrocytochrome *c* (1YCC). State IV backbone folds were generated by molecular mechanics. Ligating lysines are colored in orange and their state III counterparts are in light purple. Met^{80} is shown in all models for reference.

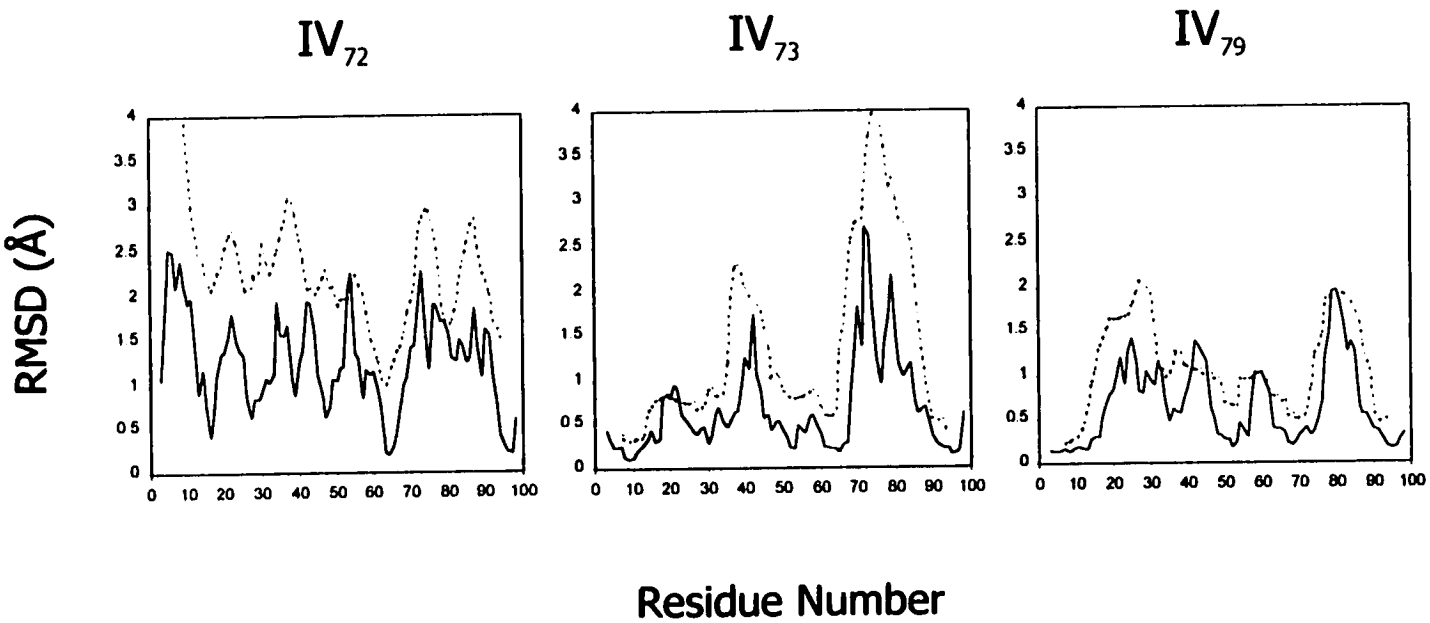

Figure 3.31a RMSD of trajectory of models of alkaline isomers. A moving RMSD windows analysis was run on each averaged model structure versus the average ferricytochrome *c* model. The scanning windows consisted in the backbone atoms of 4 residues (solid), and 12 residues (dotted). The average 12-residues RMSD are: IV_{72} = 2.26 Å , IV_{73} = 1.40 Å and IV_{79} = 1.11 Å. The RMSD of the entire models are respectively: 3.49 Å, 1.72 Å and 1.69 Å. Please refer to **Figure 3.12** for control plot.

peptide stretch of the 80s. In this model, the side chain of Met^{80} is extended outward from the protein's centre, which exposes the heme edge and the heme propionate (Hpr^{6}) to the bulk solvent.

3.3.2 **Modeling of conformer IV_{73}**

It was assumed that the formation of the Lys^{73} ligated alkaline isomer (IV_{73}) happens with a minimum of backbone rearrangement (in order to satisfy the spectroscopic evidence postulating a minimum rearrangement). The shortest and simplest way to connect the iron and the amino group of the lysine residue was chosen by biasing the isomerisation to occur through rotation of the proline double turn clockwise so the side chain of Lys^{73} would penetrate the protein and be within reach of the heme-iron ligation sphere.

The backbone rearrangement is, in this case, more extensive than in the previous model (**Figure 3.31**), although its scope is limited from position 70 to the late 80s (**Figure 3.31a**). The 70s loop is fairly rigid because of secondary structural constraint and ligation of the iron, and thus has to rearrange *en bloc* which further influences the conformation of the 80s peptide stretch.

To accommodate the displacement of $C\alpha_{Lys^{73}(III)}$ to its proposed position in IV_{73}, a distance of 7.02 Å, the architecture of the heme-crevice must be rearranged: the side chain of Ser^{40} is now in close interaction with the amide nitrogen-bound hydrogen of Asn^{52}; contact explains the perturbation in the surroundings of Ser^{40} in **figure 3.31**. Asn^{52} caps a cluster of aromatic side chains that form a network of plane-to-edge aromatic interactions involving Tyr^{74}, Trp^{59}, Tyr^{67} and the heme plane itself. Tyr^{67} is further hydrogen bonded to the amine group of Lys^{73} and its ring is in *Van der Waals* contact with Ile^{75} and the γ-methyl of Thr^{78}. This extensive packing of hydrophobic and aromatic groups is completed by a tight stabilisation of the heme propionates by Thr^{49} (HP6), Trp^{59}, Arg^{38} and Ser^{40} (HP7), bridged via the nitrogen amide of Asn^{52} and the two well ordered water molecules. In this case, the side chains of both Lys^{79} and Met^{80} are seen extending along the surface of the protein, partially covering the heme edge.

3.3.3 Modeling of conformer IV_{72}

The modeling of the alkaline species IV_{72} in yeast isoform-1 was undertaken to explore possible conformations of the untrimethylated Lys^{72} in state **IV_{72}** as postulated by Pollock

et al. (1997). This latter isomer may also be relevant to the understanding of the nature and mechanism of the alkaline transition of the horse protein.

The Tml^{72} residue was converted to a deprotonated lysine, and the smallest overall rearrangement was assumed. The subsequent minimisation and molecular mechanics steps however led to global structural rearrangement of the interaction between the protein and its prosthetic group. As we can see in **Figure 3.33**, the heme is rotated by 33° relative to the centre of mass of the protein. A backbone superposition of the whole protein yields a RMSD of 1.85 $Å^2$, which indicates a reasonable overall fold conservation despite the appearance. Closer inspection of **Figure 3.33** shows that to satisfy the bond length and angles of the Lys^{72} side chain atoms, the segment of the double proline turn has forced the 80s segment to move toward the back of the protein. The Gly^{1}-Thr^{96}, Ile^{95}/Asn^{92}-Phe^{-3} and Ser^{-1}-Asp^{93} contacts found in the native species of state III are kept, thus pushing both the N-terminal 10 amino acids and the 90s α-helix back. This pulls on the 2-14 α-helix that loses its helical conformation, altering the position of the two cysteine attachments of the heme. Furthermore, the hydrogen bond between Lys^{79} and Ser^{47} seen in state III is preserved

Figure 3.33 Lys^{72}-iron ligated state IV cytochrome c model. Native State III protein (Purple) undergoes a global shift in conformation as the omega-loop in the 70s has to rearrange to position the ε-amino group of Lys^{72}. The model protein was generated by molecular mechanics and averaged over 20 ps. Lys^{72} is shown in blue, and Lys^{79} in a lighter color to highlight some subtle structural features conserved in the model despite large conformational shifts.

(**Figure 3.33**). This results in a relative rotation of the heme with respect to the protein fold.

3.4 Study of a pH-induced transition using linear regression

3.4.1 Linearisation of a pseudosigmoid titration curve

The alkaline transition was monitored using high cytochrome c concentration to facilitate measurement of the faint signal. The irregularities of the pseudosigmoidal titration curve of the 695 nm band of ferricytochrome c were revealed as a broken line with two or three linear segments, by plotting the spectroscopic signal divided by the concentration of protons against the signal itself (**equation 8** in section 2.3.7). The linearised plots show a sharp change in slope over the course of the titration. From such a biphasic plot, it is possible to reconstitute a series of overlapping sigmoidal components from the discrete pK values and pH windows to which they are limited, as shown in **Figure 3.41**. Parameters calculated from the plot reproduce with accuracy the irregular shape of the titration curve. From such linearity, it is clear that the non-ideal character of the titration curve is not originating from the sum of multiple microscopic titration curves.

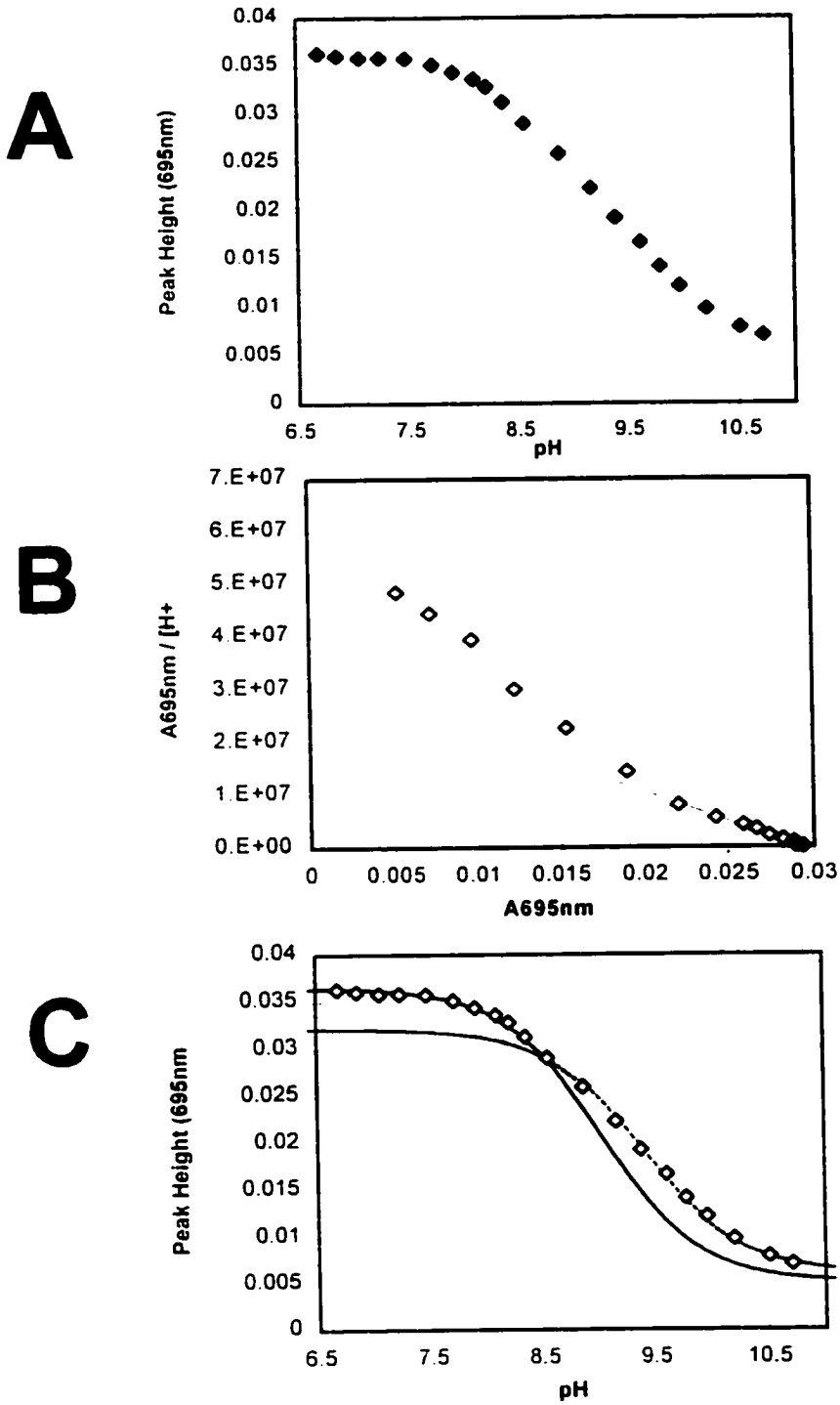

Figure 3.41 Deconvolution of transition IV -> III in horse heart cytochrome *c*. A - 695 nm Peak height titration. B - Linear regression of the transition and least-square best-fitting of its two linear segments. C - Reconstituted titration function superimposed with data as shown in A.

$$\frac{d\left[A/_{[H+]}\right]}{dA} = -\frac{1}{K_a} \qquad (10)$$

Equation 10 shows the derivative of the described linear plot, where **A** represents the absorbance at 695nm and $\mathbf{K_a}$ is the ionisation constant of a single ionizing group.

$$A = \frac{A_{max1}}{1+\left(\frac{K_1}{[H^+]}\right)} + \frac{A_{max2}}{1+\left(\frac{K_2}{[H^+]}\right)} \qquad (11)$$

$$\frac{d\left[A/_{[H+]}\right]}{dA} = -\left(\frac{[H^+]^2+(K_2)^2}{K_1([H^+]+K_2)^2}\right) \qquad (12)$$

In equation 11, $\mathbf{K_1}$ and $\mathbf{K_2}$ represent the ionisation constants of two additive groups. Its derivative (Equation 12), however, will fail to be linear, since it will be dependent on the concentration of protons in solution (**Appendix B**).

3.4.2 Asymetry of the alkaline transition in horse cytochrome c

The alkaline transition of the horse mitochondrial cytochrome c does not follow an identical path in both directions as shown in **figure 3.42**. Direct observation of this hysteresis is almost impossible, but the sensitivity provided by the linearisation of the data makes the phenomenon evident.

The hysteresis was assumed to arise from a structural or mechanistic feature in the transition mechanism. The linear regression treatment was used to determine which pathway the protein would be subjected to when the species III and IV involved would be allowed to equilibrate at mid-transition.

Table 3.42 shows the measured pK values obtained under different titration conditions. Under equilibrated conditions, the alkaline transition of the horse mitochondrial cytochrome c follows two ionisations with pK of 9.08 ± 0.03 and 9.38 ± 0.05 in either direction, which correspond to the IV->III profile. On the other hand, if the titration is performed from spectroscopic state III to state IV and equilibration is not allowed at mid-transition, the two limiting pKs are 8.9 ± 0.1 and 9.25 ± 0.02.

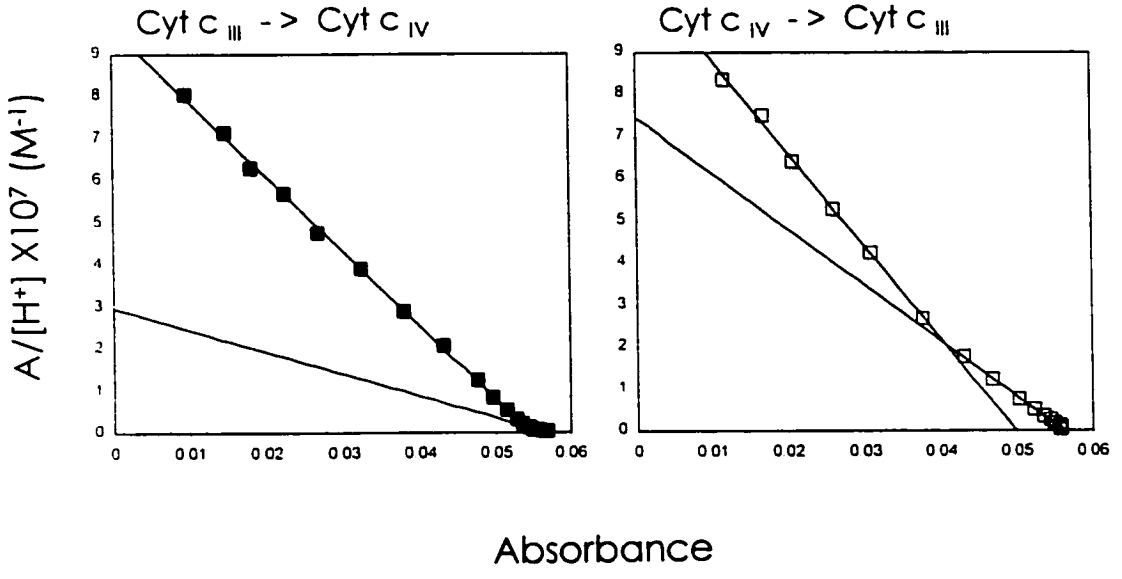

Figure 3.42 Hysteresis in the alkaline transition of horse cytochrome c. Linearised titration plot of the 695 nm band from functional state III to state IV (solid) and from state IV to state III (open).

Table 3.42 Profile of effective pKs of the horse protein alkaline transition following rapid pH change by buffer exchange.

Titration	Initial pH[a]	Delay (min)	Limiting ionisation[b]			
			pK_{F1}	pK_{R1}	pK_{F2}	pK_{R2}
Forward[c]	7.0	10+[d]	8.9(1)		9.25(2)	
	9.20[e]	0			9.24(4)	
	9.20	10				9.33(4)
Reverse	10.5	0		9.08(3)		9.38(5)
	9.20	0	8.95(6)	9.14(5)		
	9.20	10	8.82(6)	9.13(5)		

[a] All sample stocks were at pH 7.0 and then taken to the initial pH by buffer exchange.
[b] The numbers in parentheses indicate the precision of the last significant digit.
[c] Titration to alkaline pH.
[d] No buffer exchange was performed.
[e] Arbitrarily chosen pH, near the midpoint of the transition.

3.4.3 Alkylamine derivative of mitochondrial horse cytochrome c

A total lysine alkylation was performed and the effective pKs of the alkaline transition were evaluated in an attempt to determine whether the visible ionisations were due to ionisation of lysine ε-NH_2 groups. Alkylation of amino groups to secondary amines will alter their pK without changing their ability to donate, accept a hydrogen bond or coordinate the heme iron. In the isopropyl-lysine secondary amine, we observe that the limiting ionisations are shifted by about +0.6 units of pH with pKs of 9.65 ± 0.01, 10.02 ± 0.05 and 10.43 ± 0.07. It is noteworthy that the alkaline transition of this cytochrome c derivative has three limiting effective pKs and shows no hysteresis.

3.4.4 Alkaline transition of yeast cytochrome c

The 695 nm band titration of the *S. cerevisiae* cytochrome c does not show any hysteresis. As shown in **figure 3.44**, its transition is determined by two effective pKs of 8.59 ± 0.01 and 8.9 ± 0.1. A large number of *S. cerevisiae* mutant proteins are available and were screened for significant irregularity in the effective pK profile of their alkaline

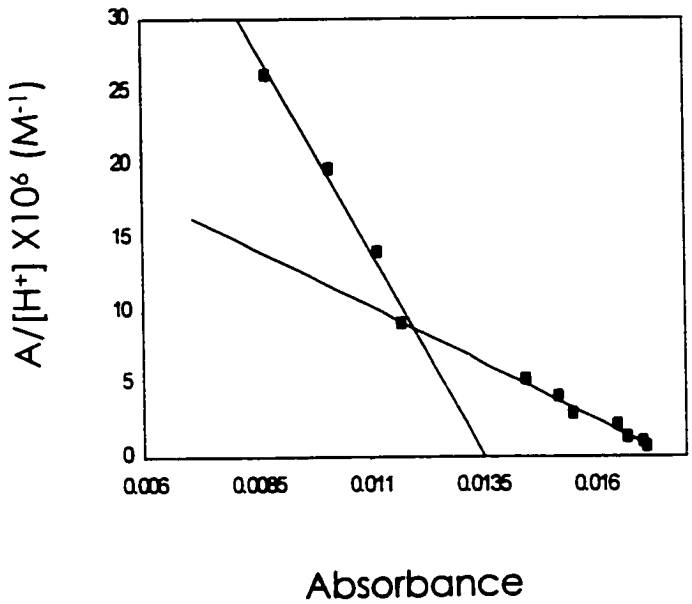

Figure 3.44 Alkaline transition of *S. cerevisiae* cytochrome c (iso-1 C102T). Resolved using a linear regression.

transition. In all cases except one (Tml72K), which will be presented later, no hysteresis was observed. The effective pK measured in 14 of these mutants group into three ionisations with pKs values of 8.01 ± 0.06, 8.53 ± 0.06 and 8.85 ± 0.09. These suggest that there are three limiting pH-dependent contributions to the relative distribution of state III and state IV in the yeast cytochrome.

3.4.5 Position 72 and hysteresis in yeast cytochrome c

E. coli-expressed yeast isoform-1 cytochrome c is identical in every way to the endogenously expressed mitochondrial cytochrome c, except for the absence of a post-translational trimethylation at position 72. However, the nature of the alkaline transition in this protein differs significantly.

First, as with the horse protein, the alkaline transition of Tml72K shows hysteresis. The two effective pKs of 8.59 ± 0.01 and 8.9 ± 0.1 in the endogenously expressed (Tml^{72}) are replaced by a different set with pK 7.84 ± 0.1 and 8.49 ± 0.06 in the state III to IV direction and 8.00 ± 0.1, 8.35 ± 0.07 and 8.56 ± 0.05 in the opposite one (**Figure 3.45**). The ionisations, although similar in pattern to these of the horse alkaline transition, are shifted by ~0.85 unit of pH.

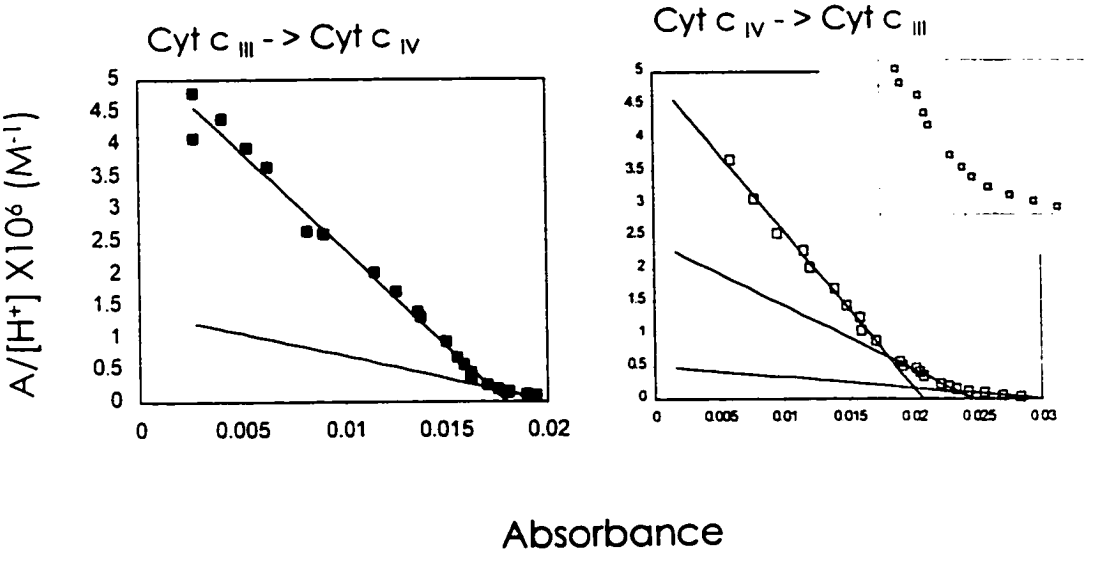

Figure 3.45 Hysteresis of the alkaline transition of *S. cerevisiae* Tml72K cytochrome c (iso-1 C102T). As resolved using a linear regression relationship. Upper part of the transition from state IV to III is magnified.

3.4.6 Resolving two independent equilibria in Tm172R

Substitution of the trimethyl-lysine at position 72 by an arginine yielded some surprising results. **Figure 3.46** shows that the bleaching of the 695 nm charge transfer band is concomitant with the appearance of a shoulder with its center at 602 nm.

These two spectroscopic characteristics are however not the consequence of a single chemical process. Linearization of these two spectroscopic events yields two different sets of effective pKs and the thermodynamics of each also differ (**Figure 3.46a**), suggesting the presence of two distinct chemical equilibria.

The appearance of a shoulder, albeit less pronounced, around 600 nm was also observed in the mutant K79R. Effective pKs for these two mutants are tabulated and presented in **Table 3.46**. Mutant K79R was targeted because of the implication of Lys^{79} in the alkaline transition of this cytochrome c. Both spectroscopic events occur with an identical effective pK of 8.2. However, the temperature dependence of its equilibrium suggests that the two spectroscopic features are diagnostic of two distinct processes.

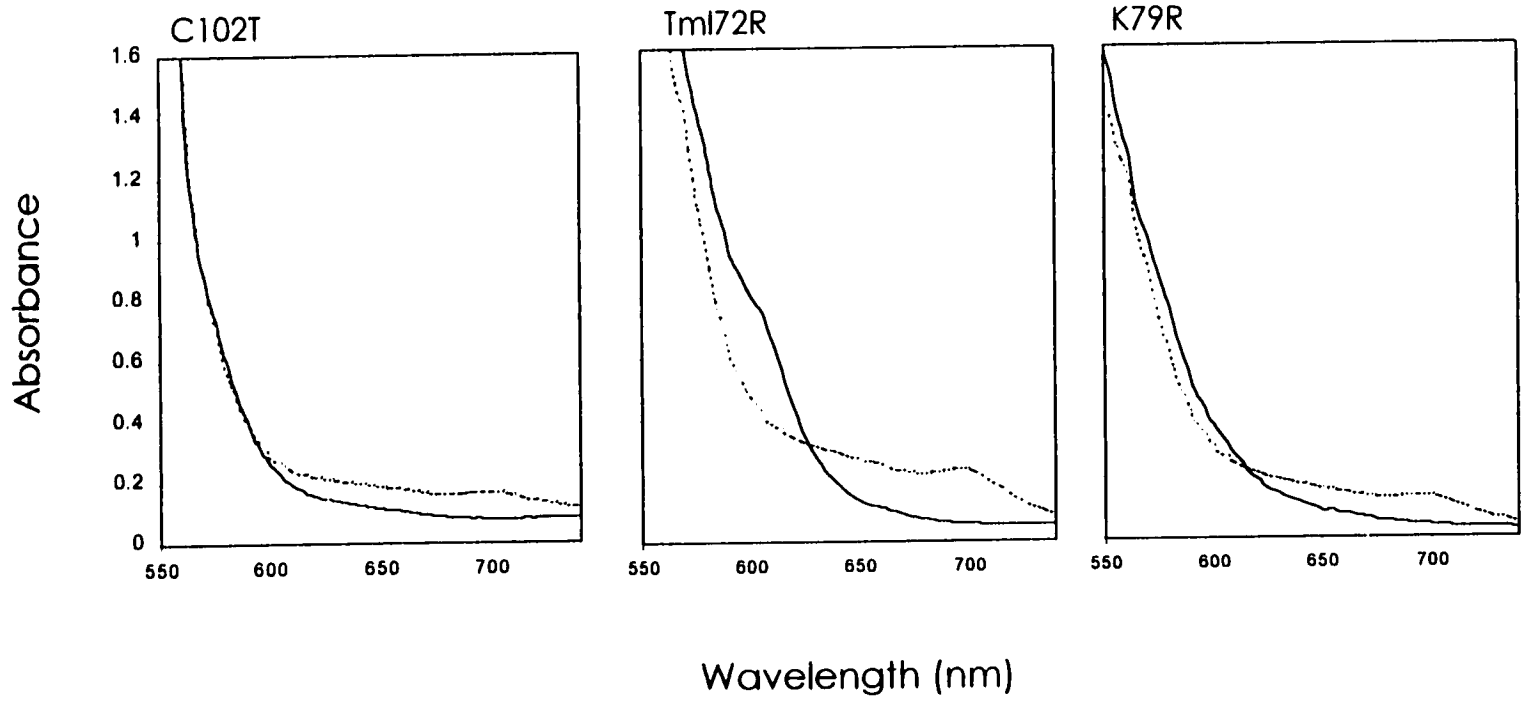

Figure 3.46 Spectra of cytochromes c in the spectroscopic states III and IV. The spectrum of the various states were measured at pH 6.96 for state III (Dotted lines) of samples and state IV (solid lines) were measured at pH 10.11 (C102T), 10.23 (Tml72R) and 9.78 (K79R).

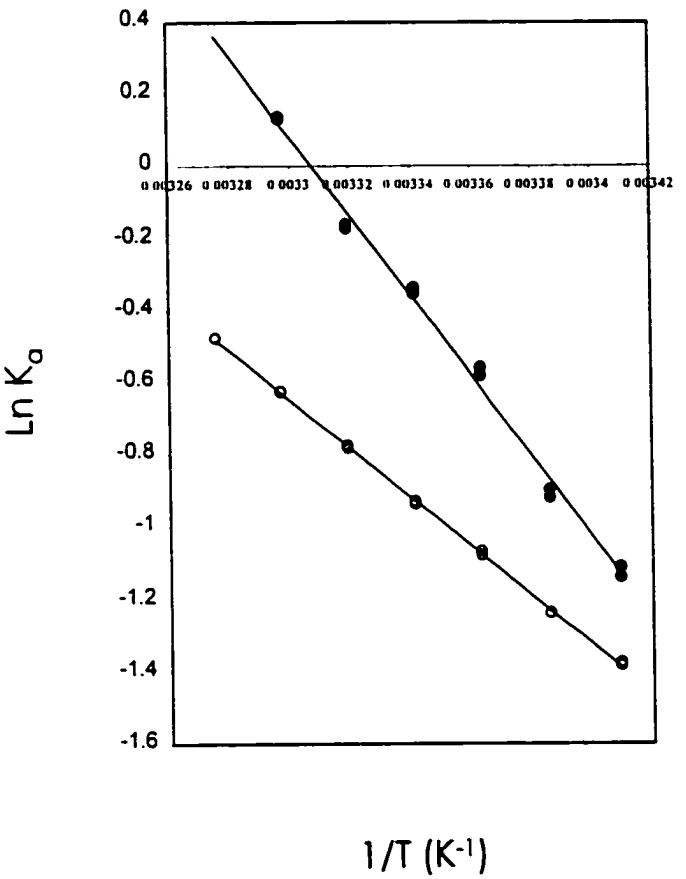

Figure 3.46a Van't Hoff plot of the spectroscopic changes observed at 695 nm (solid) and 602 nm (open) at pH 8.35 in mutant Tml72R. Both experiments were run concurently in each replicate by monitoring both wavelengths in parallel.

Table 3.46 Thermodynamic parameters calculated from Van't Hoff plots for some alkaline transition-associated equilibria.

Sample	Equilibrium[a]	Limiting pKa	Enthalpy ($kJ*mol^{-1}$)
Wild type Yeast iso-1	695 nm[c]	8.59 ± 0.01 8.9 ± 0.1	59.6 ± 0.8
Wild type Horse[b]	695 nm		54
Iso-1-K72	695 nm	Forward[e] 7.8 ± 0.1 [redacted] Reverse 8.0 ± 0.1 8.35 ± 0.07 8.56 ± 0.05	42 ± 1
Iso-1-Tm172R	695 nm	[redacted]	76 ± 4
	602 nm[d]	8.59 ± 0.07 9.25 ± 0.08	56 ± 3
Iso-1-K79R	695 nm	8.20 ± 0.02	80.3 ± 0.8
	595 nm[d]	8.20 ± 0.02	93 ± 2

[a] Temperature dependence of the conformational equilibrium detectable by the spectroscopic band of noted wavelength relative to its maximum height.
[b] As presented in Davis et al., 1974.
[c] A Sulphur-Iron charge transfer band. Characteristic of state III ferricytochrome c.
[d] Characteristic of a weak field iron-ligand replacing Met 80 as iron sixth ligand.
[e] Forward pKs refers to the limiting pKs observed in the III->IV titration while reverse refers to IV->III.

3.5 Structural aspects of an engineered protein matrix

3.5.1 Structural alterations in the Asn^{52} mutant series

Previously in this dissertation, $\Delta E_m^{\circ\prime}{}_{mut.}$ was postulated to be a measure of the perturbation of the effective dielectric of the protein matrix by a local structural modification. In order to assess the relevance of this measurement, the global structure of the fold must be ascertained to ensure that the alteration of $E_m^{\circ\prime}$ is limited to the local effect of the modification and not due to a larger alteration of the polypeptide fold.

The method chosen was circular dichroism spectroscopy (CD). The following **Figures 3.51-3.51b** compare the CD spectra of various oxidized mutants with the wild type protein, ferricytochrome *c* C102T.

The minute changes to the 180-260 nm spectra could not be interpreted in terms of secondary structure alteration using a neural network based evaluation (CDNN 2.1 Win98, Bohm *et al.*, 1992). Instead, the spectroscopic features in the characteristic region of 206 to 226 nm were compared to the wild type protein.

Position 52 is located in a small stretch of α-helix assumed to give a sensitive signal that can be monitored by CD

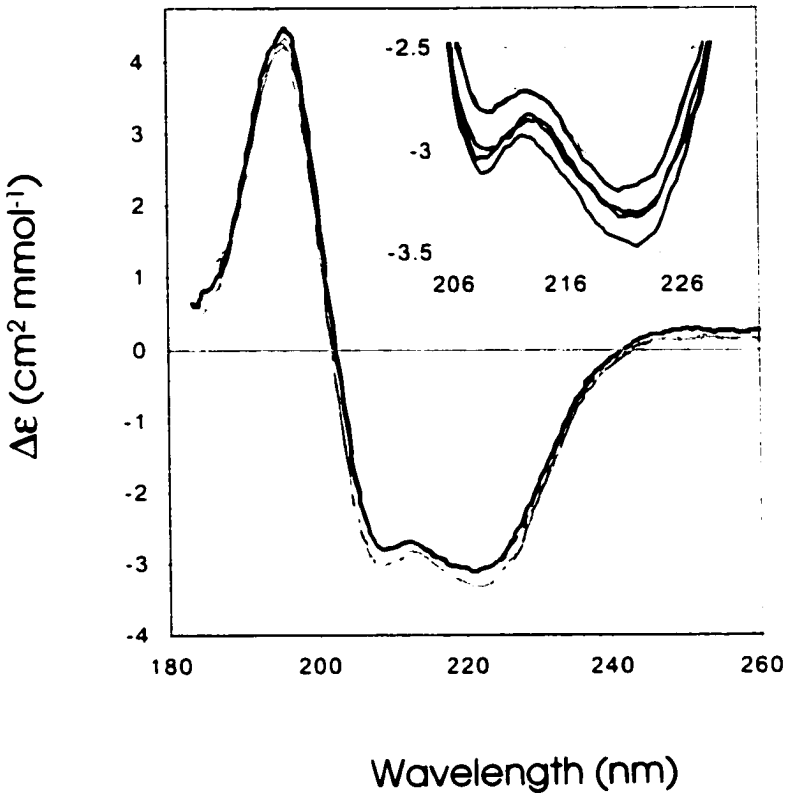

Figure 3.51 Circular dichroism spectra of replacement by site directed mutagenesis of Asn^{52} by large side chains. The superimposed spectra are of: T102 (black), N52Q (blue), N52I (green), N52H (red) and N52M (pink).

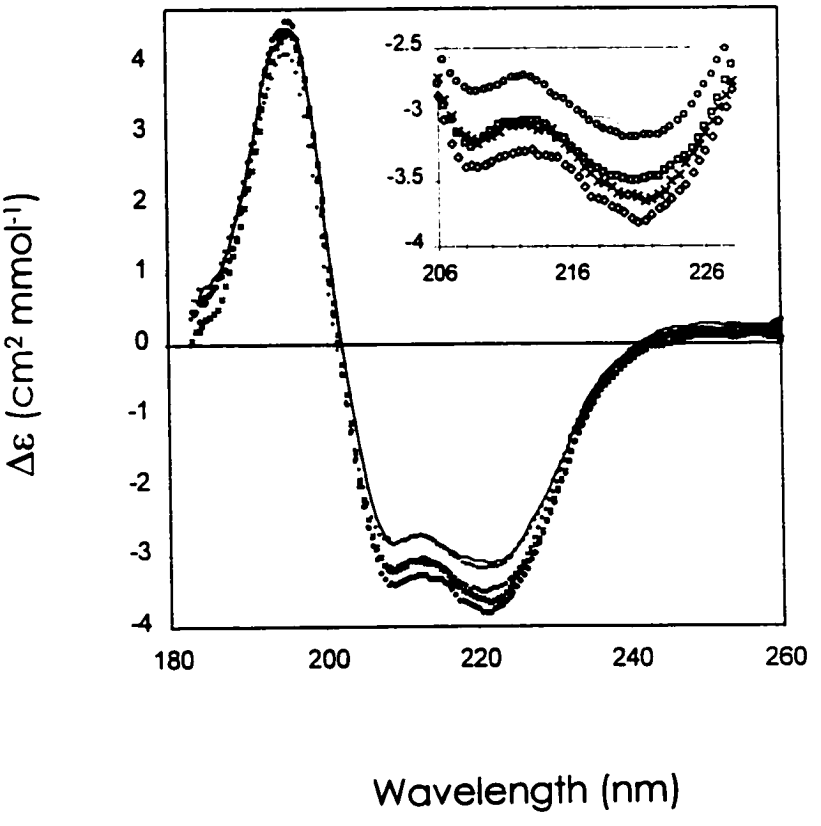

Figure 3.51a Circular dichroism spectra of replacement by site directed mutagenesis of Asn^{52} by small side chains. The overlayed spectra of N52A (diamonds), N52S (circles), N52T (squares) and N52V (X) is compared to the wild type protein (black line).

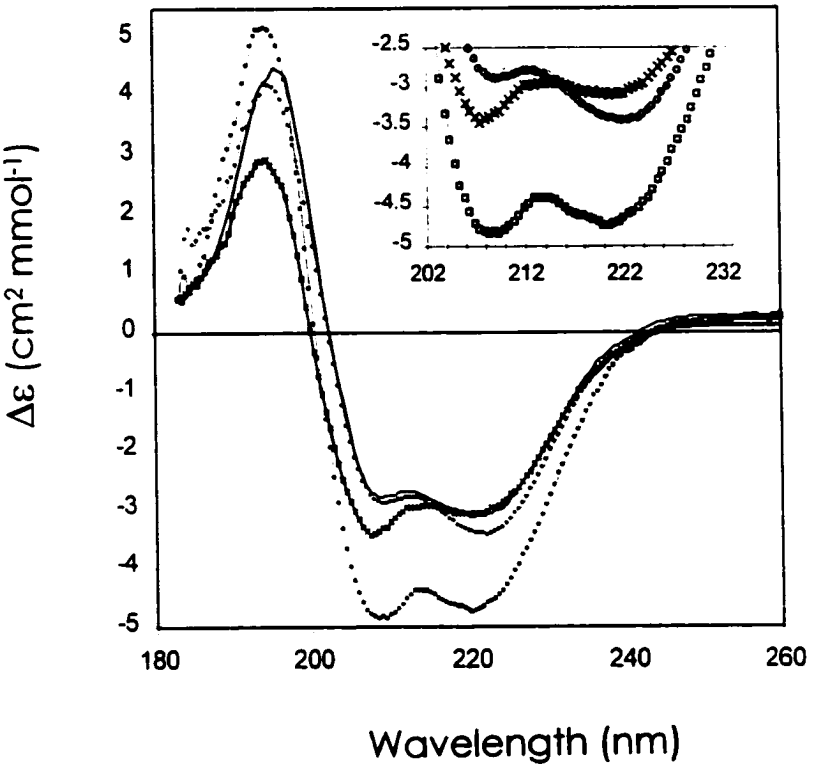

Figure 3.51b Circular dichroism spectra of mutants N52C (X), N52D (squares) and Y67F (circles). The spectrum of the wild type (T102) is shown as a plain dark line.

spectroscopy. Consistent and small changes in $\Delta\varepsilon$ (molar ellipticity) throughout the 206-226 region were not considered significant. For this reason, the mutants N52Q, N52H and N52M (**Figure 3.51**), N52V, N52S and N52T (**Figure 3.51a**) are spectroscopically similar to the structures of C102T (Wild type), N52A and N52I.

Three mutant proteins gave significantly different spectra; Y67F, N52C and N52D (**Figure 3.51b**). In N52D and N52C, the ε at 208 nm has increased compared to the wild type protein, and the major peak has undergone a blue-shift to 195 nm.

3.5.2 Modeling of Asn^{52} mutant series

A conformational search using molecular mechanics was performed for each of the mutants of the Asn^{52} mutant series. **Table 3.52** shows the assumptions made prior to setting up the initial structures for each of the modeled mutants.

Conformational searching was performed to explore the potential rearrangement within the hydrogen bond network as described in **section 1.5.4.** Four of these mutants are shown in

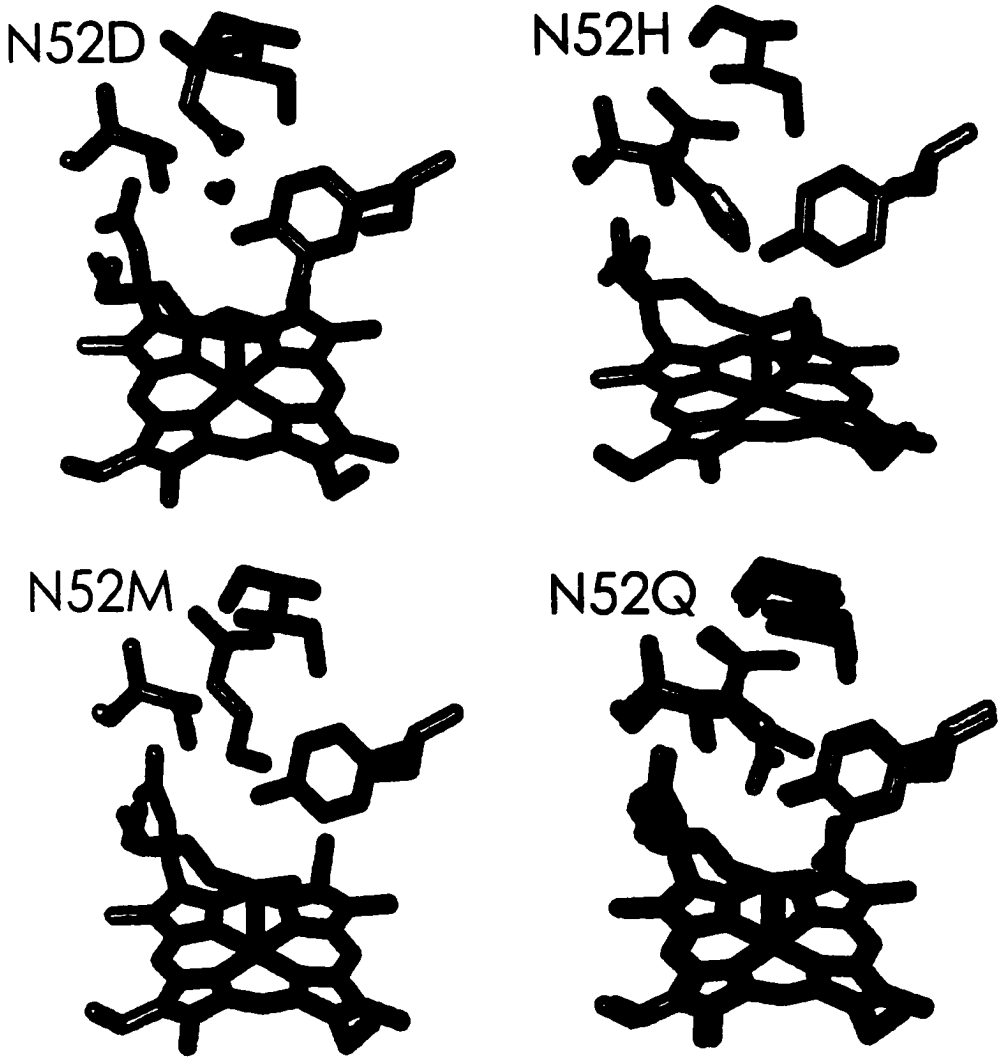

Figure 3.52 - Models of mutants of the Asn^{52} series. The modeling was carried out using molecular mechanics. Average positions of atoms of residues Thr^{78}, Tyr^{67}, Ile^{75}, Met^{80} and position 52 are displayed. Lighter colour in the N52H model indicates the nitrogen atoms. Modeling of N52Q yielded two families of conformations: the oxygen of the Gln side-chain is shown in a lighter shade of grey.

Figure 3.52. These mutations alter the nature of the cavity occupied by Wat^{166} in the wild type structure.

3.5.3 Sampling molecular dynamics for net dipolar moment

The motion of dipoles, such as water molecules, was evaluated by molecular mechanics. **Figure 3.53** shows the distribution of net dipolar moment of 2001 water molecules during the modeling of alkaline isomer IV_{73}. This simulation was chosen because some water molecules were buried during the course of the simulation, offering a suitable range of structural water molecules to analyse.

As shown in **Figure 3.53,** the water molecules distribute themselves in three general ranges of net dipolar moment, according to the position of each water molecule in the model and the length of the sampling prior to coordinate averaging.

Dipolar moment range (Debye)	
0 to 0.25	Random molecules
0.25 to 1.25	Polarized molecules
1.25 to 1.75	Fixed molecules

Table 3.52 Setup of initial structure for molecular mechanics of the Asn^{52} mutant series.

Mutation	Initial coordinates[a]	# of buried water molecules[b]	ΔG_U (Gu:HCl)[c] (kcal/Mol)
N52	**1YCC**	1	5.86
N52I	**1CRG**	0	9.96
N52A	**1IRW**	2	8.83
N52V	1IRW	2	7.88
N52S	1IRW	2	5.49
N52T	1IRW	2	7.76
N52H	1YCC	0	4.16
N52M	1CRG	0	9.90
N52Q	1YCC	0	5.02
N52D	1YCC	1	-

[a] PDB coordinates used to build the model, bold accession keys indicate actual XRD structure.
[b] Number of water molecules present in the initial coordinates.
[c] Taken from Linsk-O'Connell *et al.*, 1995.

The "random" molecules suffer little or no influence on their orientation from external constrains. They are likely to accumulate in a higher number in a dynamic simulation because of the absence of ions in solution and the existence of cutoff distances for electrostatic interactions that isolate a distal water molecule from the system. The time dependence of the distribution of net dipolar moment for the polarized molecules reflects the molecular motion of the water molecules in the two first layers of the solvation shell of the protein. The changing nature of the immediate surrounding of the solvent molecules due to a lack of geometric constraints annihilates part of their dipolar moment, which eventually drifts to values close to 0.5 at 18.5 ps. However, there is a small fraction of these water molecules that dwell in the upper range of net dipolar moment values, regardless of the sampling time. These water molecules were discretely monitored in **Figure 3.53a** from which it is evident that their net dipolar moment is stable over time. These molecules are playing key structural roles and their net dipolar moments seem to overcome the variability due to molecular tumbling after 10 ps of averaged sampling.

Not all structural water molecules, however, have a net dipolar moment stabilizing near 1.35 Debye. **Figure 3.53b**

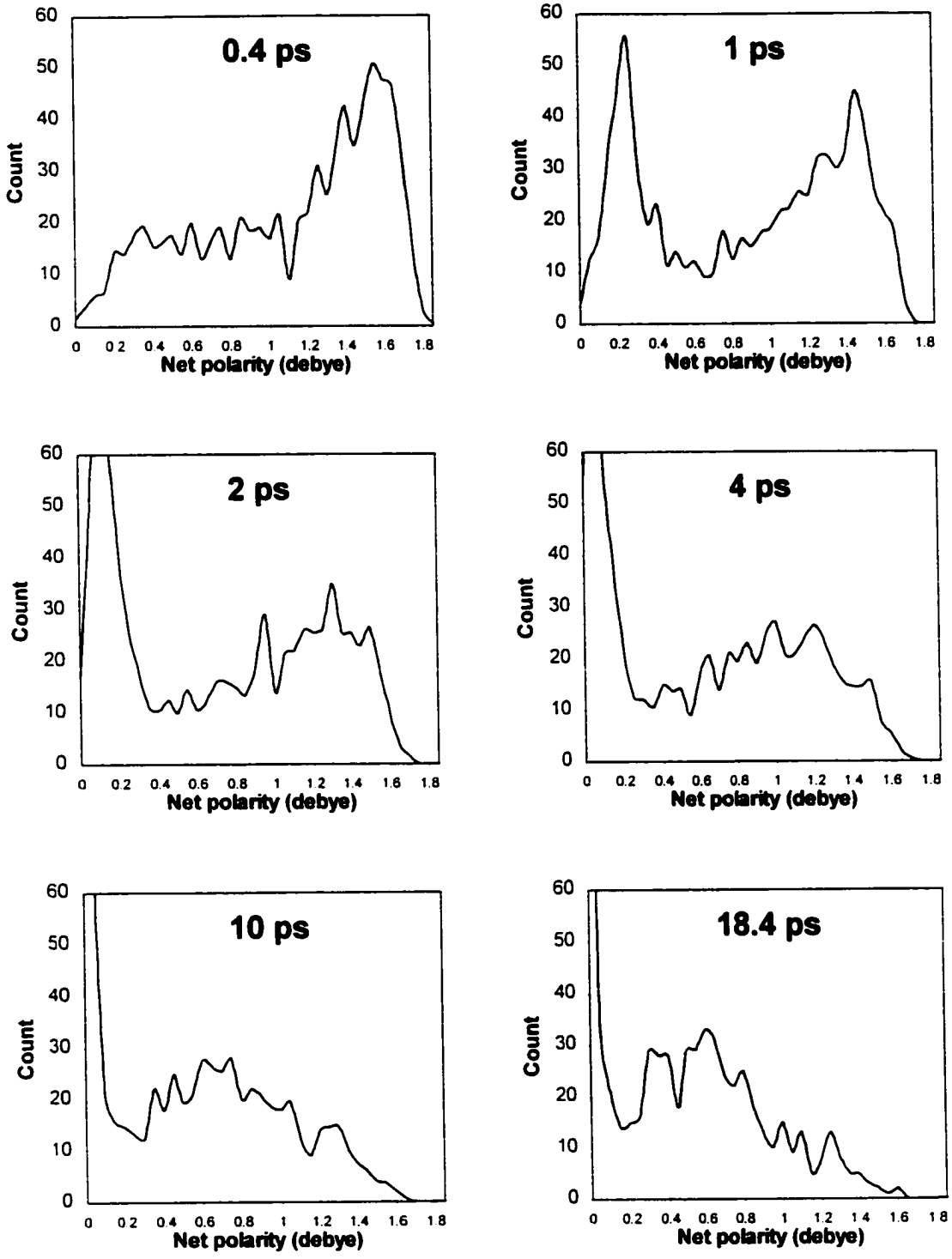

Figure 3.53 Distribution of net dipolar moment of water molecules in molecular dynamics simulation of ferricytochrome c state IV_{73}. The 2001 discretely defined water molecules of the simulation were processed and pooled in 0.05 Debye groups with respect to the sampling length.

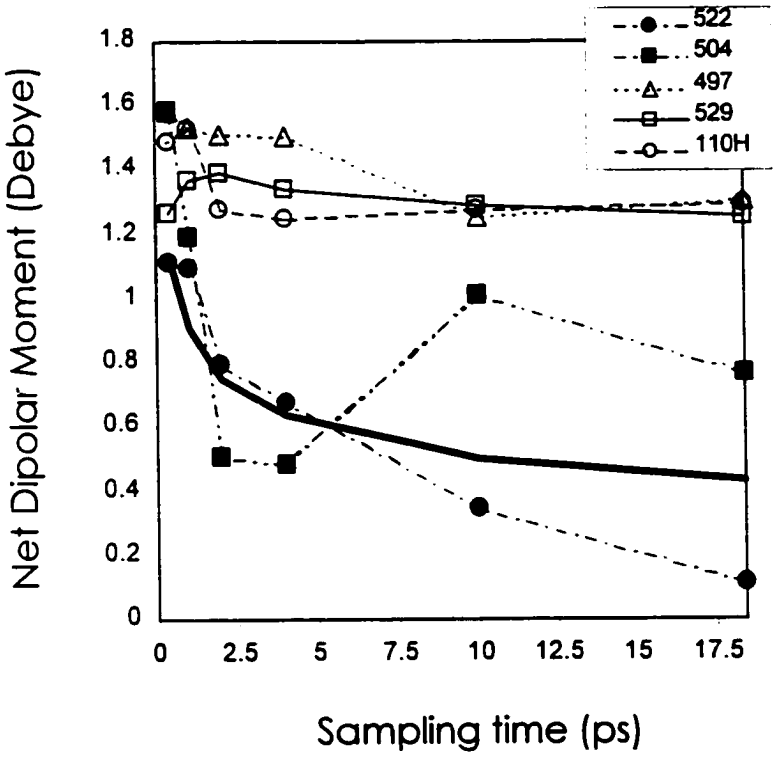

Figure 3.53a Net dipolar moment of modeled buried water molecules in ferricytochrome c state IV_{73} with respect to length of sampling time. The net dipolar moment of five buried water molecules was calculated on two set of alternate phases over 18.5 ps of simulation. Net dipolar moment average of 2001 molecules in the same simulation is plotted in bold.

shows that water molecules labelled 497, 529 and 110H are tethered in a hydrogen bond network, which explains their fixed orientation. **Figure 3.53b** also shows the singular organisation of water 522 and 504, both sharing the same internal cavity but having different stabilizing geometries to keep them in place. Water 504 is held in place by the amide carbonyl of Met^{80}, the amide N-H of Phe^{82}, and interacts with water 522. However, water 522 is merely filling the space left by the Cα of Met^{80} and is free to tumble inside the cavity. As the length of the sampling time increases, the net dipolar moment of water 522 decays along with the non-structural water molecule. This decrease, through intermolecular interaction, influences the net dipolar moment of water 504 (**Figure 3.53a**). It was, unfortunately, impossible to extend the sampling beyond 18.5 ps for practical reasons. The sensitive context of the geometry of a water molecule can then, with a sampling of 10 ps or more, be assessed by the determination of its net dipolar moment.

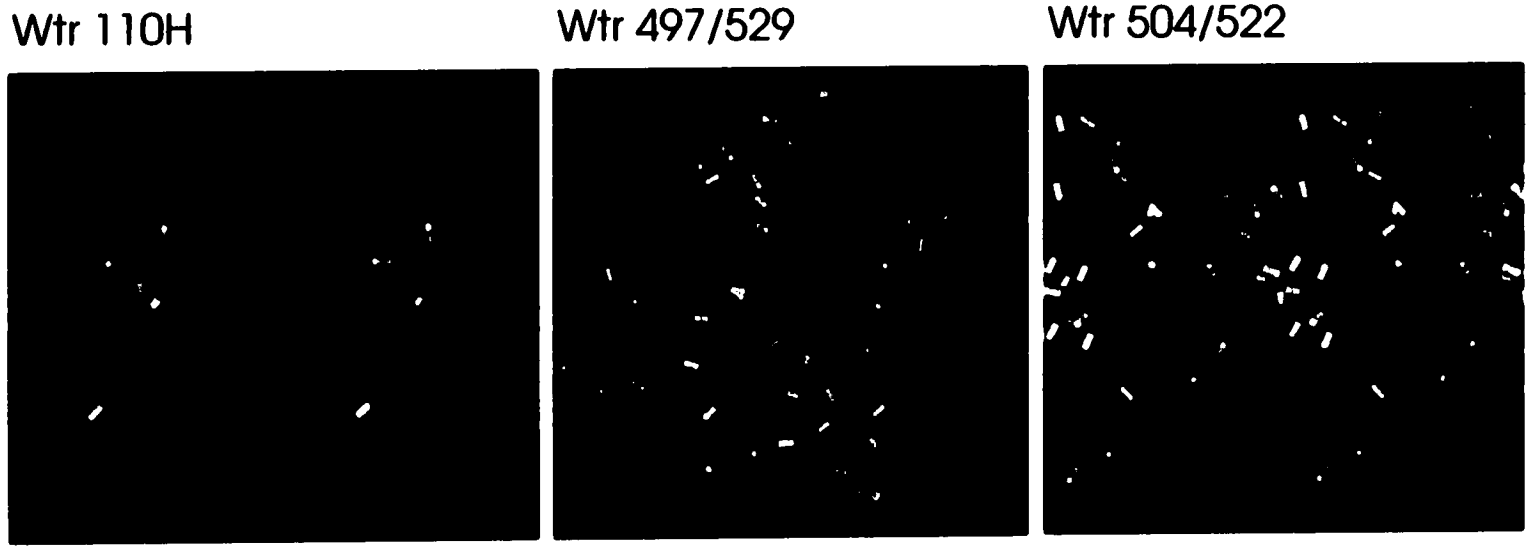

Figure 3.53b Stabilization of structural water molecules in ferricytochrome c state IV_{73}. Details of the structures are shown for each set of buried water molecules. Water coordinates are averaged over 18.5 ps.

3.5.4 Number and dynamics of buried water molecules in the heme crevice

The NDM assessment was developed to assist in determining the number and the geometrical environment of buried water molecules.

Initial structures of the following mutations: N52S, N52T and N52V were modeled using the coordinates of N52A. Therefore, two water molecules were initially buried beside the heme. Using the NDM method, the structural stability of such molecules was then assessed.

When the hydrogen bond-donating potential of the Asn side chain is lost, the oxygen of Wat^{166} flips toward Thr^{78} and the water molecule is reversed with respect to the protein. In the models of N52S and N52T, the hydroxyl group of Ser or Thr interacts with the carboxyl group of Hpr^{6}, which also reverses the polarity of Wat^{166}, despite the hydrogen-bond donor ability of these side chains.

In agreement with the crystal structure, the model of N52A shows two structurally stable water molecules, which is also observed in mutant N52S (**Figure 3.54, Table 3.54**). Mutant N52T however expels the second molecule in such a way that its average position is outside the cavity. In mutant N52V, both

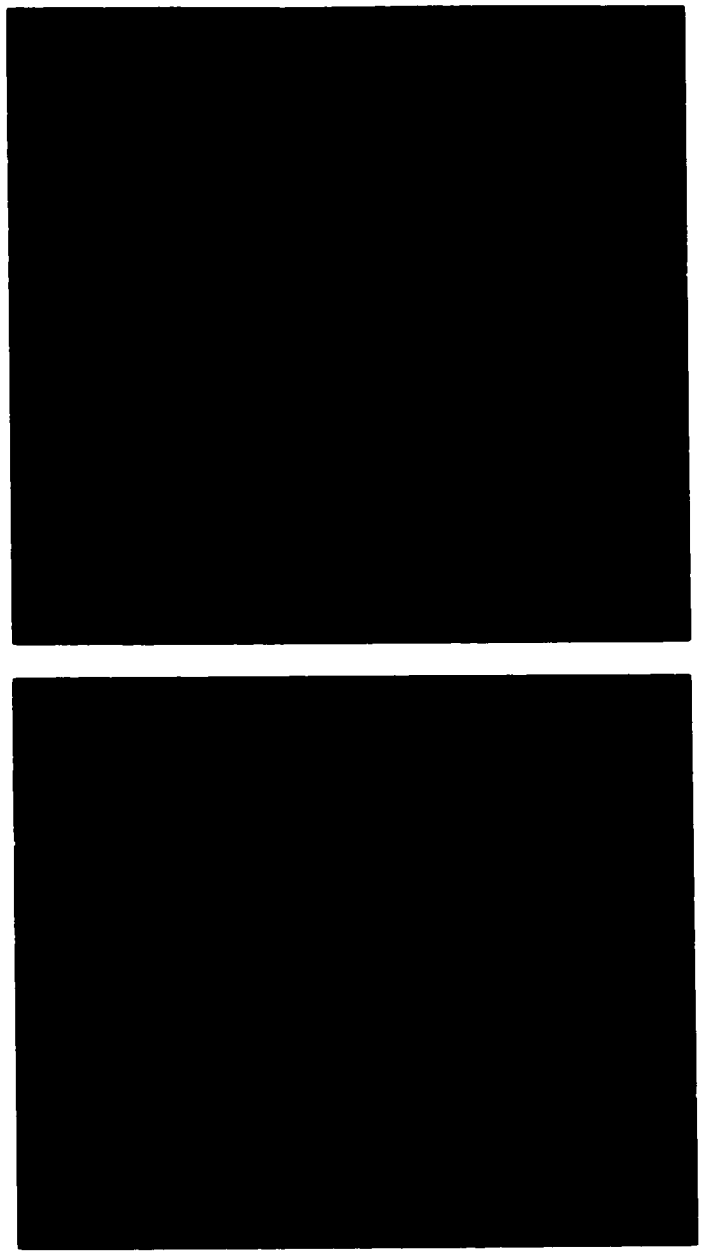

Figure 3.54 Structural water molecules in model of N52 mutants. The averaged model protein of wild type (white)[40ps], N52A (blue)[35ps], N52V (green)[35ps], N52S (red)[40ps] and N52T (purple)[40ps] were superposed using the coordinates of their backbone atoms.

Table 3.54 - Net dipolar moment of buried water molecules in model of Asn^{52} mutants series.

Model	Wat^{166}	Wat^{1300} [a]	Wat^{121} [b]
Wild type	0.92	-	1.37
N52A	1.27	1.28	1.37
N52S	1.20	1.35	1.51
N52T	1.17	1.06	1.31
N52D	1.41	-	1.49
N52V	0.78	0.63	1.63

[a] The water molecule occupying the space of the amide nitrogen of Asn^{52} in the wild type structure.
[b] The water molecule tethered between Arg^{38} and Hpr.

water molecules stay inside the protein, but their average position is such that they overlap. In these two cases, it is arguable that the cavity does not accommodate two water molecules.

3.6 Protein matrix and microscopic relaxation

3.6.1 Electrostatic probes and experimental dielectric constants

The values of the standard redox potential (E_m'') of mutant and derivative of cytochromes *c* are presented in **Table 3.21**. The thermodynamics of reduction was measured for four of these sample cytochromes *c*. One mutation, K55M, and three derivatives, with CAMMS at positions 28, 55 and 75, were chosen to measure effective dielectric constants.

As shown in **Table 3.61**, the effective dielectric constant between the site of the modification and the iron atom was calculated using two approaches. In both cases, the theoretical $\Delta U_{elec.}$ was calculated using Coulomb's law and the distances between the charges were measured on the appropriate molecular model from the iron atom to the location of the δ-S of the CAMMS side chain, except in the mutation K55M where the relevant distance is that to the ε-N of the lysine residue. The

Table 3.61 Apparent dielectric constants applying between the CAMMS probe and the redox centre.

Modification	$D_{(FE-X)}$[a] (Å)	$\Delta E_m''$ (mV)	$\Delta\Delta G_{Redox}$[b] ($kJ*M^{-1}$)	$\Delta\Delta H_{Redox}$[c] ($kJ*M^{-1}$)	$\varepsilon_{\Delta\Delta Em''}$[d]	$\varepsilon_{\Delta\Delta H}$[d]
K55M	14.6	+11 ± 4	- 1.1 ± 0.4	+ 6 ± 1	(-90)[e]	**16 ± 2**
K55M -> CAMMS55	16.0	-18 ± 5	+ 1.8 ± 0.5	- 2 ± 3	(-49)[e]	~ 44[f]
I75M -> CAMMS75	10.5	+33 ± 4	- 3.2 ± 0.4	-7 ± 2	41 ± 8	**19 ± 6**
V28M -> CAMMS28	8.0	+12 ± 2	- 1.3 ± 0.2	-7.1 ± 0.6	130 ± 20	**24 ± 2**

[a] Distance in Ångstroms from the iron atom to the site of the modification as measured in the respective molecular models.
[b] Calculated using $\Delta\Delta G_{Red.} = -RT\ \Delta\Delta E_m''$.
[c] Measured using Van't-Hoff's temperature dependence of equilibria graphical method.
[d] Ratio $\Delta U_{calculated}/\Delta U_{exp.}$. $\Delta U_{calc.} = (e^-)^2/4\pi\varepsilon_0 r$
[e] $\Delta U_{exp.}$ diverged in sign from theoretically expected $\Delta\Delta G_{Red.}$. These values have no physical meaning.
[f] Approximate value considering the large error in $\Delta\Delta H_{Red.}$.

effective dielectric constant was then calculated using either the free energy or solely the enthalpy of the redox equilibrium. When calculated from $\Delta U_{exp.} = \Delta\Delta G_{Red.}$, the calculation of dielectric effect yields very variable, indeed, irrational values.

The effect on the E_m'' of the mutant K55M and its CAMMS derivative was of the opposite sign to that of the expected values, and yielded a negative effective dielectric constant. These negative values clearly do not have any physical meaning.

However, this problem seems to be corrected if $\Delta U_{elec.}$ is taken to be $\Delta\Delta H_{Redox}$ (**Table 3.61**).

3.6.2 Thermodynamic profile of reduction of the Asn^{52} mutant series

The thermodynamic profile of enthalpy and entropy of reduction of a variety of cytochromes *c* is shown in **Figure 3.62**. The enthalpy and entropy of the redox equilibrium often vary in opposing directions with respect to one other, so that the net variation in E_m'' is attributable to the fine balance between the two components of ΔG''. In most cases except K55M, CAMMS55, Y67F/N52V and Y67F/N52I, the chemical environment

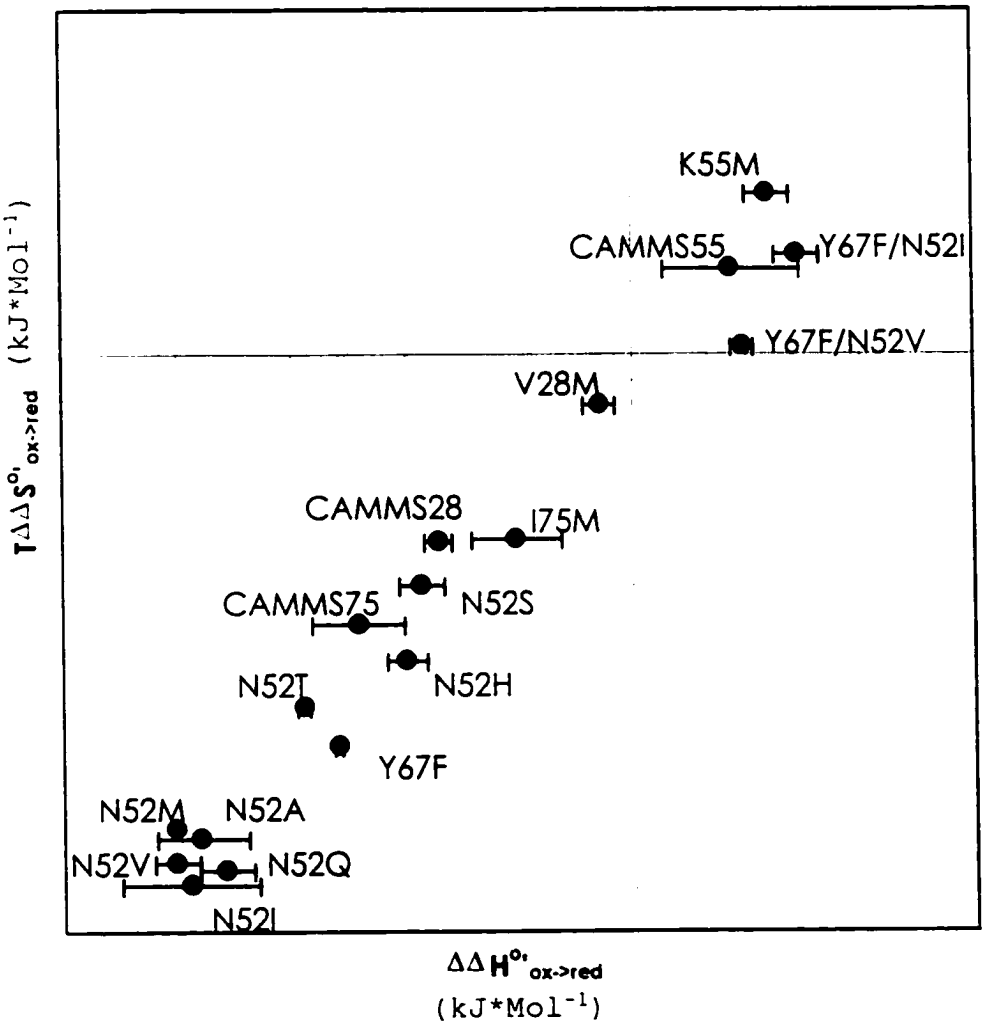

Figure 3.62 - Thermodynamic profile of reduction of cytochromes *c*. $\Delta\Delta H^{o'}$ was evaluated from temperature-dependence of the oxidized-reduced equilibrium using the graphical method of Van't-Hoff. The value of $\Delta\Delta S^{o'}$ was calculated using the equation $\Delta\Delta S^{o'} = \Delta\Delta H^{o'} + RT\ \Delta E_m^{o'}$. The dotted line shows the isocurve where $\Delta E_m^{o'}=0$. The datapoints found below the isocurve indicate a net decrease in $E_m^{o'}$.

Table 3.62 Thermodynamics of reduction of cytochromes c determined by Van't-Hoff method.

Mutation	ΔE_m'' [a] (mV)	$\Delta\Delta G_{Red.}$ [b] ($kJ*M^{-1}$)	$\Delta\Delta H_{Red.}$ [c] ($kJ*M^{-1}$)	$\Delta\Delta S_{Red.}$ [d] ($J*M^{-1}K^{-1}$)
V28M	-8 ± 4	0.8 ± 0.4	-1.5 ± 0.7	-8 ± 3
CAMMS28	5 ± 4	-0.5 ± 0.4	-8.6 ± 0.6	-27± 3
K55M	11 ± 4	-1.1 ± 0.4	6 ± 1	23 ± 4
CAMMS55	-7 ± 4	0.7 ± 0.4	4 ± 3	12 ± 11
I75M	-29 ± 4	2.8 ± 0.4	-5 ± 2	-27 ± 8
CAMMS75	4 ± 4	-0.4 ± 0.4	-12 ± 2	-39 ± 8
N52M	-5 ± 2	0.5 ± 0.2	-20 ± 0.4	-69 ± 2
N52S	-8 ± 3	0.8 ± 0.3	-9 ± 1	-34 ± 4
N52T	-9 ± 2	0.9 ± 0.2	-15 ± 0.3	-51 ± 2
N52V	-20 ± 4	1.9 ± 0.4	-20 ± 0.4	-74 ± 2
N52A	-21 ± 3	2 ± 0.3	-20 ± 2	-70 ± 8
N52H	-34 ± 2	3.3 ± 0.2	-10 ± 1	-44 ± 4
Y67F/N52I	-30 ± 2	2.9 ± 0.2	7 ± 1	15 ± 4
N52Q	-36 ± 1	3.5 ± 0.1	-20 ± 3	-77 ± 10
N52I	-47 ± 7	4.5 ± 0.7	-18 ± 1	-75 ± 3
Y67F/N52V	-47 ± 3	4.6 ± 0.3	-4.8 ± 0.5	1 ± 2
Y67F	-42 ± 1	4.1 ± 0.1	-13 ± 0.2	-57 ± 1
N52D	-96 ± 2	9.3 ± 0.2	-42 ± 7	-171 ± 25

[a] Using the method of the mixtures. Average error = 3mV (n=3)
[b] Calculated using $\Delta\Delta G_{Red.} = -RT\ \Delta E_m''$.
[c] Measured using Van't-Hoff's temperature dependence of equilibria graphical method. Average error = 1.2 $kJ*Mol^{-1}$.
[d] Calculated using $\Delta\Delta S_{Red.}'' = \Delta\Delta H_{Red.}'' - \Delta\Delta G_{Red.}''$. Average error = 6 $J*Mol^{-1}\ K^{-1}$.

favours a reduced state over the oxidized. This change in enthalpy is generally concomitant with a decrease in entropy that is responsible for the observed thermodynamic drive toward the oxidized state. In the double mutants Y67F/N52V and the Y67F/N52I and chemical derivative CAMMS55, both enthalpy and entropy favour the oxidized state. On rare occasions, (e.g. CAMMS28, CAMMS75 and K55M), E_m'' increases marginally (relative to the wild type) as described above in **section 3.6.1.** Numerical data are summarized in **Table 3.62.**

3.6.3 Entropy of reduction of mutant cytochromes *c*

The calculated entropy of reduction of mutants that did not involve change at position 52 was replotted in **Figure 3.63** as grey squares. It appears in this plot that the magnitude of the $\Delta\Delta S_{Rd}$'' is proportional to the magnitude of the change in ΔE_m''. This is however not observed for Asn^{52} mutations shown on the same graph as black circles, where the $\Delta\Delta S_{Rd}$'' values average -73 ± 3 J * Mol^{-1} K^{-1} (includes N52I, N52Q, N52V, N52A and N52M). Interestingly, this value includes a broad range of substitutions at position 52 except for the two side chains with a hydroxyl group (N52S and N52T) and mutation

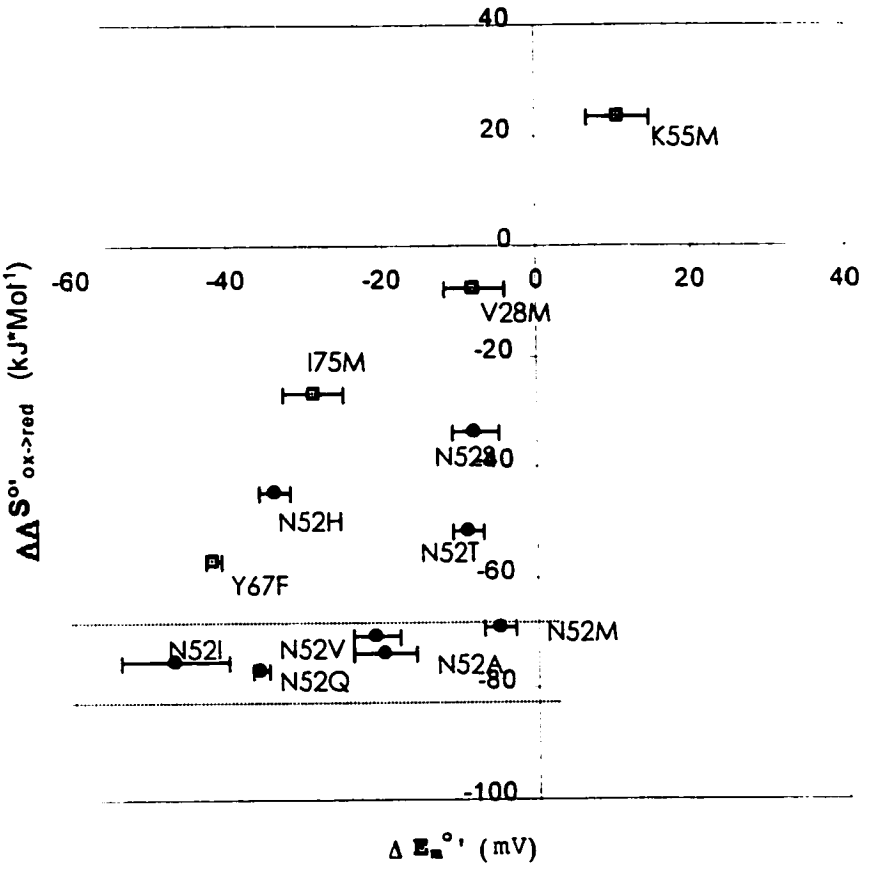

Figure 3.63 - Entropy of reduction of Asn^{52} mutants as a function of $E_m°'$. The entropy of reduction was evaluated using: $\Delta\Delta S°' = \Delta\Delta H°' + RT\ \Delta E_m°'$. Mutants that have an Asn^{52} are shown in gray and were used to generate the linear regression. Dotted lines stress the grouping of $\Delta\Delta S°'$ for the Asn^{52} mutants.

N52H **(Figure 3.63)**. The magnitude of $\Delta\Delta S_{Rd}^{\circ\prime}$, $\Delta\Delta H_{Rd}^{\circ\prime}$ and $\Delta E_m^{\circ\prime}$ is such that the mutation N52D was omitted from the plots.

3.6.4 Entropy of reduction of Tyr^{67} mutant series

The double mutations Y67F/N52V and Y67F/N52I are shown in **Figure 3.64**. The thermodynamic behaviour of these mutants differs from that of the individual substitutions. Most remarkably, the entropy of reduction of these mutants does not favour any oxidation state or slightly favours the reduced state. This radical thermodynamic behaviour will be considered in terms of the chemical nature of the heme crevice in these mutants in the following chapter.

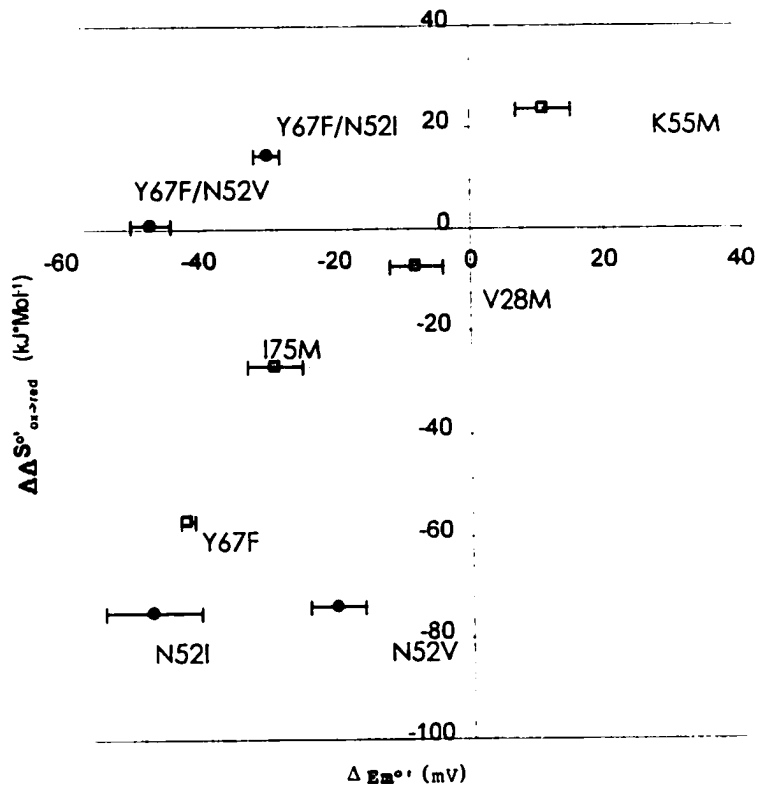

Figure 3.64 - Entropy of reduction as a function of $E_m°'$. The entropy of reduction was evaluated using: $\Delta\Delta S°' = \Delta\Delta H°' + RT\ \Delta E_m°'$. Mutants that have an Asn^{52} are shown in grey and were used to generate the linear regression.

Chapter 4: Discussion

4.1 Surface electrostatics

4.1.1 Creation of model probes using protein chemistry

In order to react with iodoacetamide, the methionine side chain must be exposed, if only transiently, to the solvent. Molecular modelling suggests that a reinsertion is possible for the CAMMS side chain at 75 due to the local internal polarity. However, in the case of reaction with L68M, the fact that no single derivative accumulates suggests that once formed, the CAMMS-68 side chain does not reinsert in the cytochrome interior. This would consequently disrupt the native conformation and expose residues that normally are unreactive (such as Met^{80}).

Iodoacetamide also reacts with lysine and histidine (there are no free cysteines in cytochrome c C102T), but at the reaction pH employed, rates with lysines are negligible, and with histidine, low (Ando *et al.*,1966). Histidines 18 and 26 are known to be quite unreactive to iodoacetamide, but partial alkylation of the

variable histidines 33 and 39 is to be expected, but will not provoke any change in net charge or functional properties. This is demonstrated by the existence of a number of CAMMS derivatives in the series that do not differ functionally from the respective parent protein.

In this series of mutants, the chemical modification of surface residues by acetamidation of methionine side chains is a simple way to alter the surface electrostatics of cytochrome c. Molecular modelling of the CAMMS derivatives showed that the modification to the protein structure, except for the derivative CAMMS75, was limited to the alteration of surface electrostatic potential. Any changes to physical or biological properties of these cytochromes then can be correlated with these local modifications.

4.1.2 Rate limiting step of the Succinate Oxidase assay

It has been argued that the rate-limiting step measured in the succinate oxidase assay is the reduction of cytochrome c by the electron transport complex III (Wallace and Proudfoot, 1986). This view is further

supported by the biological activity of the derivative CAMMS28 for which the cytochrome *c* oxidase activity is decreased ten-fold while the succinate oxidase activity, which encompasses electron transfer to the oxidase, is still at 85% of the native level. The alteration in the succinate oxidase activity can thus be regarded as a measure of the reaction rate between cytochrome *c* and the integral membrane cytochrome *c* reductase.

4.1.3 Biological function of derivatives

As illustrated in **Figure 4.13**, the changes induced by the CAMMS derivatisation in the activity of the analogs in the succinate oxidase assay relative to the parent protein seem to correlate with the proximity of the sulphonium ion to the lysines identified as critical for complex formation. The only case in which the addition of an extra positive charge has deleterious effects on activity is with the CAMMS65 derivative. This effect is not attributable to the loss of the widely variable serine residue at this position, as the activity with S65M is comparable to that of the wild type. It is interesting to note how the effects of derivatisation at position 64 in

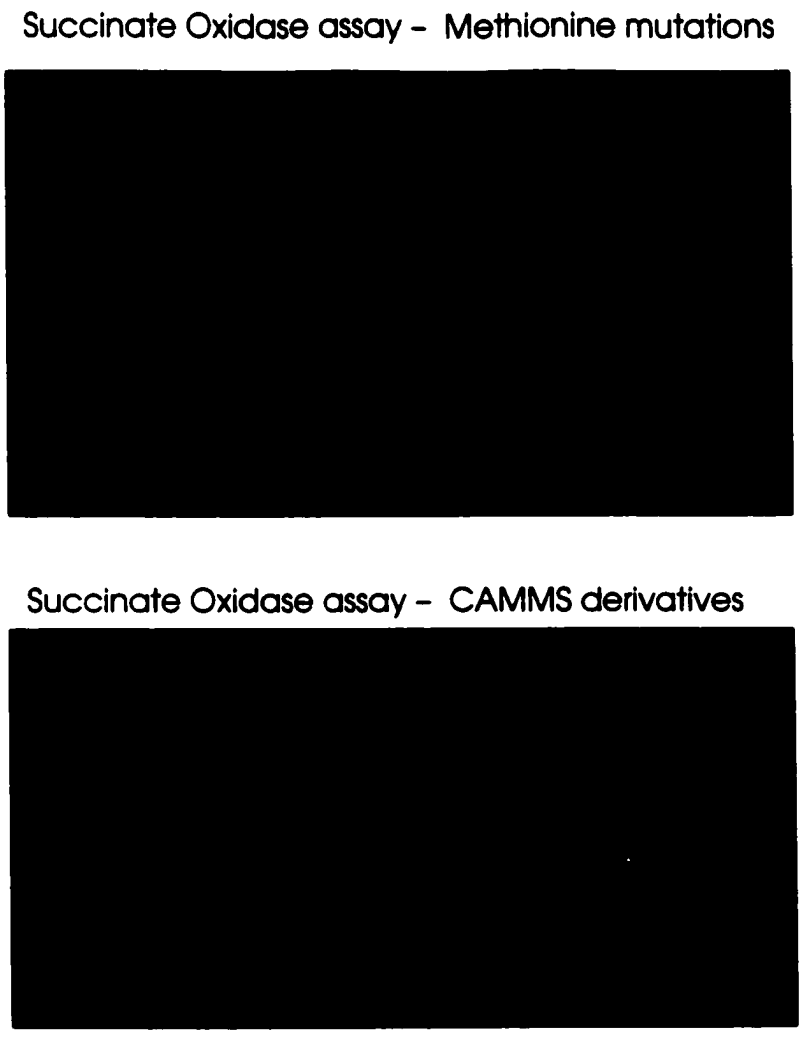

Figure 4.13 Influence of mutations and chemical derivatisations on the activity of the cytochrome c in the succinate oxidase assay. The Cα trace and the prosthetic group are displayed in purple. The sphere are centered on the Cα of the positions altered and are proportional in size to the magnitude of the effect on activity. Orange and green indicate respectively a decrease and an increase in activity. The blue Cα spheres shows the relative importance of various lysines for binding to cytochrome c reductase as presented in (Zhen *et al.*, 1999) and does not use the same scale as the presented results in this work.

the wild type protein differ from those of the CAMMS65 modification. On the basis of this data set, it is possible to suggest that the alteration of surface electrostatics in the vicinity of Lys^{86}, a residue identified as key to the interaction with the reductase (Moore and Pettigrew, 1990; Döpner *et al.*, 1999), is responsible for the apparent 3-fold reduction in activity with this physiological partner. Whether this effect is attributable to altered electrostatic steering in the docking process or by actually generating unproductive docked structures with a distorted electron tunnelling pathway (Beratan *et al.*, 1995) could not be determined, since as yet we do not know the details of the interacting surface with the reductase.

4.1.4 Interaction of derivatives with cytochrome *c* oxidase

The interaction of cytochrome *c* and subunit II of the electron transport chain complex IV has been extensively studied by spectroscopic methods (Falk *et al.*, 1983; Weber *et al.*, 1987; Michel *et al.*, 1989; Hildebrandt *et al.*, 1990; Hildebrandt *et al.*, 1993) and more recently

using *Rhodobacter sphareoides* cytochrome *c* oxidase and horse cytochrome *c* (Zhen *et al.*, 1999; Wang *et al.*, 1999). Also, a systematic search between the two partners was attempted and gave results consistent with experimental data (Roberts *et al.*, 1999).

Figure 4.14 summarizes the effect of mutation and chemical derivatisation on the activity of cytochrome *c* with the oxidase. The interaction between these two proteins is more generally influenced by the electrostatic perturbations than that with reductase. This is consistent with the observed important contribution of electrostatic forces to complex formation (Hildebrandt *et al.*, 1993; Zhen *et al.*, 1999; Wang *et al.*, 1999).

Although Lys^{55} is not thought to participate in a salt bridge between cytochrome *c* and its docking site on the oxidase (Roberts *et al.*, 1999), the mutation K55M decreased transfer rates between this pair by about 50%. However, restoration of the positive charge in CAMMS55 brought the activity of the cytochrome back to native levels (**Table 3.21**). The mutation K55M also has a substantial effect on the stability of the spectroscopic state III of the protein with a $\Delta pK'_{AT} = -0.8$ units. Yet, although the CAMMS55 derivative ($\Delta pK'_{AT} = -1.3$) restores

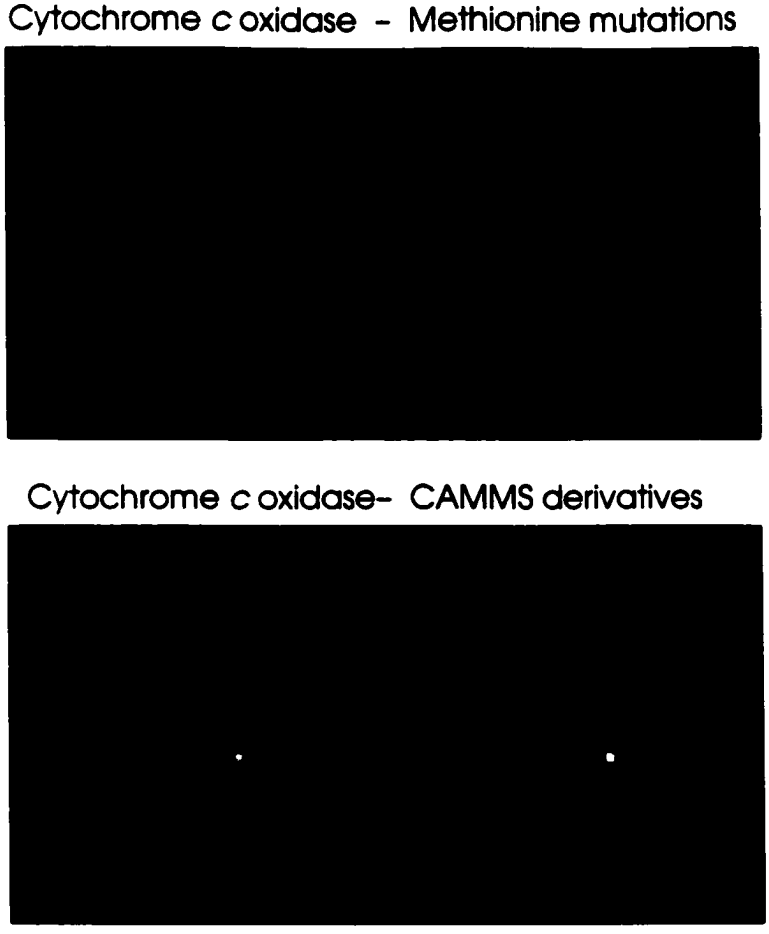

Figure 4.14 Influence of mutations and chemical derivatisations on the activity of cytochrome *c* with cytochrome *c* oxidase. The Cα trace and the prosthetic group are displayed in purple. The sphere are centered on the Cα of the positions altered and are proportional in size to the magnitude of the effect on activity. Orange and green indicate respectively a decrease and an increase in activity. The blue Cα spheres shows the relative importance of various lysines for binding to cytochrome *c* oxidase as presented in (Zhen *et al.*, 1999) and does not use the same scale as the presented results in this work.

native-level activity with the cytochrome *c* oxidase, it actually enhances the pH-lability of this conformer. This implies that the evolutionary conservation of charge at position 55, which is general but not absolute, relates not to intramolecular aspects of electron transfer, but to the global electrostatics of the intermolecular interaction.

The mutation V28M did not substantially affect electron transfer between the two proteins. This is not surprising if one accepts that the complex, proposed by Roberts *et al.*(1999), excludes the side chain of this residue from the binding interface. However, the introduction of a positive charge in the CAMMS derivatives decreased the activity with the oxidase by an order of magnitude. Although this added charge is unlikely to affect the bound complex, the proximity of such charge may divert the electrostatic steering leading to docking and thus increase the occurrence of unproductive "encounter complexes" between the partners. This interaction should be further investigated to determine if the presented results are the products of a decrease in binding or of electron-transfer kinetics.

Interestingly, the insertion/deletion of electrostatic charge on the face of cytochrome *c* that is interacting with the oxidase does not affect the activity as significantly (2-3 fold decrease in most cases). This was also noted by Zhen *et al.*, 1999 in a mutagenesis study. The authors argued that no specific interaction is crucial for binding and that the contribution of electrostatic forces relies on a general surface distribution of charges.

4.2 Electrostatics of conformational stability

4.2.1 Microscopic and macroscopic ionisations

In this study, effective pK were determined in an attempt to assign them to ionizing residues associated with a conformational transition in the protein. The two measured pK values in *S. cerevisiae* (8.60 and 8.9) can be related to the apparent pKs of the alkaline transition in mutants K79A (pK_{K73} =8.44) and K73A (pK_{K79} =8.82)(Rosell *et al.*, 1998). These investigators concluded that the apparent pK of the wild type protein was an average of the microscopic pKs for these two alternative ligands. The values extracted from **Figure 3.44** show that these two

ionisations determine the course of the alkaline transition in the wild type cytochrome c. However, the data obtained in the present study show that the titration curve is not a sum of these ionisations but rather an overlay of them.

It has been demonstrated that in cases where the sum of the curves would be operative, no linearity could ensue. Thus, at a given pH, the derivative of the titration curve would be comprised of two or more ionisations weighted by a dependence on the pH relative to their microscopic pK values (see Equation 12 in section 3.4.1).

Additivity is commonly observed over a broad pH range (Yang et al., 1993) and can be easily fitted using deconvolutive algorithms. However, in the case of a pH-induced conformational change, a lattice of cooperative interactions has to be broken over a very narrow pH range. The height of the 695 nm band is diagnostic of the distribution of spectroscopic states III and IV. Over the titration, each ionizing component appears in turn to limit the transition over a small domain of pH. This suggests that the free energy each ionizing component provides does not contribute to the energy of a continuum

of conformations but that these microscopic events are stabilizing either of the two spectroscopic products (State III and IV) in a binary fashion. The equilibrium between the states is likely to be cooperative since it was demonstrated that states IV_{73} and IV_{79} of cytochrome c are near native, stable and ordered conformers (Döpner *et al.*, 1998, Rosell *et al.*, 1998). Thermodynamics extrapolated to a null ionic strength in fact show that the transition is mostly enthalpic in nature, having small positive or even slightly negative entropy (Battistuzzi *et al.*, 1999). For this reason, I conclude that linearisation of a titration curve allows the microscopic ionizing components that limit a pH-induced cooperative conformational change in proteins to be resolved.

4.2.2 Insight into the mechanism of the alkaline transition

Evidence presented in this study seems to agree with previously published data that the microscopic course of events of the alkaline transition is determined by the deprotonation of the alternative iron ligands. Since the only difference between the variant Tm172K and the yeast

wild type is the absence of trimethylation (Pollock *et al.*, 1998), and Tm172K is the only yeast cytochrome *c* , to the author's knowledge, to show hysteresis for the alkaline transition, I conclude that this asymmetry is provoked by the ionization of the ε-amino group of Lys^{72}. Furthermore, NMR evidence indicates that a spectroscopic state IV is observed at lower pH in the titration of the Tm172K variant (Pollock *et al.*, 1998). This is confirmed in this study, and deconvolution by the linear regression approach developed allows assignment of a pK of 7.84 to this ionisation.

I therefore propose that the structural basis for hysteresis arises from the formation at a lower pH of a conformer of the spectroscopic state IV_{72}. Pollock *et al.* suggested that this low pH-induced state IV is, however, not as thermodynamically stable as the other conformers. To account for a slow rate of equilibration, this conformer must have to overcome a high-energy barrier to equilibrate with the more stable conformers IV_{73} and IV_{79}. Indeed, the computed models of conformers of spectroscopic state IV (Section 3.3.1) indicate that the local rearrangement necessary to bring Lys^{73} or Lys^{79} to the iron

coordination sphere is substantially less than the global effect of bringing Lys^{72} to ligate the heme metal ion.

4.2.3 Evidence of multiple equilibria in one transition

A band at around 600 nm is acknowledged to be diagnostic of a high-spin heme iron. Linearisation of the concomitant appearance of a shoulder in mutant Tm172R indicates that the presence of this high-spin species is not determined by the same microscopic ionisation that bleached the 695 nm band. Also, the thermodynamics of their equilibria indicate that these two events are chemically distinct. Similarly, the formation of a high-spin species in mutant K79R is part of a different equilibrium but appears to be triggered by the same microscopic ionizing group (**Table 3.46**).

The failure to replace the Met^{80} side chain by one of the lysines in these mutants may arise from the nature of the interaction of these arginine side chains with their local environment. The failure to break the hydrogen bond between Ser^{47} and position 79 (Louie *et al.*, 1990) known to be critical to the stability of the heme

crevice in the alkaline conformation of K79R (Osheroff *et al.* 1980), may forbid the backbone displacement necessary for the introduction of the ε-amine of Lys^{73}, and may instead force the introduction of a low field ligand, such as a water molecule, into the iron coordination sphere. Another factor must therefore prevent Met^{80} from keeping its place as a ligand.

The identity of this weak-field ligand that provokes the high-spin species in the alkaline conformation is unknown. In Tml72R, it appears that the formation of the high spin species coincides with ionisations found in the wild type protein (**Table 3.46**), hypothesised to be those of lysines 73 and 79. This implies that the displacement of the δ-S of Met^{80} is triggered by a third microscopic ionisation at 8.42, also visible in the transition III to IV of the variant Tml72K.

The identity of this microscopic ionisation also remains open. Some candidates have been proposed in the past, including the ionisation of Tyr67 (Davis *et al.*, 1974; Lundtz *et al.*, 1989), a buried water molecule (Takano *et al.*, 1981) that has been the topic of previous investigations (Lett *et al.*, 1996; Berghuis *et al.*, 1994), and an intriguing heme propionate with an apparent pK

similar to the apparent pK of the alkaline transition in the horse protein (Hartshorn *et al.* 1989), and which is also hypothesised to influence the apparent pK of the alkaline transition in tuna (Tonge *et al.*, 1989).

In Tml72R, the difference of pK between the displacement of the Met^{80} side chain from the iron coordination sphere and the ionisation of the alternative ligands suggests that the alkaline transition proceeds via an intermediate conformation that is not ligated by the amino group of the nearby lysines. An intermediate of the alkaline transition had already been postulated by research groups who studied the phenomenon using stop-flow kinetics (Davis *et al.*, 1974, Pierce *et al.*, 1989).

Comparisons of the horse and yeast proteins cannot explain the large difference (~0.7 units) in apparent pKs of their respective alkaline transitions, since the structure of these heme crevices are very similar. However, the difference in the structural determinants stabilising this intermediate is likely to account for the large interspecies variation. This is especially true if this third ionisation is assigned to a carboxylate with an exceptionally high pK such as Hpr^{6}.

4.3 Protein matrix and dielectric effect

The behaviour of E_m'' upon altering the electrostatic landscape of cytochrome *c*, as in most electron transport proteins, is hardly predictable. In the classical model, an electrostatic field is scaled down by a factor known as dielectric constant. This constant depends on the medium in which the field is propagated. However, at the molecular level, the uniform nature of this effect appears to be lost. For this reason, it is preferable to refer to an effective dielectric constant rather than a dielectric constant (Rees, 1980).

For appropriate biological function, the mitochondrial cytochromes *c* appear to have evolved toward higher values of E_m'' (Sober, 1970). In other words, the protein matrix has been optimized to favour the reduced state of the iron (Churg *et al.*, 1986). In practice, this is achieved by solvating the buried dipoles that would otherwise polarize to stabilize an extra positive charge of the ferric iron. This is the case in the heme crevice where every dipole is part of a hydrogen bond network (Berghuis and Brayer, 1992). The polarity of this network

intrinsically acts as a suitable dielectric environment to complement a buried, yet charged, heme without compromising the protein stability. However, this network as a whole has a sufficiently low dielectric character to differentially disfavour the triple positive charged oxidized iron. Indeed, it may be that because the structure has evolved in this direction that most mutations affecting the network lower the standard redox potential of the protein, thus favouring the oxidized form of the cytochrome *c* (Schejter *et al.*, 1994).

In this section, the value of $E_m^{\circ\prime}$ is used to quantitate the dielectric susceptibility of the protein matrix. The value of ΔG°_{redox} is a measurement of the relative thermodynamics of the ferrous and ferric states of the protein, differing by a single charge on the heme. Therefore, $\Delta\Delta G^{\circ}_{redox}$ of mutation represents the difference in the polypeptide response to the electrostatic field generated by the redox centre, including every possible factor. Assuming only a local effect on structure, $\Delta\Delta G^{\circ}_{redox}$ of mutation can thus be regarded as an alteration of the local dielectric properties of the polypeptide. The experimental determination of $\Delta\Delta G^{\circ}_{redox}$ of mutation can be done using **equation 13** from $\Delta E_m^{\circ\prime}{}_{mut}$.

$$\Delta\Delta G^{o'} = - nF \Delta E_m^{o'} \quad (13)$$

Where **n** is the number of electron exchanged in the equilibrium and **F** is the Faraday constant ($9.6487X10^4$ C mol^{-1}).

4.3.1 Redox potential of the CAMMS derivative series

The magnitude of most of the ΔE_m''s measured in the CAMMS dataset was not large enough to allow the calculation of reliable effective dielectric constants. Only four modifications incurring a ± 1 formal charge change were kept for thermodynamic analysis: the mutation K55M and the derivatives of mutants V28M, K55M and I75M.

The direct use of $\Delta\Delta G_{redox}$ to evaluate ε yielded a range of values from -90 to 130. Considering the theoretical minimum ε value of 1 and the practical maximum value of 80, it is clear that ΔE_m'' is not exclusively attributable to a change in the dielectric properties of the protein matrix (as inferred from Coulomb's law). The presence of a "negative dielectric effect" for K55M and

CAMMS55 indicate that the change in E_m'' is greater than would be expected using Coulomb's law. On the other hand, the effect of the derivatisation CAMMS28 is much smaller than would have been expected from dielectric relaxation (ε = 130 ± 20, **Table 3.61**). This value is in fact higher than the value of ε for the bulk solvent itself. The effect on standard redox potential thus extends beyond dipolar relaxation, as treated in the macroscopic scale, into factor(s) yet to be accounted for.

If, however, one uses $\Delta\Delta H_{red.}$ to calculate an effective dielectric constant, the data yields a consistent ε value (**Table 3.61**), with an average of 19 ± 6. This compares with calculated values of 25 ± 10 for the whole cytochrome *c* derived from molecular dynamics, using the Frohlich-Kirkwood theory of microscopic dielectrics (Simonson *et al.*, 1995). Derivative CAMMS55 appears to be an exception, but the standard error in the measurements is such that it is impossible to formally calculate a $\varepsilon_{\Delta\Delta H}$.

4.3.2 Physical meaning of $\varepsilon_{\Delta\Delta H}$.

A consistent $\varepsilon_{\Delta\Delta H}$ value suggests that the dielectric constant as defined by Coulomb's law applies to microscopic systems, with a value of ~20 for the heme and its immediate environment in cytochrome *c*. Or, at least, this value would apply to this system at 0 °K. This implies that, from a purely enthalpic point of view, the polypeptide relaxation to the heme electrostatic charge is consistent and independent of the position of a test charge. This more consistent dielectric susceptibility could thus be referred to as true dielectric constant, which is one of two possible components forming the apparent dielectric constant. Most importantly, this indicates that the great variability in apparent dielectric constants is due to entropy, and that the magnitude of the entropic contribution ($\varepsilon_{\Delta\Delta S}$) is larger than $\varepsilon_{\Delta\Delta H}$, and generally of an opposing sign.

4.3.3 Structures of the N52 mutant series

Modeling of the structures of mutants, and chemical derivatives in the CAMMS series, showed that the structure of cytochrome *c* is not significantly changed by surface mutation. This was also observed earlier by Parrish (1997), and permits the assumption that the extent of structural alteration of all methionine mutants and derivatives studied is limited to surface properties, and that the geometry of the iron ligation is not affected. This assumption cannot be made for the mutations at position 52. The mutants were thus screened for anomalies using CD spectroscopy of the amide band. In addition, starting from the determined structures of N52I and N52V, models are proposed for all of the N52 mutants discussed in this study.

Since position 52 is located in a small stretch of α-helix, the CD signal of the amide between 180 and 260 was expected to be sensitive to local perturbation. Spectra of two of the mutants did not resemble that of the wild type protein in a satisfactory fashion: N52C and N52D. The overall spectrum of N52C deviates from the wild type spectrum. This mutant was also reported to have an

unstable folding baseline (Linsk-O'Connell *et al.*, 1995). The molar ellipticity in the spectrum of the mutant N52D is consistently larger than that of the wild type. Since the ΔE_m'' is assumed to be a measure of the dielectric properties of the protein matrix *only* if the extent of the effects of a given mutation is limited to the local structure, mutants N52D and N52C were excluded from the analysis.

4.3.4 Molecular modeling of N52 mutant series

As described in section 3.5.2, the initial number of water molecules in the hydrophilic heme crevice was assumed based on A - similarity with known structures or B - on similar ΔG_U in guanidine hydrochloride (for N52M). The cases of N52V, N52S and N53T were treated using the Net Dipolar Moment calculation discussed below. These molecular modeling experiments helped to determine the overall hydrophilicity, volume and hydrogen bond network of the heme crevice. Molecular mechanics showed in all cases that the hydrophilic cavity adjacent to position 52 could accommodate any of the discussed mutations.

4.3.5 Net Dipolar Moment calculation and N52 series

To balance a structure through the energy barrier to be crossed in order to insert or remove a water molecule from a fully enclosed cavity would have required a nanosecond-length simulation. This was however impossible to achieve on the platform used to perform this work. To remedy this limitation, the calculation of Net Dipolar Moment (NDM) attempts to assess, in a shorter sampling time, the stability of buried water molecules. **Figures 3.53a** and **3.53b** clearly link the NDM of a buried water molecule with its context inside the protein. It also shows that much can be learned about the geometry around the water molecule with only 10 ps of sampling.

Simulation of the side-chains of Val, Ser, Thr were initialized with two water molecules in the heme crevice. Mutant N52A, for which an XRD structure has been solved, was run as a control and shows two stable water molecules with NDM of 1.28 Debye (**Table 3.54**). Mutant N52S also accomodated two water molecules inside the protein. The extra methyl found in the Thr/Val side chain seems to prevent the second molecule from settling within the

crevice. This is visible by the lower NDM values for the water molecules in mutants N52V and N52T, the overlapping position of the these molecules in N52V and the expulsion of one in N52T (**Figure 3.54**). It is thus likely that the extra methyl creates a steric clash prohibiting the presence of two water molecules in the crevice, despite the failure of molecular mechanics to expel the water during 100.5 ps of simulation.

4.3.6 Thermodynamic components of $\Delta\Delta G_{redox}$.

The behaviour of $\Delta E_m^{\circ\prime}{}_{mut}$ depends on the $\Delta\Delta G_{redox}$. As had been earlier suggested by the behaviour of the three methionine-scan mutant/derivative samples, the enthalpic relaxation leading to the dielectric effect is consistent and the variability must be attributed to an entropic factor. A treatment similar to the CAMMS series could not be applied to mutants at position 52 because of the lack of change in charge. However, the experimental determination of $\Delta\Delta H_{red.}$ as well as the $\Delta\Delta G^{o\prime}{}_{red.mut}$ (through the measurement of $\Delta E_m^{\circ\prime}$) were used to calculate $T\Delta\Delta S_{red.}$.

The elimination of the dipole of the Asn^{52} side-chain and its replacement by another residue induced a

decrease in enthalpy of reduction in all cases. This indicates that Asn^{52} enthalpically favours the oxidized state over any other single mutation at this position (**Figure 3.62**). Thus, a mutation at this position would be expected to provoke an increase in E_m''. However, most are found below the isocurve $\Delta E_m''=0$, indicating that these mutations lead to a net decrease of E_m''. The favourable enthalpy of reduction is, in these cases, opposed by a larger unfavourable entropic cost.

It is broadly recognized that in the oxidized and reduced structures of the horse cytochrome *c* (Banci *et al.*, 1997; Qi *et al.*, 1996; Qi *et al.*, 1997), and *S. cerevisiae* wild type (Berghuis and Brayer, 1992), Y67F (Berghuis *et al.*, 1994), N52I and Y67F/N52I (Berghuis *et al.*, 1994a), there is no significant conformational change. The redox dependent conformations do not differ in terms of atomic coordinates, but the differences that show up in structural determination can be conceptualized in terms of the energy necessary to keep these coordinates unchanged. This tension to keep the structure unchanged is dependent on the temperature of the system and thus is reflected by $\Delta\Delta S_{red.}$. Although Asn^{52} offers a better solvating environment from an enthalpic aspect, the Asn

side chain appears to offer fewer degrees of freedom within the heme crevice in the oxidized state. The Asn side chain will thus favour the reduced state over any other permutation at position 52.

Finally, although it is clearly observed, there is no obvious reason why enthalpy and entropy should line up along the diagonal in **Figure 3.62**. It appears that the chemical energy of reduction is gained at the expense of a higher order effect, which translates into an entropic cost. This limits the extent of the contribution of the Asn^{52}-Wat^{166}-Tyr^{67} module of $|\Delta E_m^{\circ\prime}|$ to about 50 mV (4.5 KJ/Mol).

4.3.7 Asn^{52} and $E_m^{\circ\prime}$

$\Delta E_m^{\circ\prime}$ values in the series of mutants involving Asn^{52} ranges from -5 mV in N52M to -47 mV in N52I. Mutations at this position have been reported to stabilize the fold of both oxidation states (Schejter *et al.*, 1994; Koshy *et al.*, 1994), with an enhanced preference for the reduced protein (Lett *et al.*, 1996). In mutations I75M, V28M, Y67F and K55M, $\Delta\Delta S_{red.}$ correlates with $\Delta E_m^{\circ\prime}$. This is not the case for the mutants at position 52 (**Figure 3.63**). In the Asn^{52} series, $\Delta\Delta S_{red.}$ and $\Delta E_m^{\circ\prime}$ are uncoupled. The

$\Delta\Delta S_{red.}$ of mutation is set at -74 ± 3 $J*K^{-1}*Mol^{-1}$, regardless of $\Delta E_m^{\circ\prime}$, the nature of the replacement, or the number of internal water molecules in the heme crevice. Three exceptions exist: mutants N52S, N52T and N52H. The Ser and Thr mutants have thermodynamic profiles of reduction more similar to the wild type protein (**Figure 3.63**). These mutations are the only substitutions analysed that conserve hydrogen-bond donor potential at this position. The entropic cost then appears to be due to the absence of a hydrogen bond between the water molecule and side chain at position 52, not merely to the presence of the solvent molecule. Modeling of mutant N52H shows that the histidine side chain does not leave enough space for a buried water molecule inside the heme crevice. It is unclear if this mutant protein locates along the linear regression in **Figure 3.63** by coincidence or not. In this case, the enthalpy still favours the reduced state relatively to the wild type protein, but the entropic cost is much less, halving the effect on $\Delta E_m^{\circ\prime}$. The permanent and induced dipole of the imidazole may partially compensate for the lost polarity of the Asn^{52}-Wat^{166} unit.

4.3.8 Tyr^{67} and $E_m^{\circ\prime}$

The hydroxyl group at position 67 is thought to contribute to the electron-withdrawing power of Met^{80} (Berghuis *et al.*, 1994), to the binding of Wat^{166} (Louie *et al.*, 1990), and to stabilizing the lysine ligands in the state IV alkaline isomer (Schroeder *et al.*, 1997). The $\Delta\Delta S_{red.}$ of mutant Y67F suggests that the hydroxyl group of Tyr^{67} is not part of the block Asn^{52}-Wat^{166} (**Figure 3.63**). The enthalpy of reduction upon losing the hydroxyl group also favours the reduced state. This is possible either by affecting the electron-withdrawing power of Met^{80} or more generally by deleting one dipole that is able to react favourably to the fluctuations in the electrostatic charge on the heme. Again, the enthalpic effect is counteracted by a larger entropic effect, resulting in a net decrease of E_m''.

Schroeder *et al.* (1997) determined by second derivative spectroscopy that the polarity of the environment of the aromatic ring of Tyr^{67} was higher in the reduced state of the wild type. This effect is reversed in the mutants N52I and N52V. This suggests that Wat^{166} does indeed bind the hydroxyl group of Tyr^{67} more tightly in the reduced state. Schroeder also pointed out that Tyr^{67} is not

affected by the polarity of the second water molecule in the mutant N52A.

The effects of the double mutations Y67F/N52I and Y67F/N52V have nothing in common with those of the corresponding single mutations. The enthalpy of deleting the polarity at position 52 and 67 actually favours the oxidized state. This may be caused by a more direct effect of the negatively charged heme propionate on the cationic iron ion due to the lack of screening by the protein matrix. Alternatively, since these double mutants fail to undergo an alkaline transition (Berghuis et al, 1994a; Blouin and Wallace, unpublished data), it is conceivable that the second heme propionate (Hpr^6) is ionized in these proteins, which would clearly favour a positive charge on the heme, hence a lower E_m''.

The entropies of reduction of both double mutants indicate that the temperature dependent component of the free energy of a fully hydrophobic heme crevice is similar to these of a wild type, fully hydrophilic cavity (**Figure 3.64**). This means that the resistance to thermal motion of the redox equilibrium is the same whether Asn^{52} is binding Wat^{166} or all residues in the cavity pack are using van der Waals interactions.

4.3.9 Entropy and $E_m^{\circ\prime}$

From an enthalpy perspective, the presence of the Asn^{52}-Wat^{166} bond is more favourable to the oxidized state than any other substitutions at position 52, despite the seemingly unfavourable dipolar moment of the chemical groups (Langen *et al.*, 1992). This advantage in enthalpy is countered by an entropic cost. As partial deletion of the hydrogen bond network occurs in the cavity, the unsatisfied dipoles react to the electrostatic field of the ferric heme. This increased field in the oxidized protein would offer a thermodynamic drive to rotate the dipoles away from their interacting partners. This levelling of the energetics of the hydrogen bond network would result in a crevice that is less geometrically defined, and thus becomes entropically favourable. In the extreme case of complete deletion of the polarity in the crevice, the entropic advantage in the oxidized state becomes irrelevant. This could explain why entropy and enthalpy uncouple in mutants Y67F/N52I and Y67F/N52V (**Figure 3.64**).

I therefore propose that mitochondrial cytochrome *c* evolved toward higher E_m'' by optimising a highly polar environment incapable of polarizing upon oxidation by having all of its dipoles already satisfied. This conclusion is in full agreement with the theory of microscopic dielectrics (Simonson *et al.*, 1991), with the added conformational polarisability. In addition to the dipolar and electronic polarisability, the conformational polarisability should be accounted for. This parameter cannot be calculated solely from molecular coordinates and is therefore elusive to determine.

4.3.10 Homeostasis and E_m''

There is no known theoretical reason why the datapoints in **Figure 3.62** should align along a diagonal line following the $d(T\Delta\Delta S)/d\Delta\Delta H = 1$. It appears that the changes in enthalpy and entropy cancel each other, though generally with a somewhat larger entropic effect.

Just as the structural properties of a protein are cooperatively established, a property such as the protein matrix dielectric susceptibility also seems to be set by a form of functional cooperativity. Shallow

enthalpy wells are known to have a flat bottom while deeper wells are narrower. The advantage of a decreased enthalpy would naturally be offset by an entropic penalty. The immediate environment of the heme seems to buffer cytochrome c $E_m^{o\prime}$ to fairly similar values despite low interspecies sequence identity. The mechanism would involve restraining conformational polarisability upon oxidization by restraining the dipoles from reacting to the electrostatic field. The presence of such buffering in $E_m^{\circ\prime}$ is likely to be a favourable trait as cytochrome c is part of a large array of coevolving electron transport proteins.

4.3.11 Breakdown of ε at the molecular level

It is intuitive that the constant nature of a dielectric medium will be maintained only if the dielectric material in question is homogenous between any two points in space. This assumption is true in the macroscopic world, but breaks down as the size of a system approaches the atomic scale. Also, in a macromolecule, there are no real point charges and no medium can be considered as continuous. With this in mind, there is no reason why one should expect a constant character for the

dielectric susceptibility at the microscopic level. However, it is not because a system is too small to proceed with a formal physical treatment that no rational explanation can be provided. Indeed, precise values of apparent dielectric constants are measurable, which stresses the fact that there is, somehow, a (few) simple law(s) governing the phenomenon. In fact, the problem may stem from deep within our conceptual vocabulary: the data indicate that the structure of the cytochrome *c* does not change during the redox reaction; this suggests that the structural change induced by the redox equilibration has nothing to do with the Cartesian coordinates of the atoms in the protein relative to each other.

The coordinates of the atoms of a protein define the chemical energy of a system, also referred to in molecular mechanics as *energy hyperspace*. The structure, as can be observed using XRD or NMR determines the shape of this hyperspace. The bottom of the potential energy well in which a system will tend to dwell represents the enthalpies. The very precise geometrical requirements necessary to occupy such a well will be challenged by thermal motions, constraining the chemical groups involved. The propensity to occupy a minimum against the

thermal motion reflects the entropy. If an electrostatic charge is added to a system, the hyperspace will invariably be altered without necessarily changing the physical shape of the protein.

In molecular modeling, coordinates (e.g. structure) are used as input to perform calculations. The entropy is not a function of the coordinates but more of the energy hyperspace, therefore, in molecular systems, ε cannot be calculated because of our inability to calculate $\varepsilon_{measured}$. This deficiency is reflected in the complex nature of microscopic-level dielectric behaviour.

Chapter 5: Conclusions

5.1 Methodological limitations

The experimental approaches employed, as in any research program, were limited by the availability of high-end equipment. The assumption that the biological assays presented in Section 3.2 represent an assessment of the affinity between the electron transport proteins would have been more solid if a direct determination of the affinities could have been made. However, the actual driving force ($\Delta E_m''$) of reaction was in no case greatly altered, which leaves surface electrostatics as the main factor responsible for any change in activity. This analysis should thus be regarded as qualitative.

Also, all molecular dynamics experiments were carried out on a modest size personal workstation. This means that fewer experiments were run over the years, and no attempts were made to derive biophysical constants from the models. These are presented as conformational searches, an activity for which molecular mechanics yields satisfactory results.

5.2 **Complex system**

The most interesting feature of the work I present in this dissertation concerns the fact that no matter how intertwined the components may be, non-ideal behaviour can be simplified into ideal components. Also, that simplicity in an experimental strategy can *still* provide intriguing results. My main lines of investigation pointed out that the logic behind apparently complex behaviour is in fact simple. The mathematical models are straightforward but the interpretation requires one to look at proteins less as the mechanical entities that they are usually compared to. Proteins are folded polymers folded in a unique fashion in a lattice of highly consistent interactions that have an impact both on stability and function. The depth of this self-consistency probably stems from the properties of the members of the so-called "random/variable" pool of residues in a protein's sequence.

5.3 **Further work**

Further work can be undertaken via two strategies. Firstly, the experimental approach. After spending 5 days with the most successful theoreticians in the electrostatics of macromolecules, I realized that experimental science should be promoted in order to provide data on model systems. These can then be used to validate the theoretical calculations (and obviously generate new ideas). Secondly, a computational approach. Since there are stringent technological limitations to the depth of the calculations one can perform on macromolecules, much work has to be done to extend the realm of formal treatment in computational biochemistry beyond the simple conformational sampling as presented in this thesis.

Appendix A - Corrected equation to determine standard redox Potential using the method of mixture.

Since the ideal slope (m_i) in this graph method is 1 (one electron transferred in the equilibrium), we can assume that the deviation from that slope is attributable to a constitutive error on the ratio of Fe**'cyanide setting the redox of the buffer.
Therefore: both the ideal and experimental curve must intersect at:

$$\left(-\frac{b}{2m_i} , \frac{b}{2} \right)$$

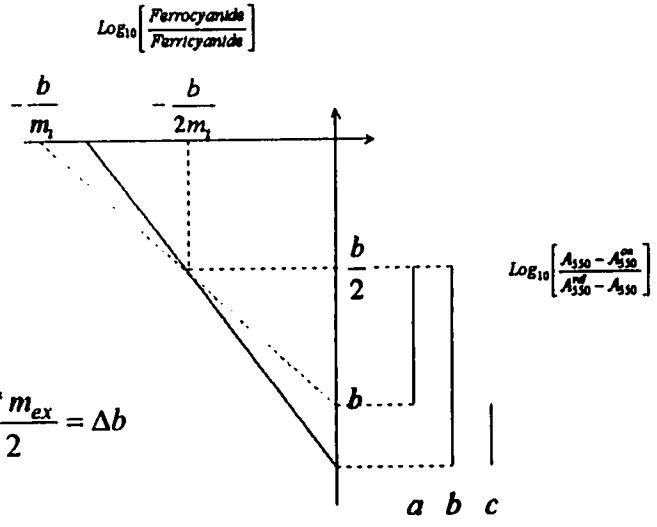

This means that the values for:

i) $a = \frac{b}{2}$ ii) $b = \frac{b * m_{ex}}{2}$ iii) $c = \frac{b}{2} + \frac{b * m_{ex}}{2} = \Delta b$

And the uncorrected intercept value is:

iv) $E_m^{o'} = 430mV - 60mV(b + \Delta b)$

v) $(b + \Delta b) = b + b * \frac{m_{ex}}{2} + \frac{b}{2} = b\left(1 + \frac{m_{ex}}{2} + \frac{1}{2}\right) = b\left(\frac{3 + m_{ex}}{2}\right)$

Which yields as corrected equation:

vi) $E_m^{o'} = 430mV - \left[60\left(\frac{3 + m_{ex}}{2}\right)b\right]mV$

Appendix B - Derivative of the linearized form of two additive ideal Ionisations.

Function of an ideal titration curve where U
Defines a function for the shape of a baseline

i $$A = \frac{A_{mx_1}}{1+\left(K_1/[H^+]\right)} + U$$

ii $$A - U = \frac{A_{mx_1}}{1+\left(K_1/[H^+]\right)}$$

iii $$A_{mx_1} = A + \frac{AK_1}{[H^+]} - \left(U + \frac{UK_1}{[H^+]}\right)$$

iv $$\frac{A}{[H^+]} = \frac{A_{mx_1}}{[H^+]} - \frac{1}{K_1}A + \left(\frac{U}{K_1} + \frac{U}{[H^+]}\right)$$

Defining U as a second ionisation:

v $$U = \frac{A_{mx_2}}{1+\left(K_2/[H^+]\right)}$$

Integrating (v) in (iv):

vi $$\frac{A}{[H^+]} = \frac{A_{mx_1}}{[H^+]} - \frac{1}{K_1}A + \left(\frac{A_{mx2}}{K_1+\left(K_1K_2/[H^+]\right)} + \frac{A_{mx2}}{[H^+]+K_2}\right)$$

Multiplying all terms by $\left(K_1+\frac{K_1K_2}{[H^+]}\right)$

vii $$\frac{A}{[H^+]}\left(K_1+\frac{K_1K_2}{[H^+]}\right)=\left(\frac{A_{mx1}K_1+\frac{A_{mx1}K_1K_2}{[H^+]}}{K_1}\right)-\left(\frac{AK_1+\frac{AK_1K_2}{[H^+]}}{K_1}\right)+A_{mx2}+\left(\frac{A_{mx2}K_1+\frac{A_{mx2}K_1K_2}{[H^+]}}{[H^+]+K_2}\right)$$

ix $$\frac{A}{[H^+]}\left(K_1+\frac{K_1K_2}{[H^+]}\right)=A_{mx1}+\frac{A_{mx1}K_2}{[H^+]}-\left(A+\frac{AK_2}{[H^+]}\right)+A_{mx2}+\left(\frac{A_{mx2}K_1+\frac{A_{mx2}K_1K_2}{[H^+]}}{[H^+]+K_2}\right)$$

Multiplying all terms by $\left([H^+]+K_2\right)$

x $$\frac{A}{[H^+]}\left(K_1+\frac{K_1K_2}{[H^+]}\right)\left([H^+]+K_2\right)=$$

$$A_{mx1}[H^+]+2(A_{mx1}K_2)+\frac{A_{mx1}K_2{}^2}{[H^+]}-\left(A[H^+]+\frac{AK_2{}^2}{[H^+]}\right)+A_{mx2}[H^+]+A_{mx2}K_2+A_{mx2}K_1+\frac{A_{mx2}K_1K_2}{[H^+]}$$

xi $$\frac{A}{[H^+]}\left(K_1+\frac{K_1K_2}{[H^+]}\right)\left([H^+]+K_2\right)=$$

$$A_{mx1}\left([H^+]+2K_2+\frac{{K_2}^2}{[H^+]}\right)+A_{mx2}\left([H^+]+K_1+K_2+\frac{K_1K_2}{[H^+]}\right)-A\left([H^+]+\frac{{K_2}^2}{[H^+]}\right)$$

Factorizing :

xii $$A_{mx1}\left([H^+]+K_2\right)\left(1+\frac{K_2}{[H^+]}\right)+A_{mx2}\left([H^+]+K_2\right)\left(1+\frac{K_1}{[H^+]}\right)-A\left([H^+]+\frac{{K_2}^2}{[H^+]}\right)$$

xiii $$\frac{A}{[H^+]}=\frac{\dfrac{A_{mx1}\left(1+\frac{K_2}{[H^+]}\right)+A_{mx2}\left(1+\frac{K_1}{[H^+]}\right)}{\left([H^+]+K_2\right)}-A\left([H^+]+\frac{{K_2}^2}{[H^+]}\right)}{\left([H^+]+K_2\right)\left(K_1+\frac{K_1K_2}{[H^+]}\right)}$$

xiv

$$\frac{d\left[\frac{A}{[H^+]}\right]}{dA} = -\frac{\left([H^+] + \frac{K_2{}^2}{[H^+]}\right)}{\left([H^+] + K_2\right)\left(K_1 + \frac{K_1K_2}{[H^+]}\right)}$$

Expanding and multiplying by 1 :

xv

$$\frac{d\left[\frac{A}{[H^+]}\right]}{dA} = -\frac{[H^+] + \frac{K_2{}^2}{[H^+]}}{K_1[H^+] + 2K_1K_2 + \frac{K_1K_2{}^2}{[H^+]}} * \left(\frac{[H^+]}{[H^+]}\right)$$

xvi

$$\frac{d\left[\frac{A}{[H^+]}\right]}{dA} = -\frac{[H^+]^2 + K_2{}^2}{K_1[H^+]^2 + 2K_1K_2[H^+] + K_1K_2{}^2}$$

xvii

$$\boxed{\frac{d\left[\frac{A}{[H^+]}\right]}{dA} = -\frac{[H^+]^2 + K_2{}^2}{K_1\left([H^+] + K_2\right)^2}}$$

Appendix C - BTCL script of moving windows RMSD analysis

```
################################
#   Calculate RMSD in structures with a range of option from sampling
#   size, filename to output and type for RMSD calculation
#      Christian Blouin, 2000
################################
#   Calculate RMS deviations down the backbone for sets of proteins
#   and plot the results (scan size = 9)
#      Jonathan Parrish, 1996
################################

Define_Macro RMSD_scan  \
     Ident Molecule_1 \
     Ident Molecule_2 \
     Int  Starting_Residue  \
     Int  Ending_Residue \
     Int  Half_Sampling_width \
     Lstring Filename \
     Enumer Scope_of_Scan
################################

     #local variables
     Float rms_value            # torsion angle value
     Lstring fn                 # filename
     Int cresidue               # current residue index
     Int midresidue             # middle residue in scan
     Int endresidue             # last residue in scan
     Ident Range_1              # molecule descriptions for superpos.
     Ident Range_2
     Param_Set_Style Scope_of_Scan PARAM_POPUP
     Def_Enum Scope_of_Scan Backbone
     Def_Enum Scope_of_Scan Heavy

################################
     # initialization
     cresidue    = $Starting_Residue
     midresidue  = $Starting_Residue + $Half_Sampling_width
     endresidue  = $Starting_Residue + (2 * $Half_Sampling_width)
     fn          = $Filename
     Print "Scope_of_Scan =" $Scope_of_Scan

     #add picking
     Set_Param_Pick Molecule_1 MOLECULE_NAME
     Set_Param_Pick Molecule_2 MOLECULE_NAME

     # check input parameters
     If ( ( $Starting_Residue < 1 ) || ( $Ending_Residue <=1 ) )
       Print "Residue number must be greater than 1"
       Return
     End

     If ((($Starting_Residue > $Ending_Residue) || \
```

```
      ( ( $Ending_Residue - $Starting_Residue) < 10) )
    Print "Ending_Residue number should be greater than"
    Print "Starting_Residue number by at least ten"
    Return
  End

  #remove rms_devs file, if present
  Bcl_Unix ("rm -f " // $fn)

  # write table description information to file
  Write $fn "InsightII V95.0\n"
  Write $fn "Date: October 1996\n#\n"
  Write $fn "TITLE:  Residue Number\n"
  Write $fn "MEASUREMENT TYPE: Dimensionless\n"
  Write $fn "UNITS OF MEASUREMENT: <no units>\n"
  Write $fn "FUNCTION: Residue Number\n#\n"
  Write $fn "TITLE: RMS deviation\n"
  Write $fn "MEASUREMENT TYPE: Distance\n"
  Write $fn "UNITS OF MEASUREMENT: Angstroms\n"
  Write $fn "FUNCTION: RMS deviation\n#\n#\n"

  #Main loop for measuring torsions
   While ($endresidue < ($Ending_Residue + 1))

        Range_1 = $Molecule_1//":"//$cresidue//"-"//$endresidue
        Range_2 = $Molecule_2//":"//$cresidue//"-"//$endresidue

        {Superimpose -End_definition \
                  $Scope_of_Scan "Label Mode" $Range_1 $Range_2 }

        $rms_value = {Superimpose End_definition}

      Write $fn "%5d %11.6f\n" $midresidue $rms_value

      cresidue = $cresidue + 1
      midresidue = $midresidue + 1
      endresidue = $endresidue + 1

   End  #end of while loop

  # close rms deviations file

  Close $fn

  #load analysis and draw the graph

  Analysis
  Get Graph $fn New_Graph "Residue Number" "RMS deviation" None

End_Macro
Add_To_Pulldown RMSD_scan User
```

References

Amati BB, Goldschmidt MC, Wallace CJA, Rochaix JD. (1988) c-DNA and deducted amino acid sequence of cytochrome *c* from *Chlamidomonas reinhardtii* : Unexpected functional and phylogenetic implication. J Mol Biol 28:151-160.

Ando K., Matsubara H. and Okunuki K. (1966) Alkylation of cytochrome *c* . I Propoerties of alkylated beef cytochrome *c*. Biochem. Biophys. Acta. 118:240-255

Ando K., Matsubara H. and Okunuki K. (1966a) Alkylation of cytochrome *c* . II Carboxymethylation of beef and huan cytochrome *c* in the reduced and oxidized form. Biochem. Biophys. Acta. 118:356-267

Banci L, Bertini I, Huber JG, Spyroulias GA, Turano P. (1999) Solution structure of reduced horse heart cytochrome *c* . J. Biol. Inorg. Chem. 4:21-31.

Banci L, Bertini I, Bren KL, Gray HB, Sompornpisut P, Turano P. (1997) Solution structure of oxidized *Saccharomyces cerevisiae* iso-1- cytochrome *c*. Biochemistry 36:8992-9001.

Banci L, Bertini I, Gray HB, Luchinat C, Reddig T, Rosato A, Turano P. (1997) Solution structure of oxidized horse heart cytochrome c. Biochemistry 36:9867-9877.

Battistuzzi GM, Borsari M, Loschi L, Martinelli A, Sola M. (1999) Thermodynamics of the alkaline transition of cytochrome c. Biochemistry 38:7900-7907.

Battistuzzi GM, Borsari M, Sola M, Francia F. (1997) Redox thermodynamics of the native and alkaline forms of eucaryote and bacterial class I cytochrome *c*. Biochem., 36:16247-58

Beratan DN, Betts JN, Onuchic JN. (1995) Electron-tunneling pathways in protein. Science. 258:1740-1

Berghuis AM, Guillemette JG, Smith M, Brayer GD. (1994) Mutation of tyrosine-67 to phenylalanine in cytochrome c significantly alters the local heme environment. J. Mol. Biol. 235:1326-1341.

Berghuis AM, Guillemette JG, McLendon G, Sherman F, Smith M, Brayer GD. 1994a. The role of a conserved internal water molecule and its associated hydrogen bond network in cytochrome c. J. Mol. Biol., 236:786-99

Berghuis AM, Brayer GD. (1992) Oxidation state-dependent conformational changes in cytochrome c. J. Mol. Biol. 223:959-976

Bohm G, Muhr R, Jaenicke R. (1992) Quantitative analysis of protein far UV circular dichroism spectra by neural networks. Protein Eng. 5:191-5

Bone S, Pethig R. 1982. Dielectric studies of binding of water to lysozyme. J. Mol. Biol. 157:175

Bosshard HR, Zürrer M. (1980) The conformation of cytochrome *c* in solution. J. Biol. Chem., 255:6694-99

Bushnel GW, Louie GV, Brayer GD. (1990) High-resolution three-dimensional structure of horse heart cytochrome *c*. J. Mol. Biol. 214:585-95

Churg AK, Warshel A. (1986) Control of the redox potential of cytochrome *c* and microscopic dielectric effects in proteins. Biochem. 25:1675-81

Craig DB, Wallace CJA. (1995) Studies of 8-azido-ATP adducts reveal two mechanisms by which ATP binding to cytochrome c could inhibit respiration. Biochemistry. 34:2686-2693

Cutler RL, Davies AM, Creighton S, Warshel A, Moore GR, Smith M, Mauk AM. (1989) Role of arginine-38 in regulation of the cytochrome *c* oxidation-reduction equilibrium. Biochem. 28:3188-97

Darley-Usmar VM, Capaldi RA, Takamiya S, Millet F, Wilson MT, Malatesta F, Sarti P. (1987) Reconstitution and molecular analysis of the respiratory chain in Mitochondria: A Practical Approach. (IRL Press, Oxford)

Davies AM, Guillemette JG, Smith M, Greenwood C, Thurgood AGP, Mauk AG, Moore GR. (1993) Redesign of the interior hydrophilic region of mitochondrial cytochrome *c* by site directed mutagenesis. Biochem. 32:5431-5

Döpner SP, Hildebrand P, Rosell FI, Mauk AG. (1998) Alkaline conformational transitions of ferricytochrome c studied by resonance Raman spectroscopy. J. Am. Chem. Soc. 120:11246-11255

Döpner S, Hildebrandt P, Rosell FI, Mauk AG, von Walter M, Buse G, Soulimane T. (1999) The structural and functional role of lysine residues in the binding domain of cytochrome *c* in the electron transfer to cytochrome *c* oxidase. Eur. J. Biochem. 261:379-391

Eaton WA, Hochstrasser RM. (1967) Electronic spectrum of single crystals of ferricytochrome-c. J. Chem. Phys. 46:2533-2539.

Edholm O, Nordlander P, Chen W, Ohlsson PI, Smith ML, Paul J. (2000) The effect of water on the Fe^{3+}/Fe^{2+} reduction potential of the heme. Bioch. Biophys. Res. Comm. 268:683-687

Eisenberg D, Crothers D. (1979) Chapter 8: Electrolyte solutions in Physical Chemistry with application to the life science. Benjamin/Cummings, Menlo Park, U.S.A.

Falk K.E. and Angstrom J. (1983) A 1H-NMR longitudinal relaxation study of the interaction between cytochrome c and cytochrome c oxidase. Biochim. Biophys. Acta 722:161-176

Feinberg BA, Petro L, Hock G, Qin W, Margoliash E. (1999) Using entropies of reaction to predict changes in protein stability: tyrosine-67-phenylalanine variant of rat cytochrome *c* and yeast Iso-1 cytochrome *c*. J. Pharm. Biomed. Anal. 19:115-125.

Ferrer JC, Guillemette JG, Bogumil R, Inglis SC, Smith M, Mauk AG. (1993) Identification of Lys79 as an iron ligand in one form of alkaline yeast iso-1-ferricytochrome c. J. Amer. Chem. Soc. 115:7507-7508.

Filosa A, Ismail AA, English AM. (1999) FTIR-monitored titration reveals different mechanisms for the isomerisation of tuna compared to horse and bovine cytochrome c. J. Biol. Inorg. Chem. 4:717-26

Guillemette JG, Barker PD, Eltis LD, Lo TP, Smith M, Brayer GD, Mauk AG. (1994) Analysis of the bimolecular

reduction of ferricytochrome c by ferrocytochrome b5 through mutagenesis and molecular modelling. Biochimie. 76:592-604

Gunner MR, Honig B. (1991) Electrostatic control of midpoint potentials in the cytochrome subunit of the *Rhodopseudomonas viridis* reaction center. Proc. Natl. Acad. Sci. USA. 88:9151-9155

Harbury HA, Cronin JR, Fanger MW, Hettinger T P, Murphy A J, Myer YP, Vinogradov SN. (1965) Complex formation between methionine and a heme peptide from cytochrome c. Proc. Natl. Acad. Sci. USA 52:1658-1664.

Hartshorn RT, Moore GR. (1989) A denaturation-induced proton-uptake study of horse ferricytochrome c. Biochem. J. 258:595-598

Hildebrandt P, Vanhecke F, Buse G, Soulimane T, Mauk AG. (1993) Resonance Raman study of the interactions between cytochrome *c* variants and cytochrome *c* oxidase. Biochemistry. 32:10912-10922

Hong XL, Dixon DW. (1989) NMR study of the alkaline isomerization of ferricytochrome c. FEBS Lett. 246:105-108.

Inglis SC, Guillemette JG, Johnson JA, Smith M. (1991) Analysis of the invariant Phe82 residue of yeast iso-1-cytochrome c by site-directed mutagenesis using a phagemid yeast shuttle vector. Protein Eng. 4:569-574

Jensen F. (1999) *Introduction to computational chemistry.* Chapter 2. John Wiley & Sons, Toronto

Koshy TI, Luntz TL, Plotkin B, Schejter A, Margoliash E. (1994) The significance of denaturant titration of protein stability: a comparison of rat and baker's yeast cytochrome *c* and their site-directed asparagine-52 to isoleucine mutants. Biochem. J., 299:347-50

Langen R, Brayer GD, Berghuis AM, McLendon G, Sherman F, Warshel A. (1992) Effect of the Asn52->Ile mutation on the redox potential of yeast cytochrome c. Theory and experiment. J. Mol. Biol. 224:589-600

Lett CM, Berghuis AM, Frey HE, Lepock JR, Guillemette JG. (1996) The role of a conserved water molecule in the redox-dependent thermal stability of iso-1 cytochrome c. J. Biol. Chem. 271:29088-93

Linsk-O'Connell L, Sherman F, McLendon G. (1995) Stabilizing amino-acid replacements at position 52 in yeast-iso-1-cytochrome *c*: *in vivo* and *in vitro* effects. Biochem. 34:7094-102

Louie GV, Brayers GD. (1990) High-resolution refinement of yeast iso-1-cytochrome c and comparisons with other eukaryotic cytochromes c. J. Mol. Biol. 214:527-555.

Luntz TL, Schejter A, Garber EA, Margoliash E. (1989) Structural significance of an internal water molecule studied by site- directed mutagenesis of tyrosine-67 in rat cytochrome *c*. Proc. Natl. Acad. Sci. USA 86:3524-3528

Mauk MR, Ferrer JC, Mauk AG. (1994) Proton linkage in formation of the *cytochrome c* - cytochrome *c* peroxidase complex: Electrostatic properties of the high- and low-affinity cytochrome binding sites on the peroxidase. Biochemistry. 33:12609-12614

Mauk AG, Mauk MR, Moore GR, Northrup SH. (1995) Experimental and theoretical analysis of the interaction between cytochrome *c* and cytochrome b_5. J. Bioener. Biomembr. 27:311-330

Michel B. and Bosshard H.R. (1989) Oxidation of cytochrome c by cytochrome c oxidase: spectroscopic binding studies and steady-state kinetics support a conformational transition mechanism. Biochemistry. 28:244-252

Moore GR, Pettigrew GW, Pitt RC, Williams RJP. 1980. pH dependence of the redox potential of *Pseudomonas aeruginosa* cytochrome *c*-551. Biochem. Biophys. Acta 590:261-271

Moore GR. 1983. Control of redox properties of cytochrome c by special electrostatic interactions. FEBS. Lett. 161:171-175

Moore GR, Pettigrew GW. (1990) Cytochrome c: Evolutionary, structural and physicochemical aspect. New-York, Springer-Verlag.

Narita K, Titani K. (1969) The complete amino acid sequence in baker's yeast cytochrome *c*. J. Biochem. 65:259-267

Osheroff ND, Borden D, Koppenol WH, Margoliash E. (1980) Electrostatic interactions in cytochrome c. The role of interactions between residues 13 and 90 and residues 79 and 47 in stabilizing the heme crevice structure. J. Biol. Chem. 255:1689-1697.

Parrish JC. (1997) Structural studies in cytochrome *c* : or cytochrome *c* allsorts. Ph.D. dissertation, Dalhousie University, Halifax, Canada.

Pearce LL, Gartner AL, Smith M, Mauk AG. (1989) Mutation-induced perturbation of the cytochrome c alkaline transition. Biochemistry 28:3152-3156.

Pollock WB, Rosell FI, Twitchett MB, Dumont ME, Mauk AG. (1998) Bacterial expression of a mitochondrial cytochrome *c*. Trimethylation of lys72 in yeast iso-1-cytochrome c and the alkaline conformational transition. Biochemistry. 37:6124-6131.

Qi PX, Beckmann RA, Wand AJ. (1996) Solution structure of horse heart ferricytochrome c and detection of redox-related structural changes by high-resolution ^{1}H NMR. Biochem. 35:12275-86

Qi PX, DiStefano DL, Wand AJ. (1994) Solution structure of horse heart ferrocytochrome c determined by high-resolution NMR and restrained simulated annealing. Biochem. 33:6408-17

Qi PX, Urbauer JL, Fuentes EJ, Leopold MF, Wand AJ. (1994a) Structural water in oxidized and reduced horse heart cytochrome *c*. Struct. Biol. 1:378-82

Rafferty SP, Guillemette JG, Berghuis AM, Smith M, Brayer GD, Mauk AG. (1996) Mechanistic and structural contributions of critical surface and internal residues to cytochrome *c* electron transfer activity. Biochem. 35:10784-92

Rees DC. (1980) Experimental evaluation of the effective dielectric constant of proteins. J. Mol. Biol. 141:323-6

Roberts VA, Pique ME. (1999) Definition of the interaction domain for the cytochrome *c* on cytochrome *c* oxidase. J. Biol. Chem. 274:38051-60

Rosell, F.I., Harris, T.R., Hildebrand, D.P., Dopner, S., Hildebrandt, P. and Mauk, G. (2000) Characterization of an alkaline transition intermediate stabilized in the Phe82Trp variant of yeast iso-1-cytochrome c. Biochemistry. 39:9047-9054

Rosell FI, Ferrer JC, Mauk AG. (1998) Proton-Linked Protein Conformational Switching: Definition of the Alkaline Conformational Transition of Yeast Iso-1-ferricytochrome c. J. Amer. Chem. Soc. 120:11234-11245.

Salemme FR. (1976) An hypothetical structure for an intermolecular electron transfer complex of cytochrome *c* and cytochrome b_5. J Mol Biol. 102:563-568

Schejter A, Koshy TI, Luntz TL, Sanishvili R, Margoliash E. (1994) Effect of mutating Asn-52 to isoleucine on the haem-linked properties of cytochrome *c*. Biochem. J. 302:95-101

Schejter A, George P. (1964) The 695-mμ band of ferricytochrome c and its relationship to protein conformation. Biochemistry. 3:1045-1049.

Schejter A, Plotkin B., Vig I. (1991) The reactivity of cytochrome c with soft ligands. FEBS lett. 280:199-201

Schroeder HR, McOdimba FA, Guillemette JG, Kornblatt JA. (1997) The polarity of tyrosine 67 in yeast iso-1-cytochrome *c* monitored by second derivative spectroscopy. Biochem. Cell. Biol. 75:191-197

Simonson T, Perahia D, Bricogne G. (1990) Intramolecular dielectric screening in proteins. J. Mol. Biol. 218:859-886

Simonson T, Perahia D, Brünger AT. (1991) Microscopic theory of the dielectric properties of proteins. Biophys. J. 59:670-690

Simonson T, Perahia D. (1995) Internal and interfacial dielectric properties of cytochrome c from molecular

dynamics in aqueous solution. Proc. Natl. Acad. Sci. USA. 92:1082-1086

Simonson T. (1998) Dielectric constant of cytochrome *c* from simulation in a water droplet including all electrostatic interaction. J. Am. Chem. Soc. 120:4875-4876

Sinha A, Yadav S, Ahmad F. (2000) A possible origin of difference between calorimetric and equilibrium estimates of stability parameters in proteins. Biochem. J. 345:711-717

Sober HA. (1970) Handbook of Biochemistry. Selected data for molecular biology. 2nd Ed. The chemical rubber Co. Cleveland, USA.

Springs ST, Bass SE, McLendon GL. Cytochrome b562 variants: A library for examining redox potential evolution. Biochemistry. 39:6075-82

Swanson R, Trus BL, Mandel G, Kallai OB, Dickerson RE. (1977) Tuna cytochrome *c* at 2.0 Å resolution. Ferricytochrome structure analysis. J. Biol. Chem. 252:759-75

Takano T, Dickerson RE. (1981) Conformation change of cytochrome *c*. I. Ferrocytochrome c structure refined at 1.5 Å resolution. J. Mol. Biol., 153:79-94

Takano T. Dickerson RE. (1981a) Conformation change of cytochrome *c* : II. Ferricytochrome c refinement at 1.8 Å and comparison with the ferricytochrome c structure. J. Mol. Biol., 153:95-115

Takashima S, Schwan H. (1965) Dielectric dispersion of crystalline powders of amino acids, peptides, and proteins. J. Phys. Chem. 69:571-575

Tanford C. (1961) Physical chemistry of macromolecules. Wiley, New-York.

Theorell H, Åkesson Å. (1941) Studies on cytochrome c. J. Amer. Chem. Soc. 63:1804-1820.

Tonge P, Moore GR, Wharton CW. (1989) Fourier-transform infra-red studies of the alkaline isomerization of

mitochondrial cytochrome c and the ionization of carboxylic acids. Biochem. J. 258:599-605.

Wallace CJA, Corthésy BE. (1987). Alkylamine derivatives of cytochrome c. Comparison with other lysine- modified analogues illuminates structure/function relations in the protein. Eur. J. Biochem. 170:293-8.

Wallace CJA, Proudfoot A. (1987). On the relationship between oxidation-reduction potential and biological activity in cytochrome c analogues. Results from four novel two-fragment complexes. Biochem. J. 245:773-779

Wallace CJA. (1989) Substitutions engineered by chemical synthesis at three conserved sites in mitochondrial cytochrome c. J. Biol. Chem. 264:15199-15209.

Wang K, Zhen Y, Sadoski R, Grinell S, Geren S, Fergusson-Miller S, Durham B, Millet F. (1999) Definition of the interaction site of cytochrome c on cytochrome c oxidase. Rapid kinetic analysis of electron transfer from cytochrome c to Rhodobacter sphaeroides cytochrome c oxidase surface mutants. J. Biol. Chem. 274:38042-50

Wang Y. and Margoliash E. (1995) Enzymic activities of covalent 1:1 complexes of cytochrome c and cytochrome c peroxidase. Biochemistry. 34:1948-1958.

Weber C., Michel B. and Bosshard H.R. (1987) Spectroscopic analysis of the cytochrome c oxidase-cytochrome c complex: circular dichroism and magnetic circular dichroism measurements reveal change of cytochrome c heme geometry imposed by complex formation. Proc. Natl. Acad. Sci. USA 84:6687-6691

Wilgus H, Stellwagen E. (1974) Alkaline isomerization of ferricytochrome c: identification of the lysine ligand. Proc. Natl. Acad. Sci. USA 71:2892-4.

Wilson, M. T. and C. Greenwood (1996) The alkaline transition in cytochrome c. In: Scott RA, Mauk AG, eds. Cytochrome c: A multidisciplinary approach. Sausalito, California, University Science Book. pp. 611-634.

Whitford D, Gao Y, Pielak GJ, Williams RPJ, McLendon GL, Sherman F. (1991) The role of the internal hydrogen bond network in first-order protein electron transfer between

Saccaromyces cerevisiae iso-1-cytochrome *c* and bovine microsomal cytochrome b_5. Eur. J. Biochem. 200:359-67

Woods A., Guillemette G., Parrish J., Smith M. and Wallace C.J.A. (1996) Synergy in protein engineering. Mutagenic manipulation of protein structure to simplify semisynthesis J. Biol. Chem. 271:32008-32015

Yang AS, Honig B. (1993) On the pH dependence of protein stability. J. Mol. Biol. 231:458-74

Zhen Y, Hoganson CW, Babcock GT, Fergusson-Miller S. (1999) Definition of the interaction domain for cytochrome *c* on cytochrome *c* oxidase. J. Biol. Chem. 274:38032-41